No. 210
March 1979

THREE DIMENSIONAL EFFECTS ON THE HYDRODYNAMIC COEFFICIENTS AND WAVE EXCITING FORCES USED IN PREDICTING MOTIONS OF SHIPS

Yung-Sup Shin

THE UNIVERSITY OF MICHIGAN
COLLEGE OF ENGINEERING
DEPARTMENT OF NAVAL ARCHITECTURE AND MARINE ENGINEERING

No. 210
March 1979

THREE DIMENSIONAL EFFECTS ON THE HYDRODYNAMIC COEFFICIENTS AND WAVE EXCITING FORCES USED IN PREDICTING MOTIONS OF SHIPS

by

Yung-Sup Shin

A dissertation submitted in partial fulfillment
of the requirement for the degree of
Doctor of Philosophy
(Naval Architecture and Marine Engineering)
in The University of Michigan
1979

Department of Naval Architecture
and Marine Engineering
College of Engineering
The University of Michigan
Ann Arbor, Michigan 48109

ABSTRACT

The three-dimensional boundary value problem for the unsteady motion of a ship oscillating on the free surface is formulated for zero forward speed. Various forms of the integral equation methods are formulated. The three-dimensional source distribution method is developed to compute the added mass and damping coefficient and the wave exciting forces on a ship.

The integral equation is solved approximately by three different methods: successive approximation by Neumann series, iterative method by use of infinite fluid solution and linear algebraic equations. The convergence of the iteration method is studied to discover why it does not converge for all frequency ranges. The improved iteration method by Buckner-Chertock series is applied for low frequency ranges to improve the convergence.

The integral equation is shown to fail at the infinite number of discrete eigenfrequencies of the interior Dirichlet problem. The difficulty near these eigenfrequencies can be removed by using a new form of Green's function. The new Green's function is constructed by adding an interior source to the fundamental Green's function. This form of the Green's function produces a new integral equation and removes the numerical difficulty near the eigenfrequencies.

The strip theory is considered to be invalid for computing hydrodynamic coefficients and exciting forces due to short waves. Comparison of the results of strip theory with those of 3-D theory shows that for the low and extremely high frequencies of oscillation, strip theory gives a poor result to compute the added mass; however, strip theory is a good approximation for fairly high frequency. The 3-D effects on the

wave exciting forces are investigated for the head sea. The axial distribution of the wave exciting forces are computed using the three dimensional theory, Haskind's formula, and a 2-D strip theory by Salvesen, Tuck, and Faltinsen (1970). The 3-D theory shows that greater forces occur near the bow than the stern for the head sea and decrease as the wave passes along the ship. This confirms Faltinsen's (1971) theory.

ACKNOWLEDGEMENTS

I would like to express my sincere gratitude to all the members of doctoral committee for guiding my thesis. Especially, I would like to thank the chairman of the committee, Professor T. Francis Ogilvie, for his technical guidance throughout the completion of my dissertation, and his continuous support during my graduate study at Michigan.

I would like to thank Professor William S. Vorus who gave invaluable suggestions and insights into the problem on various occasions. I am also indebted to Dr. Armin W. Troesch for his enthusiastic discussions and friendly help whenever it was needed. Without the help and encouragements of all the committee members, I can not think of the successful accomplishment of the dissertation. I also thank Ms. Leslie Ridgeway and Mrs. Paula Bousley who endured the laborious task of typing and corrections.

Finally, I would like to thank my parents for their continuous encouragement and moral support throughout my entire education.

This research was supported by the Department of Naval Architecture and Marine Engineering in the University of Michigan, the American Bureau of Shipping and Maritime Administration under contract number DRDA 78-88-KB1, and by the Naval Sea Systems Command General Hydromechanics Research Program, administered by the David W. Taylor Naval Ship Research and Development Center under contract number N00014-76-C-0345.

TABLE OF CONTENTS

LIST OF APPENDICES

LIST OF ILLUSTRATIONS

J_i	Bessel function of the first kind of i-th order
K	Kernel matrix of the integral equation
ℓ	distance from center to focus of spheroid
L	Ship length
M	Mass of the displaced volume
m	Added mass
m(x)	Sectional added mass
n_i	Generalized normal in i-th mode
$\vec{n}=(n_1,n_2,n_3)$	3-D normal
$\vec{N}=(0,N_2,N_3)$	2-D normal
O	Origin of the coordinate
p	Hydrodynamic pressure
P(x,y,z)	Field point
P_n^1	Associated Legendre function of the first kind
$Q(\xi,\eta,\zeta)$	Surface point
Q_n^1	Associated Lengendre function of the second kind
r	3-D distance between P and Q: $r=\sqrt{(x-\xi)^2+(z-\eta)^2+(z-\zeta)^2}$
r^*	3-D distance between P and Q^*: $r^*=\sqrt{(x-\xi)^2+(y-\eta)^2+(z+\zeta)^2}$
R	Horizontal distance between P and Q: $R=\sqrt{(x-\xi)^2+(y-\eta)^2}$
R_0	2-D distance between P and Q: $R_0=\sqrt{(y-\eta)^2+(z-\zeta)^2}$
S	Hull surface
T	Ship draft

V	Displaced volume of the ship
V_1, V_3	Constants to define the mode shape of springing $(V_1 - V_3\mu^2)$
W_i	J factor of the spheroid in i-th normal mode
Y_i	Bessel function of the second kind of i-th order
γ_i	Reciprocal eigenvalues of the kernel matrix
ε	slenderness parameter
(ξ, η, ζ)	Cartesian coordinates of surface integration variable
(κ, μ, θ)	Prolate spheroidal coordinates
λ	Wave length
μ	Dipole density or 2x/L
ν	Wave number: $\nu = \frac{\omega^2}{g}$
π	3.14159
ρ	Density of the fluid
σ	Source density
τ_i	Eigenvalues of the kernel matrix
Φ_i	Velocity potential in i-th mode
ϕ_i	Normalized velocity potential in i-th mode
χ	Wave heading angle
$\psi_i(x)$	Mode shape in the i-th mode of vertical vibration
ω	Frequency of oscillation

I. INTRODUCTION

For solving the hydrodynamic boundary-value problem of a ship oscillating at the free surface, strip theory has long been used under the assumption of the slenderness of the geometry. Another important assumption concerns the size of the wave length relative to a characteristic ship dimension, for example, the ship's beam. This leads to the short wave assumption that the wave length should be asymptotically small, of the same order of magnitude as the ship's beam. This is discussed in depth by Ogilvie (1974).

Since the introduction of the strip theory by Korvin-Kroukovsky and Jacobs (1957), various forms of strip theory have been proposed for the ship motion problem. Ogilvie and Tuck (1969) derived a more rational strip theory based on systematic perturbation analysis. Strip theory has been identified as a special case of the slender body theory which requires that the frequency of oscillation be large, $O(1/\sqrt{\varepsilon})$ where ε is the small slenderness parameter. Salvesen, Tuck, and Faltinsen (1970) derived a new strip theory which satisfies the Timman-Newman symmetry condition and provides correction terms for a transom stern.

None of these strip theories is based on a complete solution of the 3-D boundary - value problem, although some of the theories introduce the strip assumption at a later stage to minimize the effects of the 2-D assumptions. In particular, these strip theories are believed to fail near the ends, where the slenderness assumption is no longer valid. 3-D effects have not been fully investigated previously.

The purpose of this thesis is to investigate these 3-D effects and try to develop new methods of calculation that do not contain the usual errors of the strip theory. To do so, we must begin with some simpler problems. The 3-D effect

on the added mass without the presence of free surface is investigated first. Next, the 3-D effect in the presence of the free surface is studied to determine the hydrodynamic coefficients and exciting forces for a head sea. The irregular frequency phenomena of the integral equation is investigated, and a new method to cure the irregular frequency phenomena is developed by modifying the fundamental Green's function.

A. 2-D Free Surface Problem

Two methods are available to deal with the 2-D free surface problem: a multipole-expansion method and an integral-equation method.

Ursell (1949) solved the radiation problem for a heaving circular cylinder using multipole expansion method. The potential is represented by the sum of the multipole potentials. The coefficients of the multipoles are determined by satisfying the boundary condition on a circle. Tasai (1959) and Porter (1960) extended Ursell's method to non-circular cylinders.

Frank (1967) developed a completely different method, the integral equation method. He assumed that the potential could be represented by a distribution of the 2-D wave sources over the contour of the section. The unknown source strength is determined by satisfying the boundary condition at the midpoint of the segments of the section. Frank's method can be applied to a section of arbitrary shape.

The integral equation method has a defect, however: it breaks down at and near a set of discrete eigenfrequencies of the complementary interior flow. John (1950) was the first to show the existence of the phenomenon. Several researchers have proposed remedies.

Ursell (1953) developed an iteration method by modifying the fundamental Green's function to derive a convergent solution for all frequencies. He failed to mention, however, that his method overcame the difficulty because of the existence of the interior resonance. Paulling and Wood (1972)

suggested that the interior resonance could be removed by putting a lid on the free surface inside the body. Ohmatsu (1975) relieved the condition by showing that the boundary condition on the lid could be an arbitrary Neumann condition. Sayer and Ursell (1977) extended Ursell's previous work to overcome the numerical difficulty at the eigenfrequencies by modifying the fundamental Green's function. Ogilvie and Shin (1978) developed a more general method to remove the difficulty near the eigenfrequencies by choosing the proper form of modified Green's function. The fundamental form of the Green's function was modified by adding a point source at the origin. Consequently, the new form of the integral equation was obtained, and the irregular frequency phenomena were removed.

B. 3-D Infinite Fluid Problem

Lewis (1929) computed exactly the added mass of a vibrating spheroid by the method of the separation of variables in spheroidal coordinates. He devised the J factor, which represents the 3-D effect on added mass.

Hess and Smith (1962) solved the three-dimensional, infinite fluid problem for an arbitrary body in steady motion by solving the Fredholm integral equation of the second kind.

In this thesis, the boundary value problem for the oscillation problem is solved using the integral equation method by source distribution. The three-dimensional effect on the added mass is investigated for several 3-D bodies. An approximation method is developed using the two-dimensional source density as a first approximation.

C. 3-D Free Surface Problem

1. 3-D radiation problem

The formulation of the appropriate three-dimensional boundary value problem is simple and straightforward. The solution to the problem is, however, very difficult to obtain, in general. Thus, only a few cases have been solved

for bodies of simple geometry. There are two possible numerical methods which can be used for this problem: the multipole-expansion method and the integral-equation method. Recently the finite element method has been under development for the problem. It is premature to say which method is best. In general, we could say that the integral equation method is preferred for the arbitrary body oscillating periodically in a uniform depth of water.

a. Multipole expansion method

For the three-dimensional case with a free surface, Havelock (1955) was the first to solve the problem for the simple geometric body of the heaving sphere using the multipole expansion method. The velocity potential is represented by a set of higher order singularities which satisfy the free surface condition and radiation condition trivially, and a wave source or multipole at the origin within the body which satisfies the radiation condition. The unknown coefficients for the polynomials and the wave source or multipole are determined to satisfy the kinematic boundary condition on the hull. The linear algebraic equations for the unknown coefficients are solved numerically.

Barakat (1962) and Wang (1966) used a similar method for the case of the heaving sphere in a finite uniform depth.

b. Integral equation method

Various forms of Fredholm integral equations can be derived by using sources or dipoles, or by using both sources and dipoles from Green's theorem. The unknown density of singularity is determined by satisfying the kinematic boundary condition on the hull. In general, the Fredholm integral equation of the second kind is preferred over the first kind for numerical computation. Kim (1966) solved the integral equation of the second kind by using sources for the unsteady problem of the semi-spheroid oscillating at the free surface. Milgram and Halkyard (1971) solved the integral equation derived from Green's theorem by the successive approximation

method and by the linear algebraic equation method for the wave-exciting forces. Yeung (1973) solved the 3-D radiation problem by distributing wave-free sources over the entire surface of the fluid domain, such as free surface and surface at infinity, in addition to hull surface. This leads to much larger surfaces over which source density must be determined, even though the Green's function is much simpler than the wave source. Faltinsen and Michelsen (1974) followed the integral equation method using source distribution to compute the added mass and damping coefficient for large, three-dimensional offshore structures.

The integral equation method for the three-dimensional boundary value problem with free surface is complicated and time consuming. The method requires large storage space and computing time, since it involves a large number of computations for the complicated kernel and the large size of the linear algebraic equation. In the past, the three-dimensional method was not practical since computers did not have adequate computing speed and fast-access memory. However, the advent of the new generation of modern computer would make the method more practical.

The integral equation method has an inherent disadvantage over the other methods. It fails at an infinite number of discrete resonance frequencies of the complementary interior flow similarly to the 2-D free surface problem. A new method has been developed to cure the irregular frequency phenomena of the integral equation for the 3-D free surface problem. The fundamental Green's function has been modified by adding a line of sources at the free surface on the center plane. A similar interior resonance problem has been studied in acoustics by Chertock (1964, 1970), Brundrit (1965), Copley (1968), Schenck (1968), Ursell (1973), Kleinman and Roach (1974), and Jones (1974).

The integral equation by using source distribution can be solved by several approximation methods: linear algebraic equations, successive approximation by Neumann series, or frequency iteration method. The iteration methods do not

converge for all wave frequencies, however: for low wave frequency, Milgram and Halkyard (1971) have shown the successive approximation method does not converge. This occurs because the largest reciprocal eigenvalue of the kernel matrix is beyond the radius of convergence of the unit circle. This difficulty can be removed by increasing the radius of convergence using a new sequence constructed by Buckner (1948). Several other versions of the iterative methods have been developed by Wagner (1951), Samuelson (1953), Rall (1955), Petryshyn (1963), and Chertock (1968).

2. Wave excitation

In order to compute the exciting forces caused by waves, one must determine the diffracted-wave potential resulting from the presence of the ship. The boundary-value problem for the diffraction potential is, however, very difficult to solve for an arbitrary body. To avoid the difficulty of the diffraction problem, several approximation methods have been developed.

a. Strip theory

Korvin-Kroukovsky and Jacobs (1957) devised an artificial concept of the so-called relative-motion hypothesis of the 2-D strip. Consequently, they computed the sectional wave forces using the sectional added mass and damping. Although not mathematically justified, the results have shown good agreement with the experiments.

b. Haskind method and new strip theory

Haskind (1957) and Newman (1962) derived a formula by applying Green's theorem to compute the total forces without solving the direct diffraction problem. The great advantage of the formula is that the forced motion potential can be used to compute the wave-exciting forces without introducing the artifical concept of relative motion. Thus, it is not necessary to solve the additional boundary value problem for the diffraction problem. Furthermore, the 2-D strip version of the Kaskind method is derived by making the slenderness

assumption of the ship's geometry. By replacing the integrand of Haskind formula with the sectional added mass and damping coefficients, Salvesen, Tuck, and Faltinsen (1971) derived the new strip theory.

c. Direct diffraction problem

If one wants to solve the diffraction problem, there are special problems with the head sea. Faltinsen (1971) solved the head sea diffraction problem for short waves by the matched asymptotic expansion method. His results show that the wave amplitude attenuates as the wave moves along the ship. He concluded that his results agreed well with experiments for short waves ($\lambda/L=0.5$), but not for longer waves ($\lambda/L=0.75$). Maruo and Sasaki (1974) extended Faltinsen's theory for the head sea diffraction problem by including a higher order term.

The author solves the direct 3-D diffraction problem without making the usual assumptions of slenderness and high frequency wave. Therefore the 3-D effect is included in the 3-D direct solution. The results by 3-D theory are compared with Faltinsen's results. The 3-D effect on the wave exciting forces are also investigated.

II. FORMULATION OF THE BOUNDARY-VALUE PROBLEM

A. Assumptions

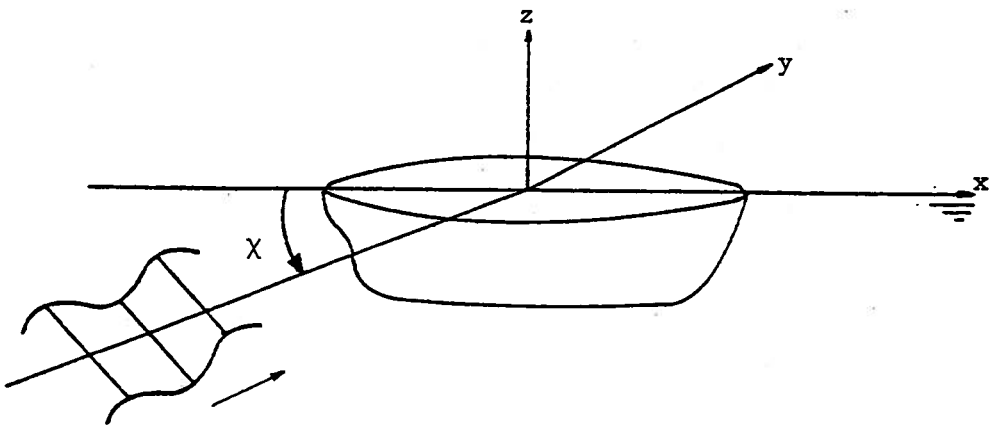

Figure 1. 3-D coordinate system and wave heading angle

Consider a ship oscillating in sinusoidal regular waves with the heading angle χ with respect to the negative x axis. It is assumed that the ship has no forward speed. The right-handed Cartesian coordinate system is used as shown in Figure 1. The origin of the coordinate system is fixed at the mean midship position in the undisturbed free surface. Positive x is to the bow, positive y is to port and positive z is vertically upwards. The plane z=0 represents the undisturbed free surface.

The following assumptions are used throughout the paper:

(i) The fluid is inviscid and incompressible, and the flow is irrotational. Thus a velocity potential exists in the fluid domain. The boundary-value problem can be formulated in terms of the velocity potential.

(ii) The waves have small amplitude. Linear free-surface wave theory will be used. The surface tension also is neglected.

(iii) The resulting motion of the ship is small. The hydrodynamic problem can be linearized with respect to a small-motion parameter.

The total hydrodynamic problem can be separated into a problem of wave excitation on the restrained body and the resulting forced motion due to the excitation. The hydrodynamic forces on the ship due to its own motion are computed without the incident waves (in calm water).

The total velocity potential is decomposed into one associated with the wave system and one due to the forced motion of the ship. We can write*:

$$\Phi(x,y,z) = \Phi_0 + \Phi_7 + \Sigma\ \Phi_i \quad , \tag{1}$$

where

Φ_0 is the complex amplitude of the incident-wave potential,

Φ_7 is the complex amplitude of the diffracted-wave potential,

Φ_i is the complex amplitude of the velocity potential due to forced motion in the i-th mode.

B. Radiation Problem

Consider a ship forced to oscillate periodically with frequency of oscillation ω. The motion is described by

$$a_i(t) = \mathrm{Re}\{a_i\ e^{i\omega t}\} \quad , \tag{2}$$

where a_i is the complex amplitude of the motion in i-th mode.

Then the complex velocity potential due to the forced motion in the i-th mode, $\Phi_i(x,y,z)$, satisfies the 3-D Laplace equation,

$$\left(\frac{\partial^2}{\partial x^2} + \frac{\partial^2}{\partial y^2} + \frac{\partial^2}{\partial z^2}\right)\Phi_i(x,y,z) = 0 \quad , \tag{3}$$

in the region exterior to the ship.

---

* It should be noted that the velocity potential corresponds to the real part of $\Phi(x,y,z)e^{i\omega t}$. Time factor $e^{i\omega t}$ will be suppressed unless otherwise specified.

It also satisfies the free surface conditions. The kinematic free surface condition is

$$\frac{\partial \Phi_i}{\partial x}\frac{\partial \eta}{\partial x} + \frac{\partial \Phi_i}{\partial y}\frac{\partial \eta}{\partial y} - \frac{\partial \Phi_i}{\partial z} + i\omega\eta = 0 \quad \text{on } z=\eta(x,y) \quad . \tag{4}$$

The dynamic free surface condition is derived from the Bernoulli equation,

$$g\eta + i\omega\Phi_i + \frac{1}{2}|\nabla\Phi_j|^2 = 0 \quad \text{on } z=\eta(x,y) \quad , \tag{5}$$

where g is the gravitational acceleration.

Combining the kinematic and dynamic free surface conditions, we get a linearized free surface condition for zero forward speed.

$$\frac{\partial \Phi_i}{\partial z} - \nu\Phi_i = 0 \quad \text{on } z = 0 \quad , \tag{6}$$

where

$$\nu = \frac{\omega^2}{g} \quad .$$

The potential also should satisfy the bottom boundary condition.

At a large distance from the body, the wave should travel outward, which gives a radiation condition,

$$\lim_{R\to\infty} \sqrt{R}\left(\frac{\partial \Phi_i}{\partial R} + i\nu\Phi_i\right) = 0 \quad , \tag{7}$$

where

$$R = \sqrt{x^2+y^2} \quad .$$

The radiation condition is needed to make the solution unique.

The velocity potential should satisfy the kinematic boundary condition on the mean position of the ship,

$$\frac{\partial \Phi_i}{\partial n} = i\,\omega\,a_i\,n_i \quad , \tag{8}$$

where n_i is the generalized normal for the i-th mode of motion.

Let us redefine the velocity potential to derive a non-dimensional form of the hull boundary condition:

$$\Phi_i(x,y,z) = i\,\omega\,a_i\;\phi_i(x,y,z) \quad . \tag{9}$$

Then the hull boundary condition becomes

$$\frac{\partial \phi_i(x,y,z)}{\partial n} = n_i \quad \text{on the hull} \quad . \tag{10}$$

The other conditions are unchanged if Φ_i is replaced by ϕ_i.

Once the forced motion potential is computed from the boundary value problem, the hydrodynamic coefficients (added mass and damping) in the equations of the motion are computed independently of the wave exciting forces.

C. Diffraction Problem

The velocity potential for the diffracted waves is computed as if the ship were restrained from moving. The diffracted-wave potential should satisfy the 3-D Laplace equation (3), the free surface condition (6), and the radiation condition (7), as does the radiation potential except for the hull boundary condition.

Since the ship is assumed to be restrained, the boundary condition on the hull becomes

$$\frac{\partial \Phi_7}{\partial n} = -\frac{\partial \Phi_0}{\partial n} \quad , \tag{11}$$

where the incident wave potential is given by

$$\Phi_0 = \frac{igh}{\omega} e^{\nu z}\, e^{-i(\nu x \cos\chi + \nu y \sin\chi)} \quad . \tag{12}$$

Once the diffracted wave potential is computed from the boundary value problem,(3), (6), (7), and (11), the wave pressure distribution and exciting forces on the restrained ship can be computed from the incident-wave potential and diffracted-wave potential.

D. Method of Solution by Various Integral Equations

The exterior Neumann problem for the three dimensional unsteady water-wave problem can be solved by integral equation methods. There are at least four different ways to formulate the integral equation:

i) integral equation of the second kind, by using sources,
ii) integral equation of the first kind, by using dipoles,
iii) integral equation of the second kind from Green's theorem (Helmholz representation in acoustics),
iv) integral equation of the first kind from Green's theorem.

We can get an integral equation either of the first kind or of the second kind. In general, it is easier to solve the second kind than the first kind. The integral equation of the second kind usually has the dominating diagonal terms in the influence matrix, and so the solution is more stable than the first kind for the numerical computation.

We can get two different forms of the Fredholm integral equation of the second kind, one by using a source distribution and the other from Green's theorem. The kernel matrices of these two integral equations are transposes of each other.

1. Integral equation of the second kind by using sources

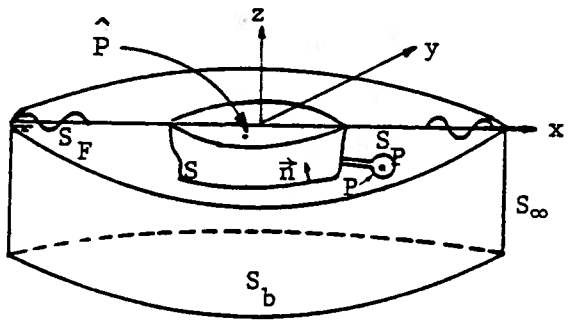

Figure 2. Exterior Neumann problem by using sources

Let us apply Green's theorem to the exterior flow[†]:

$$\iint_{\Sigma S}\left[\bar{\phi}_i(Q)\frac{\partial G}{\partial n_Q}(P,Q)-\frac{\partial \phi_i}{\partial n_Q}G(P,Q)\right]dS(Q)=\iiint_{V}\left[\bar{\phi}_i(Q)\nabla_Q^2 G(P,Q)-G\nabla_Q^2\phi_i\right]dV, \tag{13}$$

where Green's function, $G(P,Q)$, represents the potential at field point $P(x,y,z)$ due to a source of strength -4π at point $Q(\xi,\eta,\zeta)$:

$$G(x,y,z;\xi,\eta,\zeta)=\frac{1}{r}+\frac{1}{r^*}+2\nu e^{\nu z}\int_{-\infty}^{z}\frac{e^{-\nu w}dw}{\sqrt{(x-\xi)^2+(y-\eta)^2+(w+\zeta)^2}}$$

$$-2\pi i\,\nu\, e^{\nu(z+\zeta)}H_0^{(2)}(\nu R) \tag{14}$$

where

$$r=\sqrt{(x-\xi)^2+(y-\eta)^2+(z-\zeta)^2}\ ;$$

$$r^*=\sqrt{(x-\xi)^2+(y-\eta)^2+(z+\zeta)^2}\ ;$$

$$R=\sqrt{(x-\xi)^2+(y-\eta)^2}\ .$$

(Various forms of the Green's functions are derived in Appendix A.) ΣS represents all the bounding surfaces, that is, hull, free surface, surface at infinity, bottom surface, and control surface around P.

Since ϕ and G are harmonic in V, the volume integral in the right hand side becomes zero. Furthermore the surface integrals over the free surface and the surfaces at infinity and bottom do not give any contribution because of cancellation, since G satisfies the same boundary conditions on those surfaces as ϕ (radiation and diffraction potential only).

[†]Since we are employing linear theory throughout the paper, subscript i of ϕ_i and Φ_i will be deleted. Φ and ϕ imply Φ_i and ϕ_i, respectively unless otherwise specified.

However, the integral over the small sphere isolating the singularity gives, in the limit as its radius approaches zero,

$$\lim \iint_{S_P} \left[\bar{\phi}(Q) \frac{\partial G}{\partial n_Q}(P,Q) - \frac{\partial \phi}{\partial n_Q} G(P,Q) \right] dS(Q) = 4\pi\phi(P) \quad . \qquad (15)$$

Note that only the first integrand gives $4\pi\phi$, since the second integrand does not contribute to the integral.

Thus we can represent the potential by sources and dipoles only over the hull surface,

$$\phi(P) = -\frac{1}{4\pi} \iint_S \left[\bar{\phi}(Q) \frac{\partial G}{\partial n_Q}(P,Q) - \frac{\partial \phi}{\partial n_Q} G(P,Q) \right] dS(Q) \, . \qquad (16)$$

We can also formulate a complementary interior problem similarly: Let $\hat{\phi}(\hat{P})$ be a solution of the 3-D Laplace equation for $\hat{P}$ inside S , satisfying the free surface condition. Note that the radiation condition cannot be applied to the interior flow. Keeping the same sign of $\vec{n}$, we get a similar expression from Green's theorem,

$$\hat{\phi}(\hat{P}) = \frac{1}{4\pi} \iint_S \left[\bar{\hat{\phi}}(Q) \frac{\partial G}{\partial n_Q}(\hat{P},Q) - \frac{\partial \hat{\phi}}{\partial n_Q} G(\hat{P},Q) \right] dS(Q) \quad . \qquad (17)$$

We can also apply Green's theorem to $\hat{\phi}(Q)$ and $G(P,Q)$ for P outside of S. Since both functions are harmonic inside S , we get

$$0 = \frac{1}{4\pi} \iint \left[\bar{\hat{\phi}}(Q) \frac{\partial G}{\partial n_Q}(P,Q) - \frac{\partial \hat{\phi}}{\partial n_Q} G(P,Q) \right] dS(Q) \quad . \qquad (18)$$

By adding (16) and (18) together, we get

$$\phi(P) = -\frac{1}{4\pi} \iint_S \left[\{\bar{\phi}(Q) - \bar{\hat{\phi}}(Q)\} \frac{\partial G}{\partial n_Q}(P,Q) + G(P,Q) \{ \frac{\partial \hat{\phi}}{\partial n_Q} - \frac{\partial \phi}{\partial n_Q} \} \right] dS(Q) \, . \qquad (19)$$

The velocity potential is represented by sources and dipoles distributed over the hull surface S. Further, if we specify that

$$\phi(Q) = \hat{\phi}(Q) \qquad \text{for} \quad Q \quad \text{on} \quad S \ , \tag{20}$$

then we can represent the potential solely by the distribution of sources of density $\sigma(Q)$ on the surface S:

$$\phi(P) = -\frac{1}{4\pi} \iint_S \sigma(Q)\ G(P,Q)\,dS(Q) \quad , \tag{21}$$

where

$$\sigma(Q) = \frac{\partial \hat{\phi}}{\partial n_Q}(Q) - \frac{\partial \phi}{\partial n_Q}(Q) \quad . \tag{22}$$

Since the Green's function satisfies the Laplace equation, free surface condition, and radiation condition at infinity, the velocity potential automatically satisfies those three conditions of the boundary-value problem. The remaining condition is the hull boundary condition. Therefore the source density in the integral representation must be determined so that the given hull boundary condition is satisfied. By applying the boundary condition on the hull, we get the Fredholm integral equation of the second kind,

$$-\frac{\sigma(P)}{2} - \frac{1}{4\pi} \iint\limits_S \sigma(Q)\ \frac{\partial G}{\partial n_P}(P,Q)\ dS(Q) = f(P)^* \ . \tag{23}$$

*It should be noted that the right hand side of the integral equation is defined as

$$\begin{aligned} f(P) &= n_i(P) \quad \text{for radiation problem} \\ f(P) &= -\partial \Phi_0 / \partial n\ (P) \quad \text{for diffraction problem,} \end{aligned} \tag{24}$$

henceforth unless otherwise specified. The bar through the integral signs denotes that a principal value interpretation should be made.

We can solve the two dimensional Fredholm integral equation of the second kind approximately by various methods. These methods will be discussed in detail in later sections.

2. Integral equation of the first kind by dipole

If we specify that, in the equation (19),

$$\frac{\partial \hat{\phi}}{\partial n_Q}(Q) = \frac{\partial \phi}{\partial n_Q}(Q) \qquad \text{for } Q \text{ on } S \,, \tag{25}$$

then we can represent the potential only by the distribution of the dipoles of density $\mu(Q)$ on the surface S

$$\phi(P) = -\frac{1}{4\pi} \iint \mu(Q) \frac{\partial G}{\partial n_Q}(P,Q)\, dS(Q) \,, \tag{26}$$

where

$$\mu(Q) = \phi(Q) - \hat{\phi}(Q) \,. \tag{27}$$

By applying the boundary condition on the hull we get an integral equation of the first kind,

$$-\frac{1}{4\pi} \frac{\partial}{\partial n_P} \iint_S \mu(Q) \frac{\partial G(P,Q)}{\partial n_Q}\, dS(Q) = f(P) \,. \tag{28}$$

3. Integral equation of the second kind from Green's theorem (Helmholz representation in acoustics)

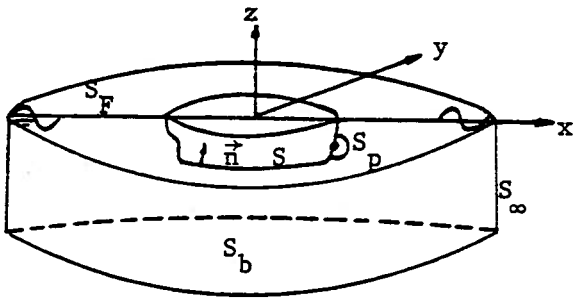

Figure 3. Exterior Neumann problem by using sources and dipoles

Let us apply Green's theorem to the exterior region with field point P(x,y,z) on S. Since ϕ and G are harmonic in V, we get

$$\iint_{\Sigma S} \left[\phi(Q)\frac{\partial G}{\partial n_Q}(P,Q) - \frac{\partial \phi}{\partial n_Q} G(P,Q)\right] dS(Q) = 0 \; , \qquad (29)$$

The surface integrals over the free surface and the surfaces at infinity and bottom drop out because of cancellation. The integral over the small hemisphere, S_P, is

$$\iint_{S_P} \left[\phi(Q)\frac{\partial G}{\partial n_Q}(P,Q) - \frac{\partial \phi}{\partial n_Q} G(P,Q)\right] dS(Q) = 2\pi\phi(P) \quad . \qquad (30)$$

Note that the second integral does not contribute. Substitution of the equation (30) into equation (29) yields the integral equation of the second kind with unknown ϕ on S,

$$\frac{\phi(P)}{2} + \frac{1}{4\pi} \iint_S \phi(Q) \frac{\partial G}{\partial n_Q}(P,Q) = \frac{1}{4\pi} \iint_S G(P,Q) \frac{\partial \phi}{\partial n_Q} dS(Q) \; . \qquad (31)$$

The right hand side is known from the given hull boundary condition. It is interesting to note that the operator of integral equation (31) is the transpose of the operator of integral equation (23) by using source distribution. It will be shown in section II-E that both operators have the same eigenfrequency.

4. Integral equation of the first kind from Green's theorem

Alternatively, we can get another form of the integral equation from Green's theorem for the exterior Neumann problem. Differentiating ϕ with respect to the normal at point P in equation (31) and substituting hull boundary condition(24), we get the integral equation of the first kind,

$$\frac{1}{4\pi} \iint_S \phi(Q) \frac{\partial}{\partial n_P} \frac{\partial G}{\partial n_Q}(P,Q) dS(Q) = -\frac{1}{2} f(P) + \frac{1}{4\pi} \iint_S \frac{\partial G}{\partial n_P}(P,Q) f(Q) dS(Q) \; . \qquad (32)$$

The integral in the left hand side is worse than just improper. Burton and Miller (1971) proposed a method to deal with the non-integrable singular kernel.

E. Irregular Frequency Phenomenon

John (1950) showed that the integral-equation (23) by source distribution has numerical difficulty at the eigen-frequency of the interior Dirichlet problem. It can be considered that the integral equation (31) derived directly from Green's theorem is more general in the sense that no assumption about the interior flow has been made. In fact, we have not defined the interior flow in the derivation of equation (31). However, this alternative form of integral equation also has the same difficulty at those eigenfrequencies of the interior Dirichlet problem. This will be discussed in more detail in later sections II-E and III-B.

It can be shown that the operator of the integral equation for the interior Dirichlet problem is identical to that of the integral equation (23) by sources for the exterior Neumann problem.

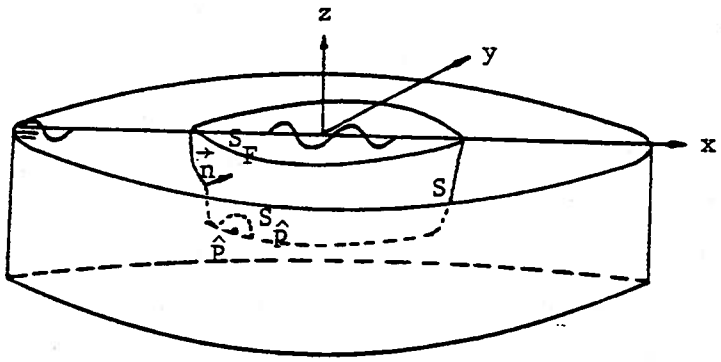

Figure 4. Interior Dirichlet problem

Applying Green's theorem to the interior flow with field point $\hat{P}(x,y,z)$ on the surface S, we get

$$\iint_{S+S_{\hat{P}}+S_F} \left[\hat{\phi}(Q)\frac{\partial G}{\partial n_Q}(\hat{P},Q) - \frac{\partial \hat{\phi}}{\partial n_Q}(Q)\,G(\hat{P},Q)\right] dS(Q) = 0 \quad \text{for } \hat{P} \text{ on } S. \tag{33}$$

The integral over the free surface vanishes since $\hat{\phi}$ and G satisfy the same free surface condition. The integral around the hemisphere, S_P, gives $-2\pi\hat{\phi}(\hat{P})$ with the same sign of $\vec{n}$. Thus, we get directly the integral equation of the first kind with unknown $\partial\hat{\phi}/\partial n_Q$,

$$\iint_S \frac{\partial\hat{\phi}}{\partial n_Q} G(\hat{P},Q)\,dS(Q) = -2\pi\hat{\phi}(\hat{P}) + \iint_S \hat{\phi}(Q)\,\frac{\partial G}{\partial n_Q}(\hat{P},Q)\,dS(Q) \quad . \tag{34}$$

In order to get the integral equation of the second kind, let us differentiate $\hat{\phi}$ with respect to the normal vector at $\hat{P}(x,y,z)$ on S. Then we get the integral equation of the second kind with unknown normal velocity:

$$-\frac{1}{2}\frac{\partial\hat{\phi}}{\partial n_P} - \frac{1}{4\pi}\iint_S \frac{\partial\hat{\phi}}{\partial n_Q}\,\frac{\partial G}{\partial n_P}(\hat{P},Q)\,dS(Q) = -\frac{1}{4\pi}\iint_S \hat{\phi}\,\frac{\partial}{\partial n_P}\,\frac{\partial G}{\partial n_Q}(\hat{P},Q)\,dS(Q) \quad . \tag{35}$$

The right hand side is known since $\hat{\phi}$ is known. The left hand side is identical to that of the integral equation (23) for the exterior Neumann problem by source distribution. If the homogeneous equation corresponding to (35) has a non-trivial solution, the integral equation (35) for the interior Dirichlet problem does not have a unique solution, nor does the integral equation (23) by source distribution for the exterior Neumann problem.

The integral equation method for the exterior Neumann problem has been widely used in other field of wave problem, especially in acoustics. Many authors, such as Chertock (1964), Brundrit (1965), Copley (1968) and Schenck (1968), considered the exterior Neumann problem for the 3-D Helmholz equation and pointed out that both the integral-equation methods by source distribution and Helmholz representation are inadequate near the interior eigenfrequency. Kleinman and Roach (1974) discussed the relationship between various cases of the integral equation of the interior and exterior Dirichlet problems and Neumann problem for the three dimensional Helmholz equation.

F. Existence and Uniqueness Theorem

The integral equation by source distribution , (23), is rewritten as

$$\sigma(P) - \tau K(\sigma) = -2\, f(P) \ , \tag{36}$$

where K denotes an operator or kernel matrix of the integral equation, which is defined as

$$K(\sigma) = -\frac{1}{2\pi} \iint_S \sigma(Q)\, \frac{\partial G}{\partial n_P}(P,Q)\, dS(Q) \ . \tag{37}$$

$-\tau$ is taken to conform to the standard form of $(I-\tau K)$, where I is the identity matrix. Mikhlin (1960) gives the derivation of the adjoint integral equation. It is given by

$$\sigma(P) - \bar{\tau} K^*(\sigma) = -2\, f(P) \ , \tag{38}$$

where K^* , the adjoint operator of K, is defined as

$$K^*(\sigma) = -\frac{1}{2\pi} \iint_S \sigma(Q) \frac{\overline{\partial G}}{\partial n_Q}(Q,P)\, dS(Q) \ . \tag{39}$$

The asterisk denotes the adjoint, and the bar denotes the complex conjugate. The complex conjugate of the adjoint operator is defined as

$$\bar{K}^*(\sigma) = -\frac{1}{2\pi} \iint_S \sigma(Q)\, \frac{\partial G}{\partial n_Q}(Q,P)\, dS(Q) \ . \tag{40}$$

This is the same operator of the integral equation (31) of the second kind derived directly from Green's theorem.

If the associated homogeneous equation of (36) has a non-trivial solution, τ is called the characteristic value of K, and $\phi(P)$ is called a characteristic function of K belonging to τ.

Theorem 1. If τ is not a characteristic value of K, the solution to the integral equation (36) is unique, as is its adjoint system. Both homogeneous equations have only trivial solutions.

(Corollary) If τ is a characteristic value of K, τ is also a characteristic value of $\bar{K}^*$ and $\bar{\tau}$ is a characteristic value of $\bar{K}$ and K^*.

When τ is one of the characteristic values of K, the solution of the integral equation (36) is not unique since we can add any homogeneous solutions to the particular solution. Furthermore, we can not compute the particular solution correctly due to numerical difficulty near the characteristic values.

Theorem 2. If τ is a characteristic value of K, then the inhomogeneous equation has a solution if and only if $f(P)$ is orthogonal to the every solution of the adjoint homogeneous equation:

$$\iint_S \sigma^*(Q)\ f(Q)\ dS(Q) = 0 \quad , \tag{41}$$

where

$$\sigma^* - \bar{\tau}K^*(\sigma^*) = 0 \quad .$$

The operator K also depends on the frequency of oscillation ω for the unsteady water wave problem. For each wave frequency, there is a set of characteristic values corresponding to K. Any wave-frequency that includes $\tau=1$ in its set of characteristic values is called an eigenfrequency or characteristic frequency.

Theorem 3. If the frequency of oscillation is that of the eigenfrequency of operator K, the homogeneous equation of (36) has a non-trivial solution, and solution of the integral equation is not unique. Furthermore, if τ is real, the eigenfrequency of operator K also is an eigenfrequency of K^*, $\bar{K}$, and $\bar{K}^*$.

Various forms of integral equations are derived in the previous section. All the integral equations of the second kind involve the operator K in some form or another. By Theorem 3, all the integral equations have the same eigen-

frequency of oscillation. Thus, all the integral equations fail to give unique solutions at the same eigenfrequencies.

From Theorem 1, the integral equation has a unique solution if τ is not any of the characteristic values of K. This condition implies only that the kernel matrix is invertible, since the determinant of the matrix is not singular. However, the condition does not guarantee that the iteration-method converges. A more restrictive condition should be satisfied to ensure convergence of the iteration-method. Petryshyn (1963) gives the following condition.

Theorem 4. (Convergence theorem of the iteration-method)

The integral equation (36) has a convergent and unique solution by successive iteration if any one of the following conditions is satisfied. The degree of restriction increases in the given order.

$$\text{(i)} \qquad \lim_n \sqrt[n]{\|K^n f\|} < 1 \quad , \tag{42}$$

$$\text{(ii)} \qquad \lim_n \sqrt[n]{\|K^n\|} < 1 \quad , \tag{43}$$

$$\text{(iii)} \qquad \|K\| < 1 \quad , \tag{44}$$

where $\|K\|$ denotes the norm of the operator which is defined by

$$\|K\| = \iint \left| \frac{\partial G(P,Q)}{\partial n_P} \right|^2 dS(P)\, dS(Q)$$

The following equalities hold:

$$\lim_n \sqrt[n]{\|K^n f\|} \leq \lim_n \sqrt[n]{\|K^n\|} \leq \|K\| \quad . \tag{45}$$

Condition (ii) is equivalent to a more practical condition that the maximum reciprocal characteristic value, $\gamma_{max}\left(\frac{1}{\tau_{min}}\right)$, is less than 1. Condition (iii) is equivalent to more practical condition that the maximum singular

value* is less than 1. Conditions (ii) and (iii) become identical for the symmetric operator in Hermitian sense.

Singular value is the square root of the reciprocal characteristic value of [K][K].

III. 2-D FREE SURFACE PROBLEM

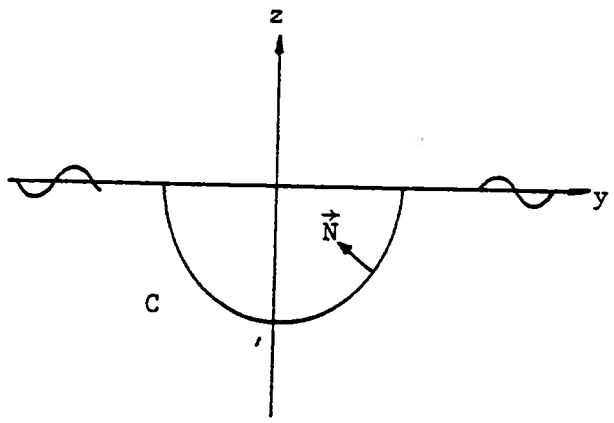

Figure 5. 2-D coordinate system

Many strip theories have been developed either heuristically or by systematic perturbation techniques. Even though some strip theories introduce strip assumptions at a later stage of derivation to minimize the effect of the 2-D assumptions, all the strip theories eventually lead to a 2-D boundary value problem for each section. In this chapter, a 2-D boundary value problem with the free surface is solved using the integral equation method* by 2-D wave source distribution. The irregular frequency phenomenon of the integral equation is corrected by a modified form of the Green's function.

A. Integral Equation Using the 2-D Wave Source

The boundary value problem for a 2-D oscillating body

*Integral equation refers to the Fredholm-type integral equation unless otherwise specified.

in calm water is formulated in terms of complex velocity potential $\phi_i(y,z)$. The 2-D velocity potential* should satisfy the following equation:

$$\frac{\partial^2 \phi_i}{\partial y^2} + \frac{\partial^2 \phi_i}{\partial z^2} = 0 \qquad \text{in the 2-D fluid region,}$$

$$\nu\phi_i - \frac{\partial \phi_i}{\partial z} = 0 \qquad \text{on } z = 0,$$

$$\lim_{z \to -\infty} \frac{\partial \phi_i}{\partial z} = 0 \qquad ,$$

$$\frac{\partial \phi_i}{\partial N} = N_i \qquad \text{on C,}$$

and the radiation condition which requires outgoing waves as $|y| \to \infty$.

The velocity potential can be represented by the distribution of the 2-D wave sources over the contour of the section:

$$\phi_i(P) = \frac{1}{2\pi}\int_C \sigma_i(Q)\, G(P,Q)\, d\ell(Q), \tag{46}$$

where 2-D Green's function is given by

$$G(y,z;\ \eta,\zeta) = \log\sqrt{(y-\eta)^2+(z-\zeta)^2} - \log\sqrt{(y-\eta)^2+(z+\zeta)^2}$$
$$-2\int_0^\infty \frac{e^{k(z+\zeta)}\cos k(y-\eta)\ dk}{k-\nu} - 2\pi i e^{\nu(z+\zeta)}\cos\ \nu(y-\eta). \tag{47}$$

The 2-D Green's function is derived from the 3-D Green's function in Appendix A. Since the 2-D Green's function satisfies the 2-D Laplace equation, free surface condition, and radiation condition, the velocity potential of (46) satisfies the same conditions. The unknown source density is determined so as to satisfy the 2-D kinematic boundary condition on the hull. The Fredholm integral equation of the second kind in terms of the complex source density is given by,

$$-\frac{\sigma_i(P)}{2} + \frac{1}{2\pi}\int_C \sigma_i(Q)\frac{\partial G(P,Q)}{\partial N_p} d\ell(Q) = N_i(P). \tag{48}$$

---

*The velocity potential is the normalized form of Φ_i by the relationship (9).

B. Irregular Frequency Phenomenon

The integral equation (48) by using the source distribution can be approximated by a set of the simultaneous linear algebraic equations which can be solved by matrix inversion. However, the integral equation fails to produce solutions at certain frequencies associated with the resonance of interior flow. At these eigenfrequencies, the determinant of the kernel matrix becomes singular. The solution of the integral equation cannot be computed at these eigenfrequencies of the interior flow (Theorem 3 in chapter II-E).

The Green's function can be modified by adding or subtracting a harmonic function which satisfies the radiation condition and free surface boundary condition. The singular nature of the Green's function is not changed. Ursell (1953) used a simple form of modified Green's function to compute the high frequency asymptotic solution of the integral equation from Green's theorem:

$$^{*}\tilde{G}(P,Q) = G(P,Q) - Ce^{\nu\zeta}\, e^{-i\nu b} G(P,O). \tag{49}$$

where G(P,Q) is the original Green's function, b is half beam, and O denotes the origin. Ursell determined the constant C specifically as 1/2, thus making the kernel small enough to yield the convergent solution by iteration method. This restriction turns out to be a weak one, however. Ogilvie and Shin (1978) proved that constant C can have a rather arbitrary magnitude. A more general form of the modified Green's function is given by

$$\tilde{G}(P,Q) = G(P,Q) - Ce^{\nu\zeta}\, e^{-i\nu|\eta|} G(P,O), \tag{50}$$

The modified Green's functions (49) and (50) do not satisfy the symmetry requirement of the Green's function. The symmetrical form of the modified G can be constructed in the following form:

$$\tilde{G}(P,Q) = G(P,Q) - \frac{C}{2\pi i} G(P,O)G(O,Q). \tag{51}$$

---

*$\tilde{G}$ denotes a modified Green's function.

The modification term G(P,O) represents a source at the origin. This modified Green's function (51) satisfies the requirements of the Green's function. The modification would not affect the potential in the exterior region. It would, however, change the magnitude of the source density on the hull.

The integral equation is solved by using the modified Green's function which removes the numerical difficulty at the eigenfrequency. The numerical result shows that the symmetry condition of the modified G is not very important. Any of the modified Green's functions (49), (50) and (51) can be used for the purpose. The eigenfrequencies of the 2-D rectangle can be predicted by the method of separation of variables. For the symmetrical mode (heave), the eigensolution is given by

$$\phi_n = \cos \frac{\gamma_n Y}{B} \sinh \gamma_n (z+T), \text{ where } n = 1,2,3,...$$

and $\gamma_n = \frac{(2n-1)\pi}{B}$, B is the beam, and T is the draft.

Note that 2-D coordinate system from Figure 5 is used.

The eigenfrequency of oscillation is given by

$$\frac{\omega_n^2 B}{2g} = \frac{(2n-1)\pi}{2} \coth \frac{(2n-1)\pi T}{B} .$$

For the anti-symmetrical mode (sway), the eigensolution is given by

$$\phi_n = \cos \frac{\mu_n Y}{B} \sinh \mu_n (z+T), \text{ where } n = 1,2,3,...$$

and $\mu_n = \frac{2n\pi}{B}$.

The eigenfrequency of oscillation is given by

$$\frac{\omega_n^2 B}{2g} = n\pi \coth \frac{2n\pi T}{B} .$$

Figure 6 shows that source density becomes very large at the irregular frequency. The source density should become infinite if we hit the exact irregular frequency. As a consequence, the pressure, added mass coefficient, and damping coeffcient blow up. If we modify the Green's function, we

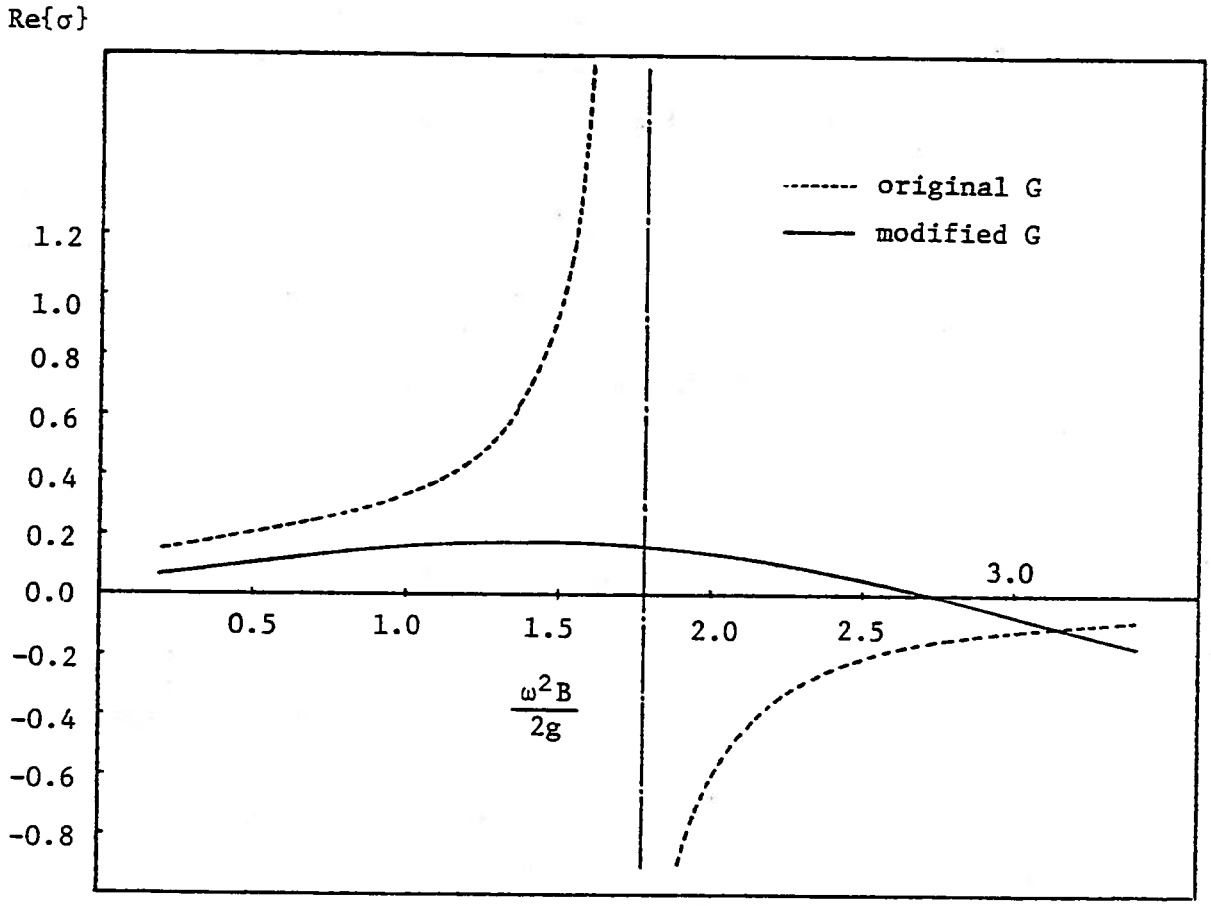

Figure 6. Source density at the free surface for the heaving rectangle

can solve the integral equation. Figure 6 also shows that the discontinuity in source density can be corrected by the modified Green's function.

C. Approximation Methods

Three different methods will be used to solve the integral equation (48): linear algebraic equation, successive approximation by Neumann series, and frequency iteration.

1. Linear algebraic equation method

Frank (1967) solved the 2-D boundary value problem by the method of source distribution over the contour. He divided the hull into segments of straight lines and assumed the source density to be constant over each segment. By applying the hull boundary condition at the midpoint of each segment, he got a set of simultaneous linear algebraic equations. This was solved by matrix inversion.

Troesch (1976) made the more reasonable assumption that source density varies linearly along the given segment. Thus, for him, the source density is a continuous function over the given section, while Frank's assumption gives jump in source density from segment to segment. The body boundary condition is applied at the nodal point of the section. These simultaneous linear algebraic equations for the unknown source density are solved by matrix inversion or lower and upper triangular decomposition method. In this paper, Troesch's method is employed.

2. Successive approximation by Neumann series

Let

$$\sigma = \Delta\sigma^{(1)} + \Delta\sigma^{(2)} + \Delta\sigma^{(3)} + \text{----} \ . \tag{52}$$

Substituting (52) into the integral equation (48) produces a series of source densities as follows:

$$\Delta\sigma^{(1)} = -2N_i \ , \tag{53}$$

and

$$\Delta\sigma^{(2)} = \frac{1}{\pi}\int_C \Delta\sigma^{(1)} \frac{\partial G(P,Q)}{\partial N_p} \, d\ell(Q) \ .$$

By induction, we get

$$\Delta\sigma^{(n)} = \frac{1}{\pi} \int_C \Delta\sigma^{(n-1)}(Q) \frac{\partial G}{\partial N_p}(P,Q) \, d\ell(Q) \quad . \tag{54}$$

In order to get the convergence of the iteration method, some bounded conditions on the kernel are required. This is presented in detail in section II-F. When the numerical calculation is performed by using the original form of the Green's function, the iterative solution does not converge at irregular frequencies as expected. By using the modified Green's function, however, the iterative solution converges very well. Even at irregular frequencies, the convergence is good. The rate of convergence is much faster for the high frequency of oscillation than for the low frequency.

3. Frequency iterative method

We can extend Ursell's (1953) high frequency asymptotic analysis to practical problems of finite frequency. The solution of the finite frequency case can be considered as the high frequency limit problem, with successive corrections of the frequency effect in accordance with the asymptotic analysis. Then we only need to solve a canonical problem corresponding to infinite frequency. When the problem is solved once, the same kernel matrix can be used iteratively to find successive corrections for free surface effect.

The Green's function consists of two parts: one for the infinite fluid and the other for the presence of the free surface boundary. By separating these parts of the Green's function, the integral equation (48) can be written as

$$-\frac{\sigma}{2} + \frac{1}{2\pi}\int_C \sigma \frac{\partial G^I}{\partial N} \, d\ell = N_i - \frac{1}{2\pi}\int_C \sigma \frac{\partial G^F}{\partial N} d\ell \quad , \tag{55}$$

where

$$G^I = \log\sqrt{(y-\eta)^2 + (z-\zeta)^2} - \log\sqrt{(y-\eta)^2 + (z+\zeta)^2} \quad ,$$

and $G^F = G - G^I$.

Assuming that there is an asymptotic series for σ and

that $\partial G^F/\partial N$ is of a higher order than $\partial G^I/\partial N$ for high frequency, we get a sequence of integral equations. As a first order approximation, we get

$$-\frac{\Delta\sigma^{(1)}}{2} + \frac{1}{2\pi}\int_C \Delta\sigma^{(1)} \frac{\partial G^I}{\partial N} d\ell = N_i \ . \tag{56}$$

This corresponds to the case of infinitely high frequency of oscillation. More precisely, it is the case of $\phi=0$ free surface condition. Equation (56) would be a good approximation for the vibration problem of extremely high frequency of oscillation. The free surface effect is taken into account in the higher order approximation. Thus, the second iteration is given by

$$-\frac{\Delta\sigma^{(2)}}{2} + \frac{1}{2\pi}\int_C \Delta\sigma^{(2)} \frac{\partial G^I}{\partial N} d\ell = -\frac{1}{2\pi}\int_C \Delta\sigma^{(1)} \frac{\partial G^F}{\partial N} d\ell \ . \tag{57}$$

The right-hand side of the integral equation (57) is known from the first iteration (56). The n-th iteration is given by

$$-\frac{\Delta\sigma^{(n)}}{2} + \frac{1}{2\pi}\int_C \Delta\sigma^{(n)} \frac{\partial G^I}{\partial N} d\ell = -\frac{1}{2\pi}\int_C \Delta\sigma^{(n-1)} \frac{\partial G^F}{\partial N} d\ell \ . \tag{58}$$

The kernel matrix of the integral equation (58) does not have eigenfrequencies. There is no resonance of the interior flow, since there is no free surface involved in the left-hand side. The free surface effect is reflected as a forcing term in the right-hand side of the equation. This can be interpreted as a corrective normal velocity resulting from the presence of a free surface. Similar to the successive approximation by Neumann series, this iterative method does not converge for all frequency ranges unless we modify the original form of the Green's function.

Figure 7 shows that the corrective normal velocity diverges by using the original Green's function. It also shows that the corrective normal velocity converges with the modified Green's function. Figure 8 shows that the velocity potential converges well when the modified Green's function is used for the heaving circle. Figure 9 shows that the iterative solution converges for the heaving rectangle.

$$V^{(n)} = -\frac{1}{2\pi}\int \Delta\sigma^{(n-1)} \frac{\partial G^F}{\partial n} d\ell$$

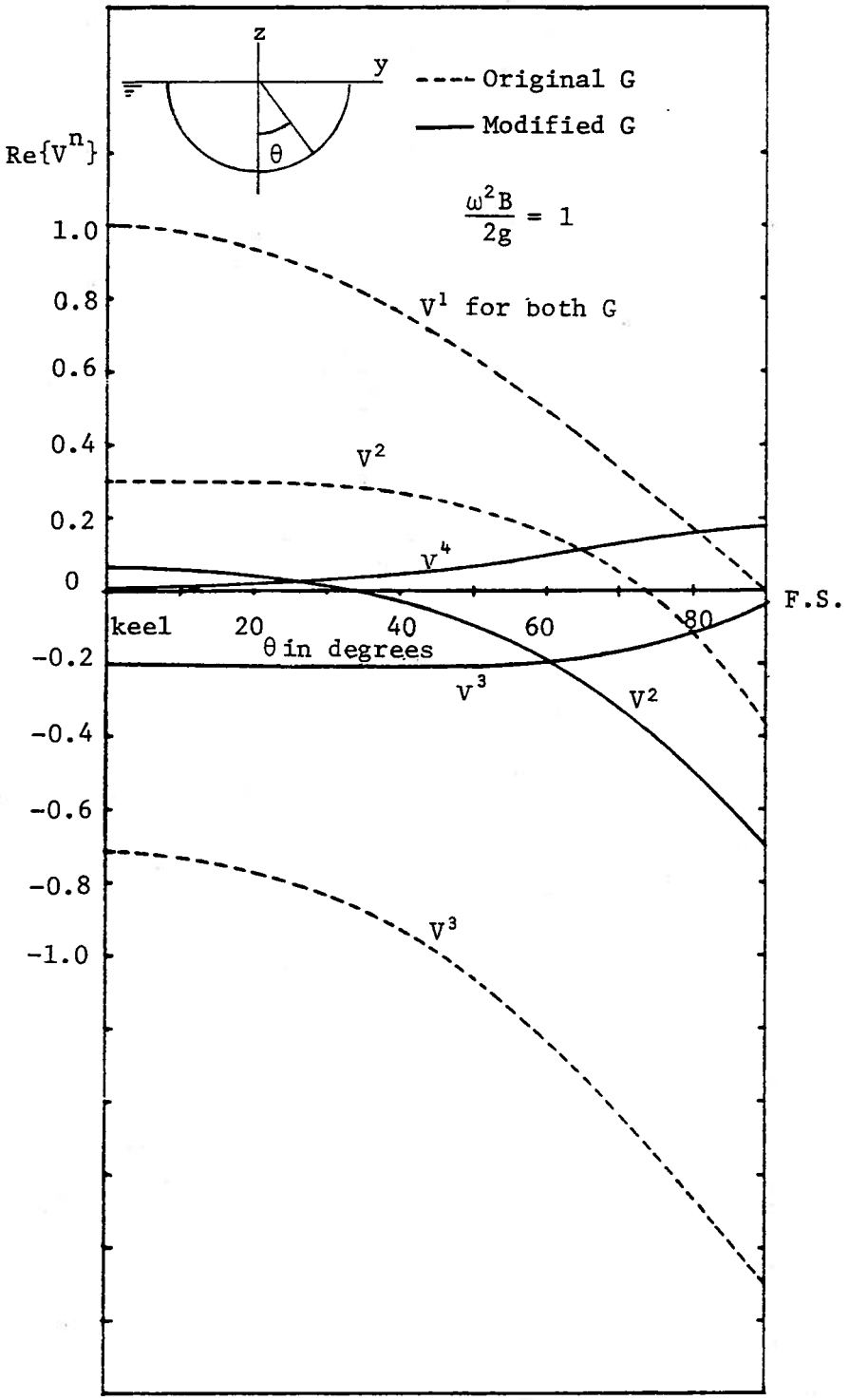

Figure 7. Corrective normal velocity for the heaving circle by the frequency iteration method

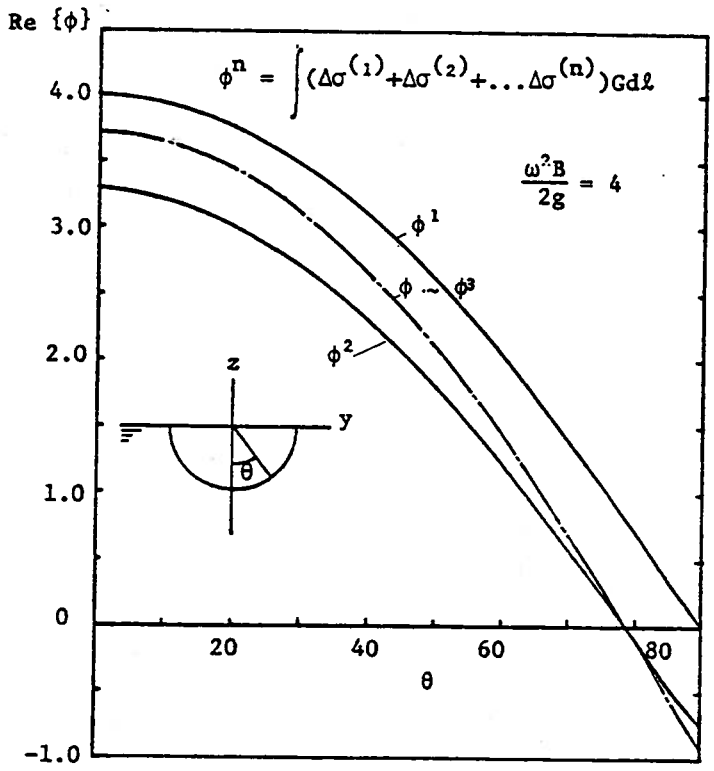

Figure 8. Iterative solution of the velocity potential for the heaving circle

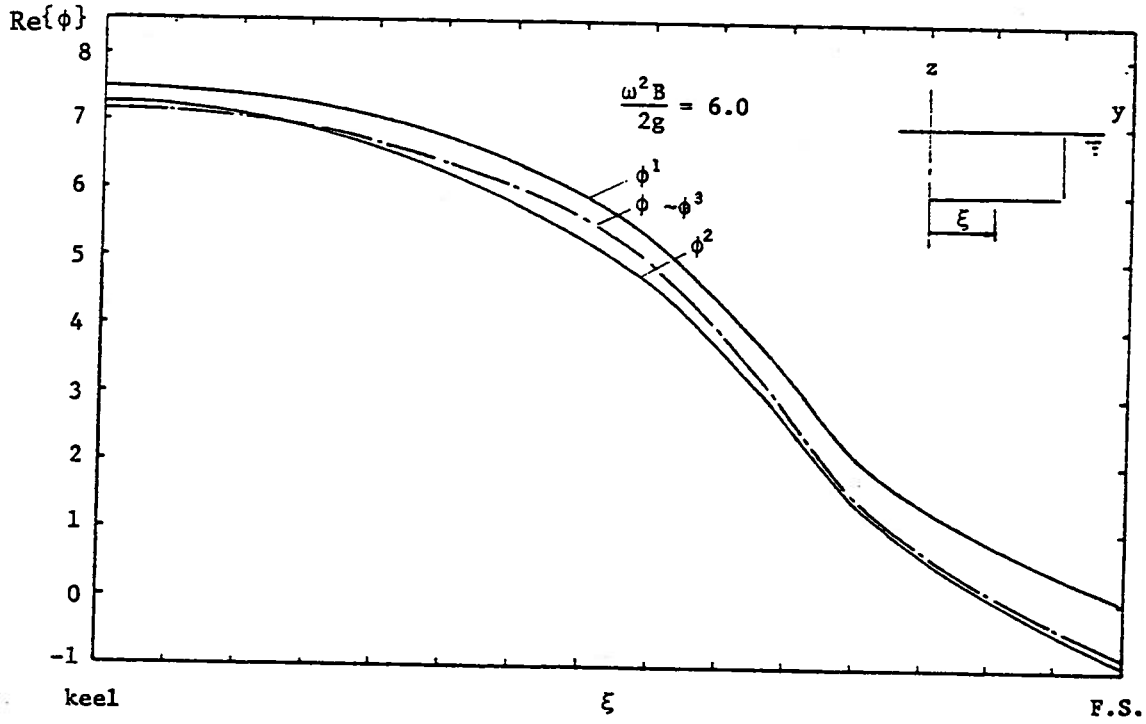

Figure 9. Iterative solution of the velocity potential for the heaving rectangle (B/T=4)

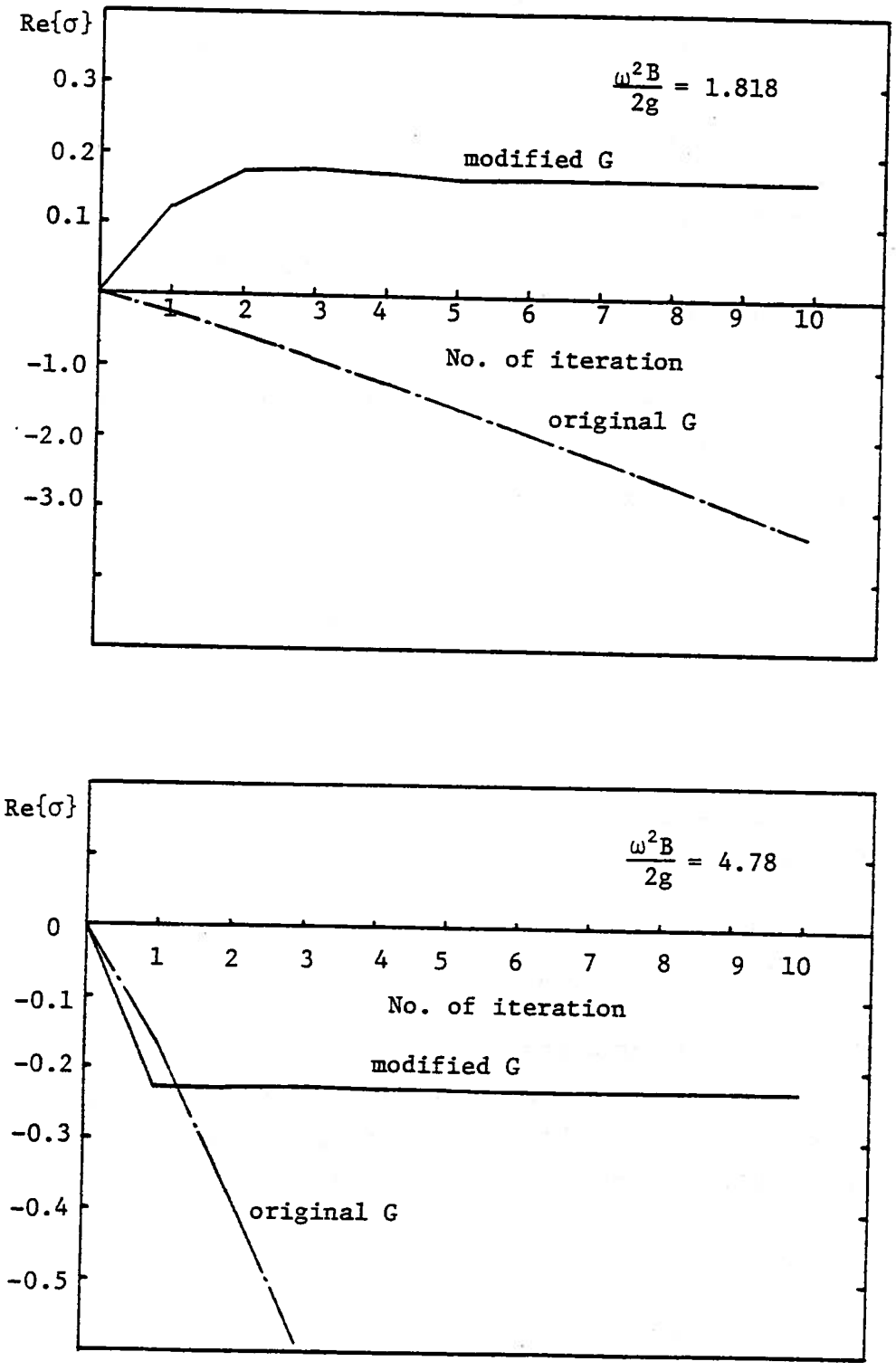

Figure 10. Convergence of source density at the free surface for the heaving circle.

Figure 10 shows that the iterative solution converges well when the modified Green's function is used. The rate of convergence is slow for low frequencies, and is faster for the high frequencies. The rate also depends on the shape of the section. For example, the rate of convergence is better for the circular cylinder than for the flat rectangular cylinder (B/T = 4.0). Four to ten iterations yield a good approximation from which to compute the source density. They give sufficient accuracy for the computation of the added mass and damping coefficients.

D. Hydrodynamic Pressure, Sectional Added Mass, and Damping

The hydrodynamic pressure is obtained from the linearized Bernoulli equation as,

$$p = -i\omega\rho\Phi, \tag{59}$$

where ω is the frequency of oscillation, and ρ is the density of the fluid. By replacing Φ with $i\omega a\phi$, we get

$$p = \rho a\omega^2\phi, \tag{60}$$

where a is the amplitude of the body motion, and ϕ is the normalized form of the velocity potential. The pressure is non-dimensionalized by hydrostatic pressure ρga:

$$\frac{p}{\rho ga} = \nu\phi \quad , \quad \text{where } \nu = \frac{\omega^2}{g} \quad . \tag{61}$$

The real and imaginary parts of the hydrodynamic pressure are related to added mass and damping coefficients, respectively. The sectional hydrodynamic force is computed from the pressure integration over the contour:

$$F_i = \int_C p(Q)\ N_i(Q)\ d\ell(Q), \tag{62}$$
$$= \rho ga\nu\tilde{F} \ ,$$

where $\tilde{F} = \int_C \phi \, N_i \, d\ell$. (63)

The complex amplitude of the hydrodynamic force is represented by

$$F = -(-\rho A \, C_a \, \omega^2 a + i\rho A \, C_d \, \omega^2 a), \tag{64}$$

where A is the sectional area, C_a is the added mass coefficient, and C_d is the damping coefficient. By equating (62) and (64), the sectional added mass and damping coefficients are defined by

$$C_a = \frac{Re[\tilde{F}]}{A}$$

and

$$C_d = \frac{-Im[\tilde{F}]}{A} \quad . \tag{65}$$

Figures 11 and 12 show the hydrodynamic pressure at keel and at the free surface on the heaving circle, respectively. The 2-D added mass coefficient and damping coefficient for the heaving circular cylinder are shown in Figure 13.

The added mass coefficient and damping coefficient for the rectangular cylinder with a beam draft ratio of 2.0 is shown in Figure 14.

E. Summary

The integral equation of the second kind derived by using a 2-D wave source can be solved approximately by several numerical methods: simultaneous linear algebraic equation, frequency iteration using the infinite fluid solution, or successive approximation by Neumann series.

All of these methods, however, fail at the eigenfrequency of the interior Dirichlet problem. The irregular frequency phenomenon for the Fredholm integral equation which results from the source distribution can be removed by

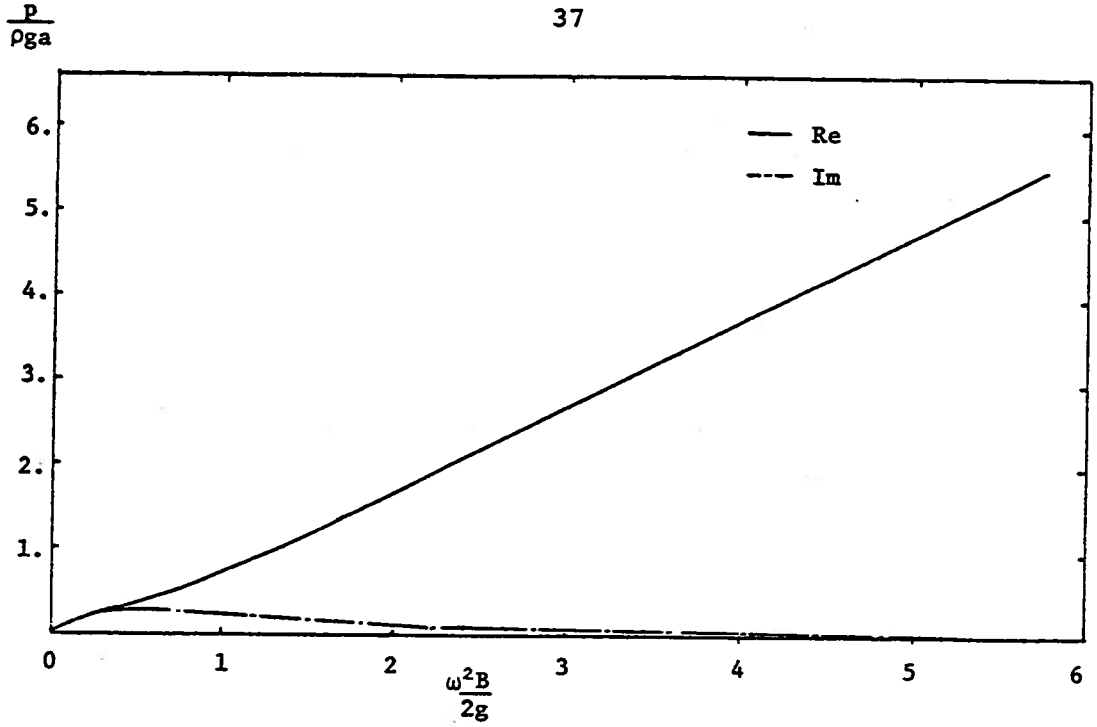

Figure 11. Pressure at the keel for the heaving circle

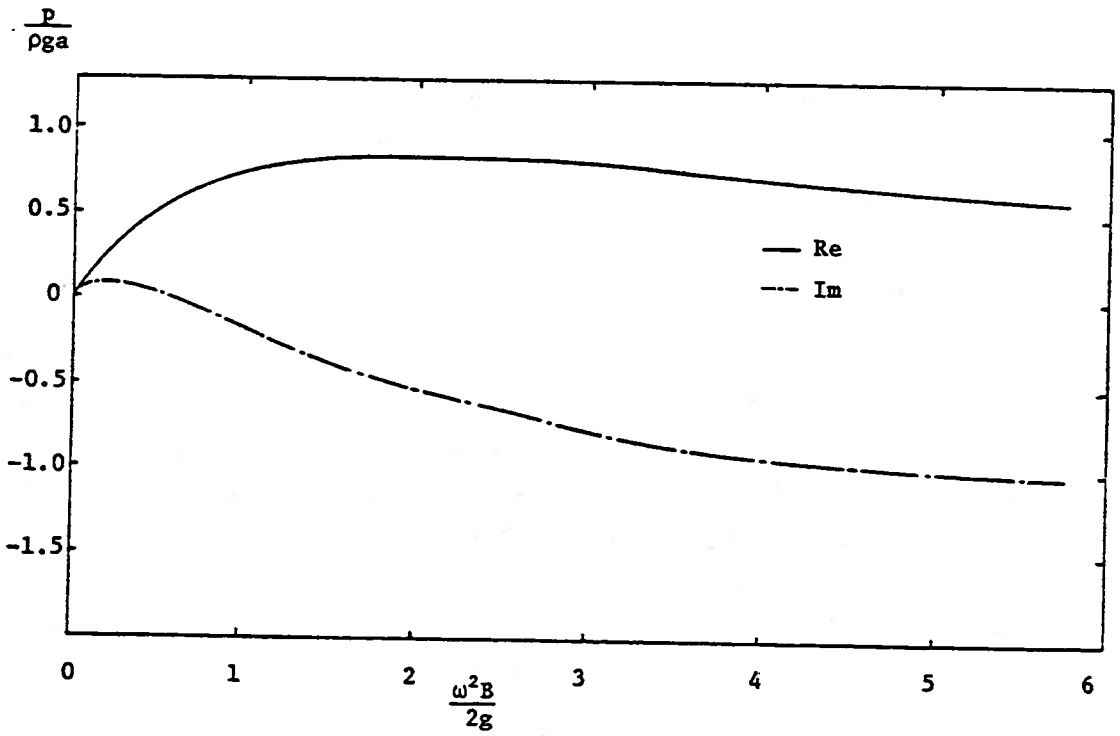

Figure 12. Pressure at the free surface for the heaving circle

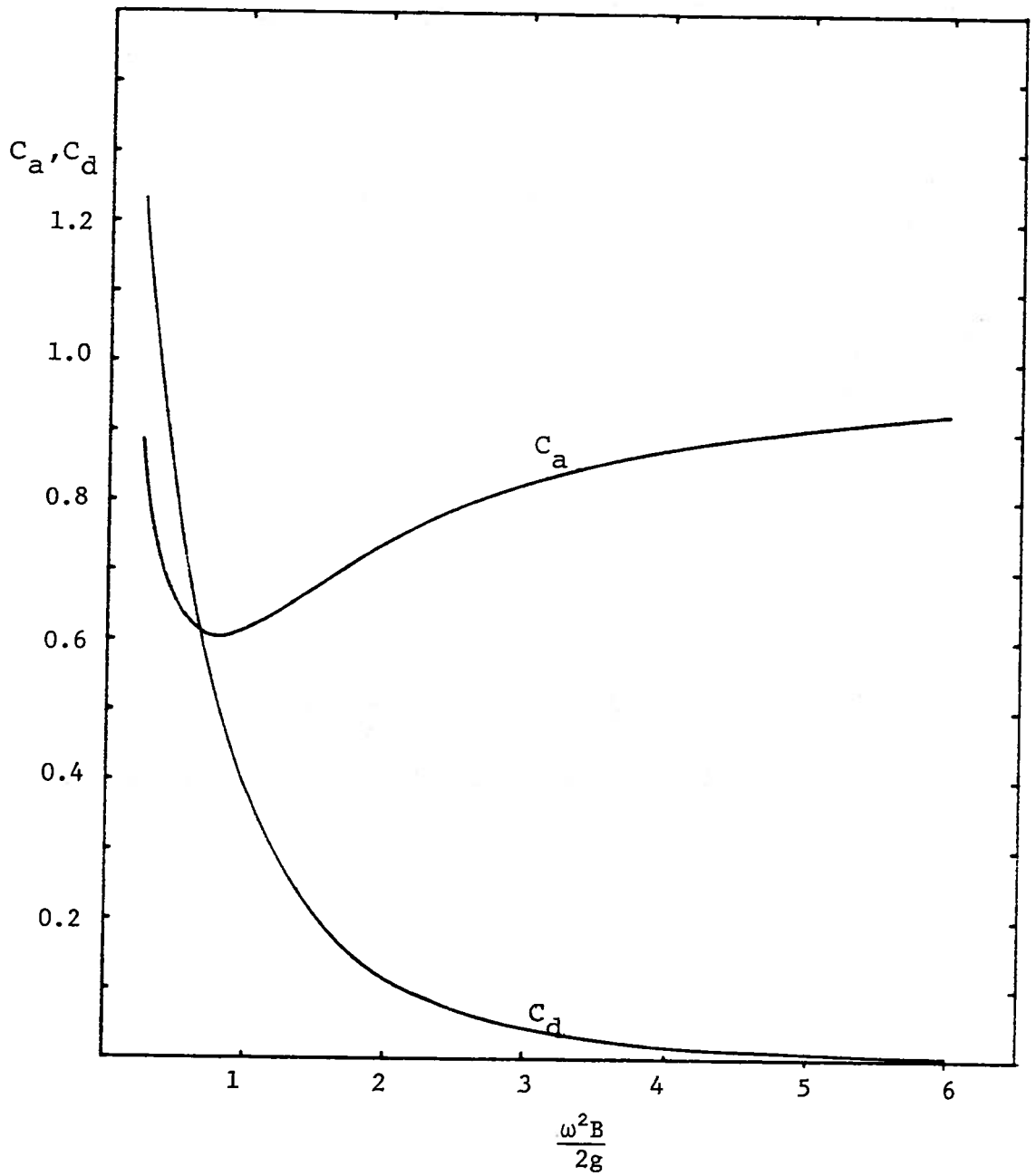

Figure 13. Added mass and damping coefficients for the heaving circle

modifying the fundamental form of the Green's function.

When the modified Green's function is used, both the successive approximation by Neumann series and frequency iterative method can also be used. The iterative methods converge well for the high frequencies of oscillation. The rate of convergence is slow for the low frequencies. For the computation of the added mass and damping coefficients, four to ten iterations give a good approximation.

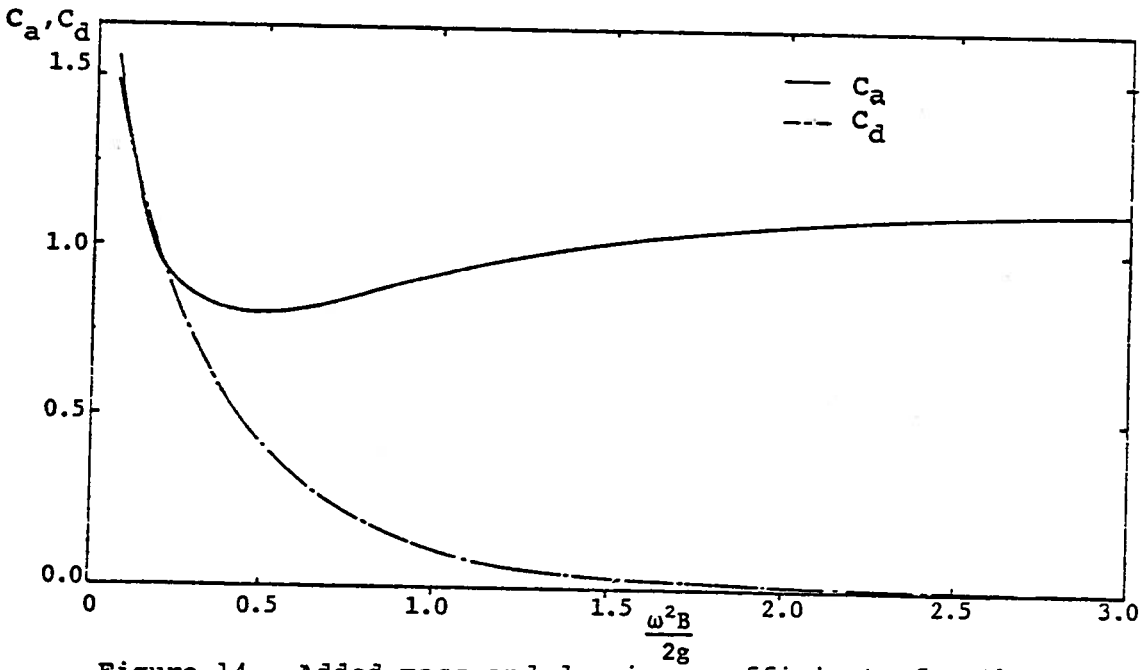

Figure 14. Added mass and damping coefficients for the heaving rectangle (B/T=2)

IV. 3-D INFINITE FLUID PROBLEM

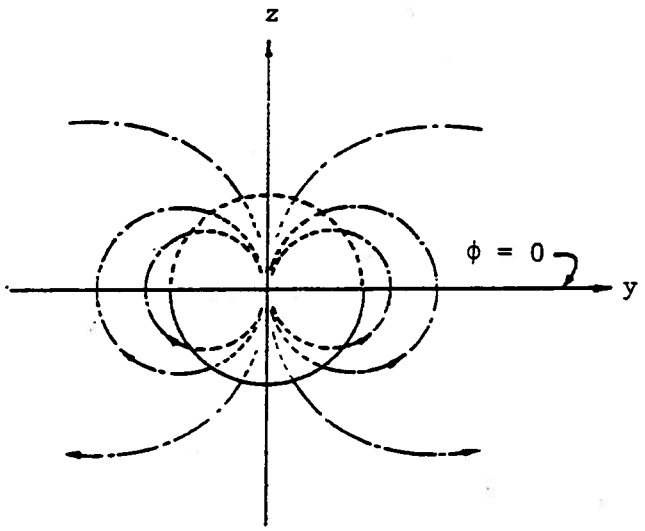

Figure 15. Free-surface problem for infinitely high frequency

As the frequency of oscillation increases, the free surface wave is contained only in the thin layer near the free surface. In the limit, the wave disappears and the free surface becomes a zero equi-potential surface. The problem in the lower-half space can be extended into the upper-half space by reflecting the body into the upper-half plane. This corresponds to the flow around the so-called "double body"* The flow is qualitatively similar to that caused by a vertical dipole at the origin for a sphere and by a line of dipoles at the centerline for a slender spheroid. For simple geometric bodies such as the sphere and spheroid, the exact solution can be obtained by the method of separation of variables in a suitable coordinate system.

A similar subject has been treated by Lamb (1932), Lewis (1929), Landweber and Macagno (1957), Kumai (1966), Vorus

*It should be noted that this applies only to heave motion.

(1971), and Tein (1976) for the study of vibration in the infinite fluid.

For the arbitrary 3-D body, no simple solution exists. It can be solved either by multipole expansion method or by an integral equation method. Various forms of integral equations are available by sources, by dipoles, and by both sources and dipoles (see Lamb). Since the Green's function for the infinite fluid case is simple, the integral equation by source distribution is relatively simple to solve. This method is applied to compute the hydrodynamic pressure for the unsteady motion of 3-D body with the infinitely high frequency of oscillation. This also is equivalent to the oscillation problem of the deeply submerged body.

A. Integral Equation Methods

The integral equation using the 3-D wave-free source is given by

$$-\frac{\sigma}{2}(P) - \frac{1}{4\pi}\iint_S \sigma(Q)\frac{\partial G^{3-D}(P,Q)}{\partial n_P}\, ds(Q) = n_3(P), \qquad (66)$$

where the Green's function is given by

$$G^{3-D} = \frac{1}{\sqrt{(x-\xi)^2 + (y-\eta)^2 + (z-\zeta)^2}} - \frac{1}{\sqrt{(x-\xi)^2 + (y-\eta)^2 + (z+\zeta)^2}}.$$

The integral equation (66) is the same as the integral equation (23) except for the simple form of Green's function. The first term is a point sink. The second term is a point source. The numerical procedure to solve the integral equation is described in Appendix B. The basic numerical scheme is the same as in the 3-D free surface problem which uses the more complicated Green's function to satisfy the free surface and radiation conditions. The induced velocity potential is evaluated in Appendix B.

No irregular frequency phenomena has been found for the infinite fluid case, because interior resonance cannot occur without the presence of free surface inside the

body. Mathematically there is no eigensolution for the interior Dirichlet problem in the infinite fluid case, as described in Kellogg (1929).* The reciprocal eigenvalues of the kernel matrix are within the unit circle of convergence. Any numerical methods for the integral equation would work. The linear algebraic equation method gives a stable solution since the determinant of the kernel matrix never becomes zero. The iterative method with successive approximation converges very well. In general, 4 to 8 iterations are sufficient to give 4-significant-digit accuracy.

The integral equation also can be solved, approximately, by the 2-D iteration method. Instead of solving the 3-D integral equation** directly, a sequence of two-dimensional integral equations is solved section by section. Considering the slenderness of the parallel middle body, the 2-D source density is assumed to be a first approximation to the 3-D source density along most of the length of the parallel middle body. For each section of parallel middle body, we get a 2-D integral equation such as

$$-\frac{\Delta\sigma^{(1)}}{2} + \frac{1}{2\pi}\int_{C(x)} \Delta\sigma^{(1)} \frac{\partial G^{2\text{-}D}}{\partial N_P}(P,Q)\, d\ell(Q) = N_3(P), \qquad (67)$$

where

$$G^{2\text{-}D} = \log\sqrt{(y-\eta)^2+(z-\zeta)^2} - \log\sqrt{(y-\eta)^2+(z+\zeta)^2}\ .$$

The 2-D approximation of source density begins to fail as it approaches the ends, where the slenderness assumption is not valid. For the rapidly varying sections near the end, the 3-D integral equation is solved directly by taking into account the 3-D onset velocity on the end section which is caused by the strip motion of the parallel middle body:

---

*If the velocity potential is harmonic, is continuously differentiable in a closed regular region, and vanishes at all points of the boundary of the region, it vanishes at all points of the region.

**The 3-D integral equation and 2-D integral equation are defined as the integral equation derived from the 3-D and 2-D boundary value problems, respectively.

$$-\frac{\Delta\sigma^{(1)}}{2}-\frac{1}{4\pi}\iint_{S_E}\Delta\sigma^{(1)}\frac{\partial G(P,Q)}{\partial n_P}\,dS(Q) = n_3(P)+\frac{1}{4\pi}\iint_{S_M}\Delta\sigma^{(1)}\frac{\partial G(P,Q)}{\partial n_P}\,dS(Q), \tag{68}$$

where S_E denotes end section, and S_M denotes the slowly changing middle section. The contribution from the other end is small and can be neglected.

The integral in the right-hand side of (68) is the onset velocity from the parallel middle body. The integral vanishes for the infinitely long uniform cylinder. The 3-D integral equation becomes the exact 2-D integral equation. The first order approximation becomes the exact solution. In Appendix A-5, the 2-D source density is derived from the 3-D source density for the infinitely long uniform cylinder. The iteration can continue further. In this paper, only the first iterative solution is computed.

The velocity potential is obtained by integrating the product of the source density and the 3-D Green's function over the hull surface:

$$\phi(P) = -\frac{1}{4\pi}\iint_S \sigma(Q)G^{3\text{-}D}(P,Q)\,dS(Q) \quad . \tag{69}$$

The velocity potential (hydrodynamic pressure) distribution as computed by the 2-D iteration method is compared with the 3-D solution and the strip theory solution in Figure 16 through 18. Even the first order solution gives better accuracy than the strip theory, especially for heave. It becomes less accurate for the springing mode. More iterations are needed for the higher mode of vibration because we assume that 2-D strip source density is a good approximation of 3-D source density along the parallel middle body, which is not quite true. The assumption is valid for heave, but not for 2-node vibration. Figure 19 shows the axial distribution of the source density along the keel of the rectangular cylinder. Figure 20 shows the girthwise distribution of the velocity potential at the midship of the heaving rectangular cylinder.

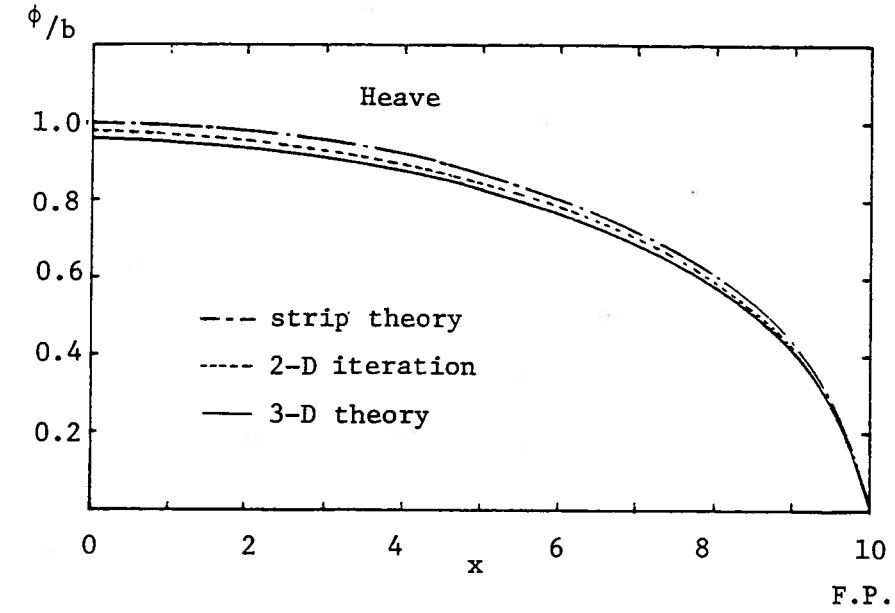

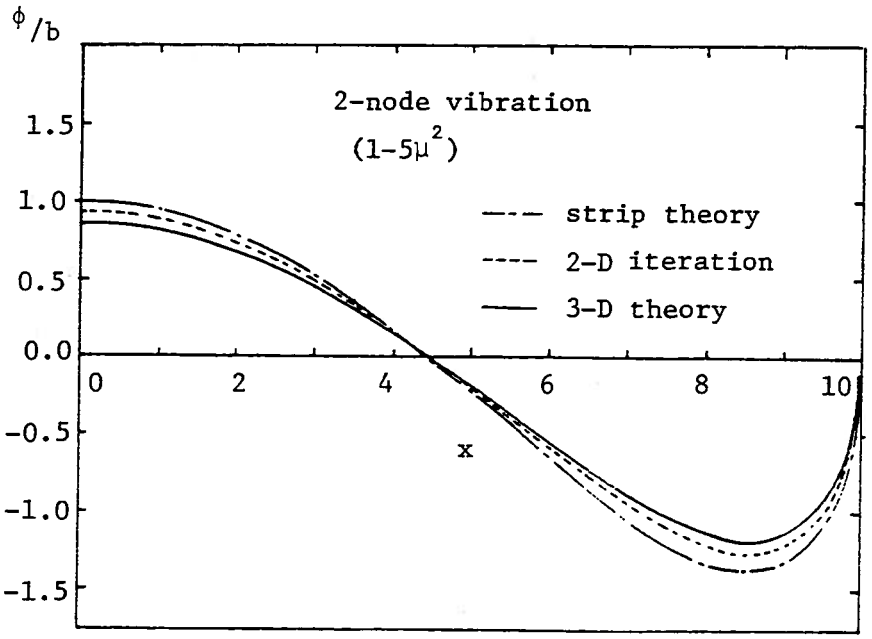

Figure 16. Velocity potential along the keel of the spheroid (L/B=10)

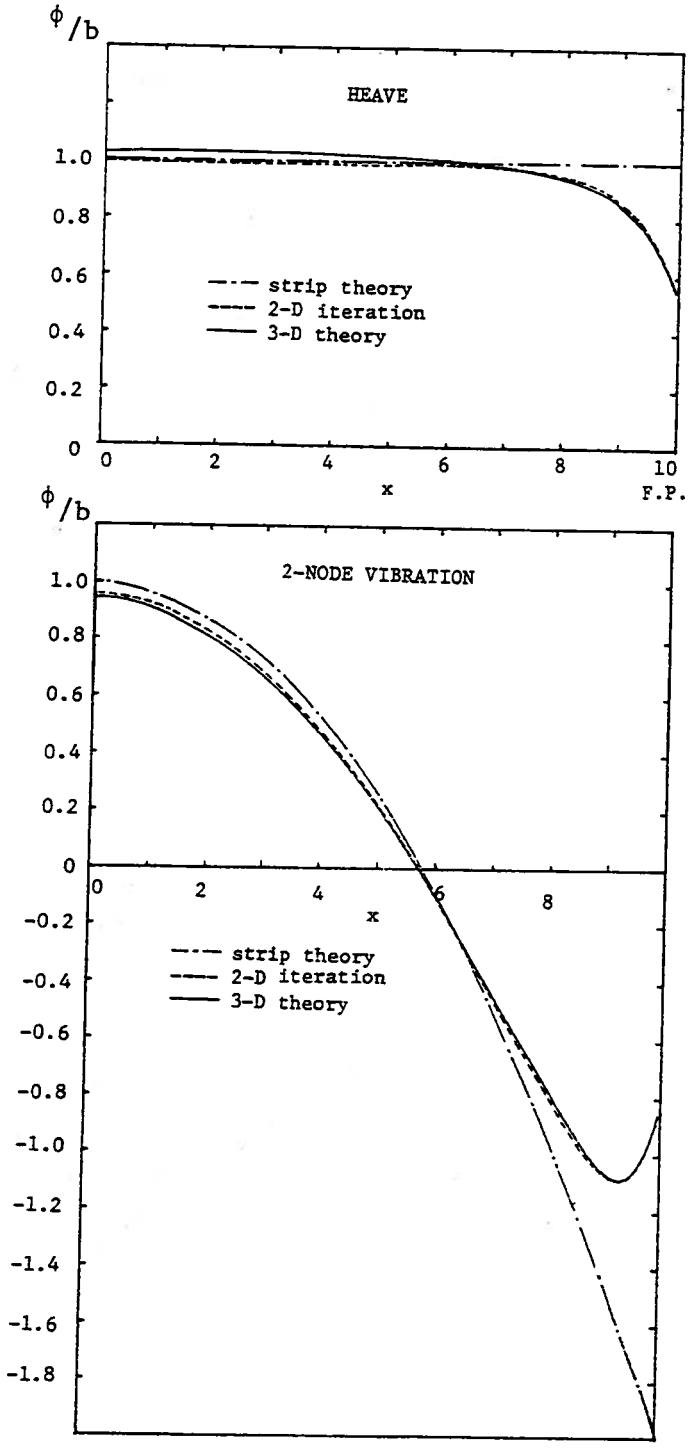

Figure 17. Velocity potential along the keel of the circular cylinder (L/B=10)

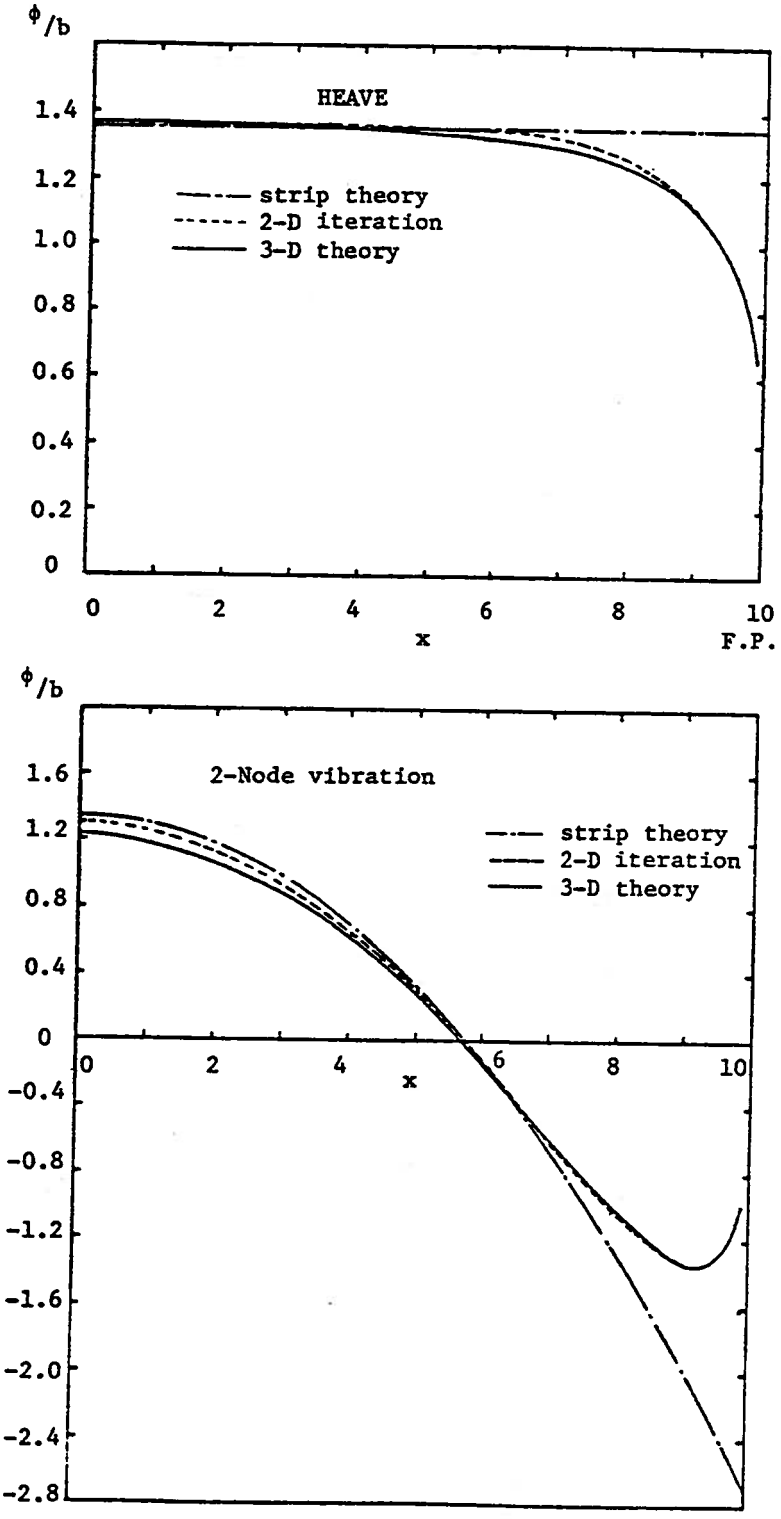

Figure 18. Velocity potential along the keel of the rectangular cylinder (L/B=10)

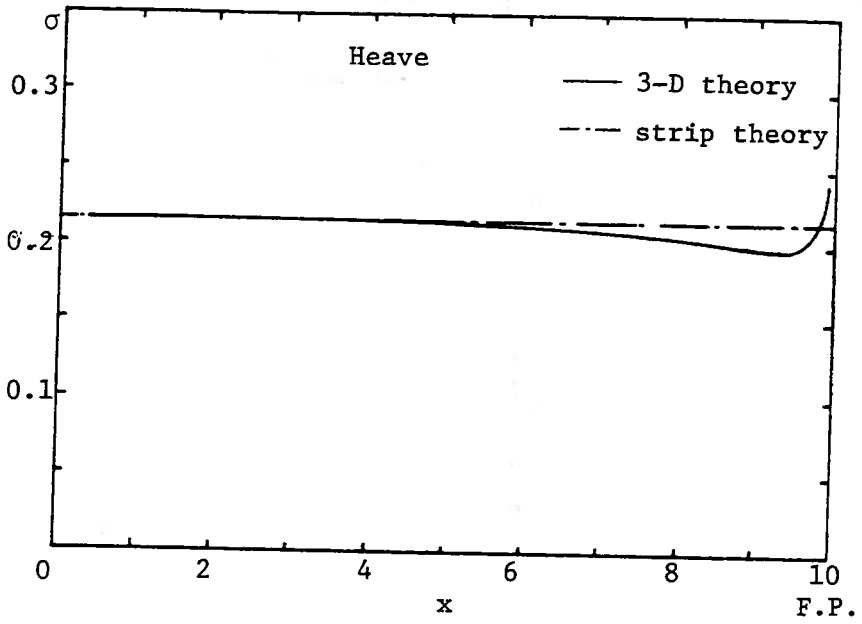

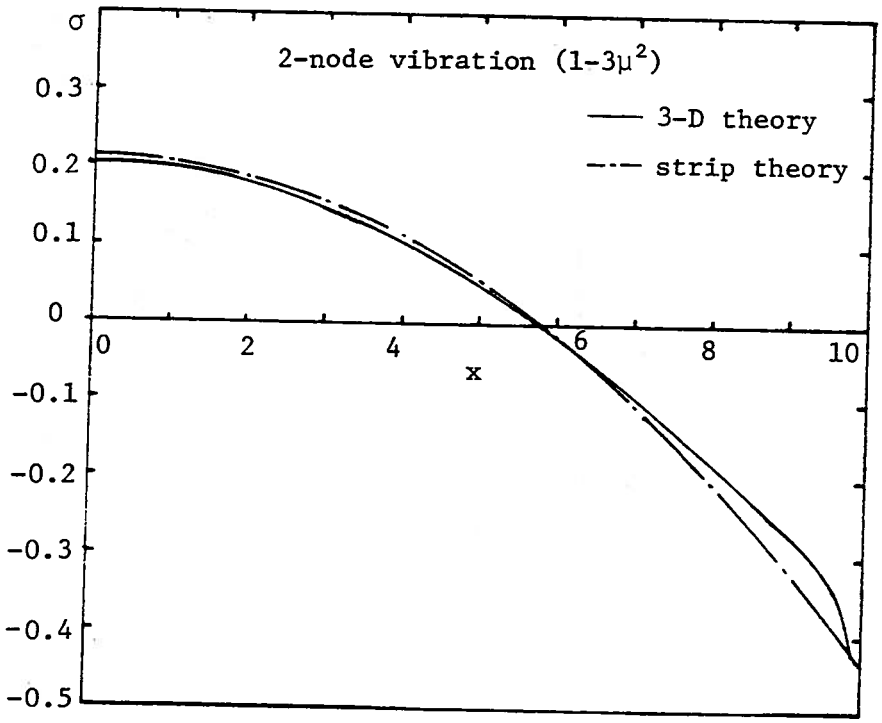

Figure 19. Axial distribution of the source density along the keel of the rectangular cylinder (L/B=10)

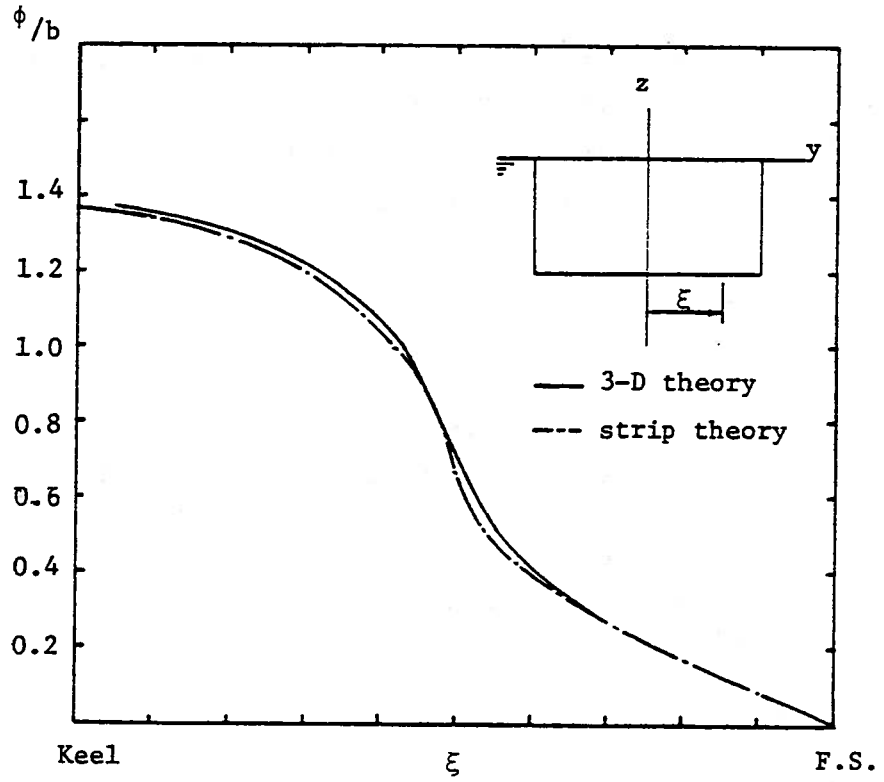

Figure 20. Girthwise distribution of the potential at the midship for the heaving rectangular cylinder (L/B=10)

B. Hydrodynamic Pressure and Added Mass

The non-dimensional hydrodynamic pressure is represented in terms of velocity potential,

$$\frac{p}{\rho a \omega^2} = \phi. \tag{70}$$

Note that the hydrodynamic pressure has only a real part for the infinite fluid case.

The added mass* is the hydrodynamic force caused by unit acceleration, since the total force is in phase with the acceleration. The sectional added mass is obtained through pressure integration around the section:

$$m(x) = \rho \int_{C(x)} \phi \psi_i(x) n_3 \frac{d\ell}{\sqrt{1-n_1^2}}, \tag{71}$$

where $\psi_i(x)$ is the mode shape of the vertical vibration. The sectional added mass coefficient is defined by

$$C_a(x) = \frac{m(x)}{\rho A_0}, \tag{72}$$

where A_0 is the sectional area at midship. The total added mass coefficient is defined by

$$C_a = \frac{1}{\rho \nabla} \int_{-L/2}^{L/2} m(x)\, dx,$$

where ∇ is the volume of the displaced fluid.

C. 3-D Exact Solution of the Vibrating Spheroid

The velocity potential for the vibrating spheroid is solved by the method of separation of variables in spheroidal coordinates by Lewis (1929). It is assumed that the mode shape is approximately a simple shear of transverse sections of the spheroid. Then the velocity potential for the

---

*Added mass for the heave is mass and for the pitch it is added moment of inertia dimensionally. For the vibration mode, it should be interpreted as generalized added mass.

vertical vibration can be expressed by the spherical harmonics. The transformation of the cylindrical coordinate system (x,R,θ) to the prolate spheroidal coordinate system (κ,μ,θ) is given by

$$x = \ell\,\mu\,\kappa \qquad 1<\kappa<\infty \ ,$$

$$R = \ell\sqrt{(1-\mu^2)(\kappa^2-1)} \qquad -1\leq\mu\leq 1 \ ,$$

and

$$\theta = \theta \qquad 0\leq\theta<2\pi \ ,$$

where ℓ is the distance from center to focus of spheroid.

The velocity potential at field point (κ,μ,θ) due to the 2-node vibration mode $(V_1-V_3\mu^2)$ is represented in spheroidal coordinates:

$$\phi = C(\kappa,\mu)\cos\theta, \tag{73}$$

where

$$C(\kappa,\mu) = \beta_1(\kappa_0)P_1(\mu)Q_1(\kappa) + \beta_3(\kappa_0)P_3(\mu)Q_3(\kappa) \ ,$$

$\beta_n(\kappa_0)$ is constant for the given shape of the spheroid $(\kappa=\kappa_0)$ and given mode shape of vibration, β_1 and β_3 are given by

$$\beta_1 = \left.\frac{\left(V_1 - \frac{V_3}{5}\right)L}{2\sqrt{\kappa^2-1}\,\frac{\partial}{\partial\kappa}Q_1(\kappa)}\right|_{\kappa=\kappa_0} \ ,$$

$$\beta_3 = \left.\frac{V_3 L}{15\sqrt{\kappa^2-1}\,\frac{\partial}{\partial\kappa}Q_3(\kappa)}\right|_{\kappa=\kappa_0} \ ,$$

where L is the length of the spheroid.

$P_n(\mu)$ is the associated Legendre function of the first kind, and $Q_n(\kappa)$ is the associated Legendre function of the second kind. After some algebraic manipulation, we get the velocity potential on the surface of the spheroid, where $\kappa=\kappa_0$, as

$$\phi(\kappa_0,\mu,\theta)=R_0(\mu)\left[\left[V_1-\frac{V_3}{5}\right]W_1(\kappa_0)+\frac{V_3}{5}(1-5\mu^2)W_3(\kappa_0)\right]\cos\theta \quad , \tag{74}$$

where $R_0(\mu)$ is the local radius at section $\mu(2x/L)$ of the spheroid, and $W_n(\kappa_0)$ is J factor of the spheroid for n-th normal mode:

$$W_1 = \left.\frac{\frac{3}{2}\kappa\log\frac{\kappa+1}{\kappa-1}-\frac{3\kappa^2}{\kappa^2-1}}{\frac{3}{2}\kappa\log\frac{\kappa+1}{\kappa-1}-\frac{3\kappa^2-6}{\kappa^2-1}}\right|_{\kappa=\kappa_0} ,$$

$$W_3 = -\left.\frac{\frac{3}{2}(5\kappa^3-\kappa)\log\frac{\kappa+1}{\kappa-1}-\frac{15\kappa^4-13\kappa^2}{\kappa^2-1}}{\frac{3}{2}(15\kappa^3-11\kappa)\log\frac{\kappa+1}{\kappa-1}-\frac{45\kappa^4-63\kappa^2+16}{\kappa^2-1}}\right|_{\kappa=\kappa_0} .$$

The added mass can be computed either from the kinetic energy of the fluid or by the direct integration of the pressure over the hull surface. By applying Green's theorem in the fluid domain, the generalized added mass for the vibration modes can be represented by the kinetic energy of the surrounding fluid caused by the unit velocity in the given mode. This relationship does not hold when the free surface exists, however, since the kinetic energy expression has contributions from the free surface and surface at infinity.

The sectional added mass for the springing spheroid is obtained through pressure integration around the section:

$$m(\mu) = \rho\int_{-\pi/2}^{\pi/2}(V_1-V_3\mu^2)n_3\frac{\sqrt{\kappa_0^2-\mu^2}}{\sqrt{1-\mu^2}}R_0(\mu)\,d\theta \quad .$$

Thus, the sectional added mass coefficient of a springing spheroid is given by

$$C_a(\mu) = \frac{m(\mu)}{\frac{\rho\pi b^2}{2}} = (1-\mu^2)(V_1-V_3\mu^2)\left[W_1\left(V_1-\frac{V_3}{5}\right)-\frac{1}{5}W_3V_3(5\mu^2-1)\right] . \tag{75}$$

The total added mass coefficient is obtained by integrating the sectional added mass along the axial direction:

$$C_a = \frac{m}{\rho V} = W_1\left(V_1-\frac{V_3}{5}\right)^2 + \frac{8}{175}W_3V_3^2 . \tag{76}$$

The total added mass agrees with Lewis' result computed from the kinetic energy of the fluid for the 2-node vibration.

D. 2-D Strip Theory for the Vibrating Spheroid

Instead of solving the 3-D boundary value problem, a set of 2-D boundary value problems is solved sequentially by section based on slenderness of the body. It is assumed that each section performs 2-D vertical motion independently, without the interaction between sections. The 2-D flow of any section of the spheroid can be computed by the method of separation of variables. The flow is basically that caused by the 2-D vertical dipole at the centerline with a strength proportional to $V_1-V_3\mu^2$. The velocity potential in the fluid field computed by strip theory is given in cylindrical coordinates:

$$\phi(\mu,R,\theta) = \frac{(V_1-V_3\mu^2)R_0^2(\mu)\cos\theta}{R} , \tag{77}$$

where

$$R = \sqrt{y^2+z^2} ,$$

and

$$R_0(\mu) = b\sqrt{1-\mu^2} .$$

The velocity potential on the surface of the spheroid for the 2-node vibration is given as

$$\phi(\mu,R_0,\theta) = (V_1-V_3\mu^2)R_0(\mu)\cos\theta \quad . \tag{78}$$

The strip-theory sectional added mass is obtained by integrating the pressure along the girth of the section:

$$m(\mu) = \rho(V_1-V_3\mu^2)\int_C \phi N_3 d\ell = \rho\pi R_0^2(\mu)\ (V_1-V_3\mu^2)^2 \quad . \tag{79}$$

The total added mass of the spheroid is obtained by integrating (79) along the axial direction. The added mass coefficient by strip theory becomes

$$C_a = \left(V_1 - \frac{V_3}{5}\right)^2 + \frac{8}{175}V_3^2 \quad . \tag{80}$$

This is the same as 3-D results (76) except for the W_n factor.

E. Local J(μ) Factor and the 3-D Effect

The local J factor is defined as the ratio of the sectional added mass of the 3-D body to the added mass of the 2-D cylinder at the section μ. For the vibrating spheroid with mode shape $V_1-V_3\mu^2$, the local J factor becomes

$$J(\mu) = \frac{W_1(V_1-\frac{V_3}{5})+\frac{1}{5}W_3V_3(1-5\mu^2)}{V_1-V_3\mu^2} \quad . \tag{81}$$

For heave, the local J(μ) factor becomes W_1, which is constant. This is surprising since it means that the relative error of the strip theory computation is the same for any section of the spheroid. In other words, the 2-D strip-theory value for the added mass near the ends is no worse than that along midship of the heaving spheroid. Furthermore, the absolute error created by strip theory is greater at midship than near ends. Figure 21 compares strip theory and 3-D theory for the added mass distribution of the heaving and springing spheroid.

For a normal mode of 2-node vibration $(1-5\mu^2)$, the local J factor becomes a constant value of W_3. Thus, the same conclusion about the end effect can be made for the 2-node

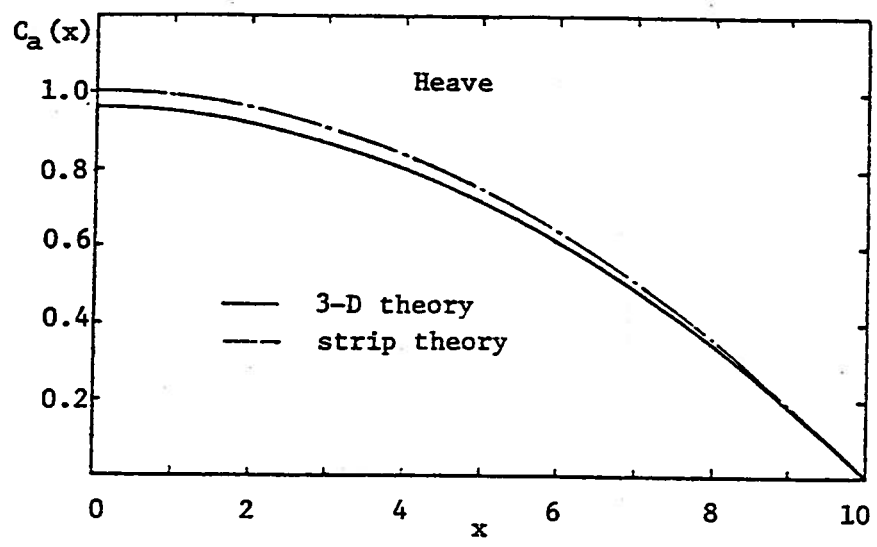

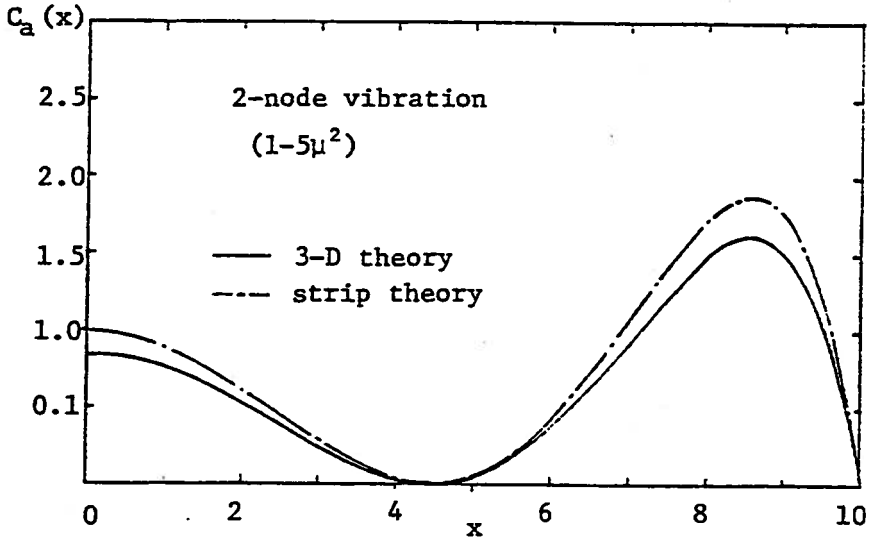

Figure 21. Axial distribution of the added mass for the spheroid (L/B=10)

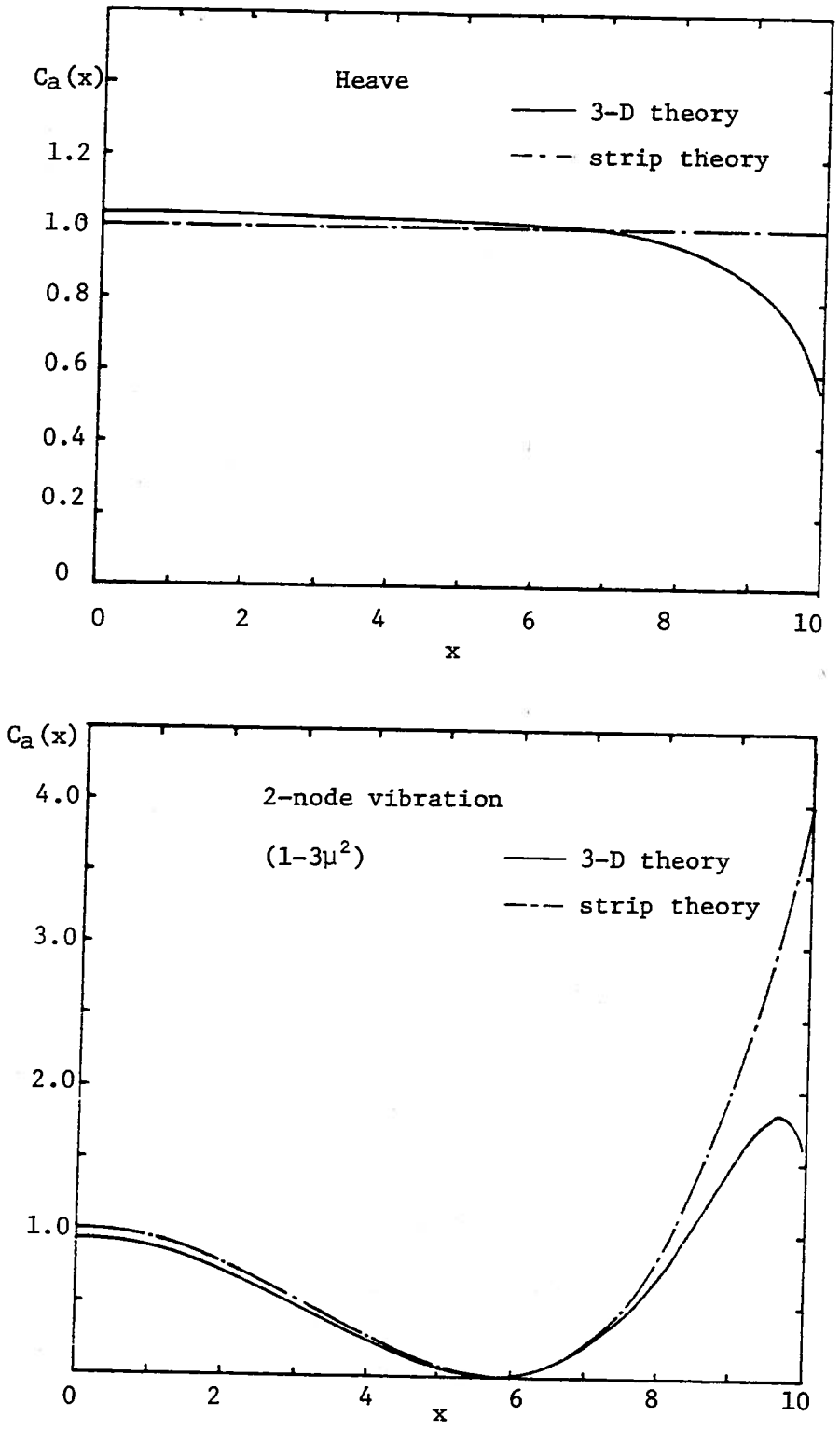

Figure 22. Axial distribtuion of the added mass for the circular cylinder (L/B=10)

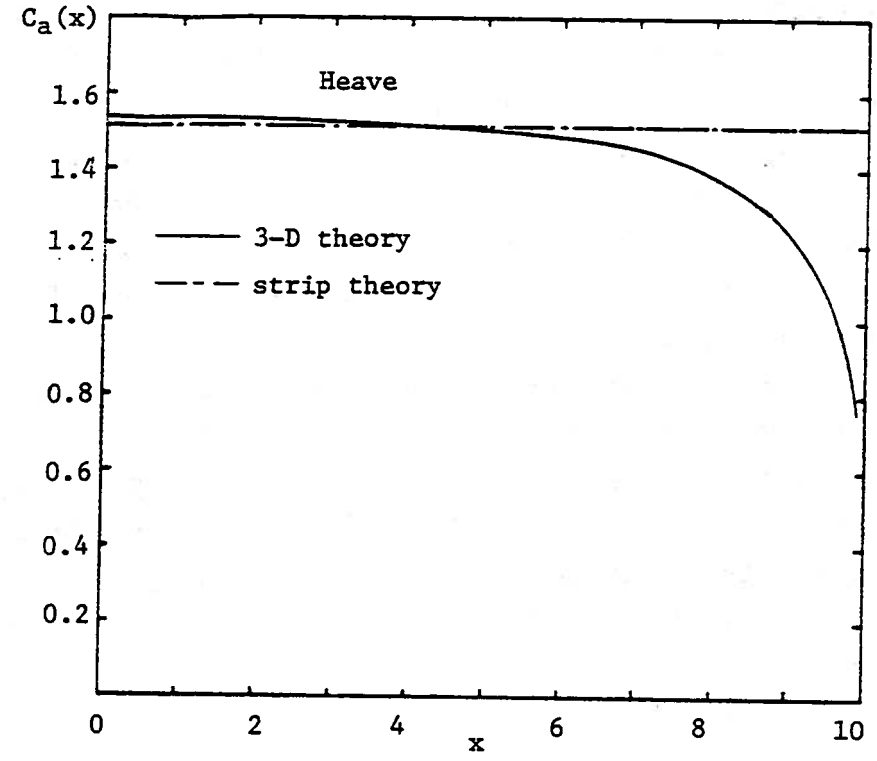

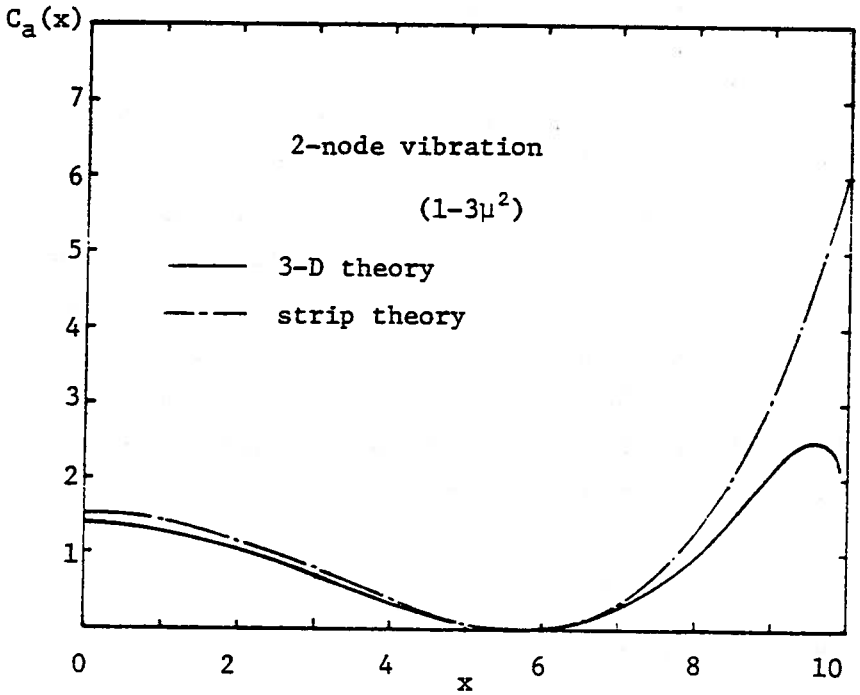

Figure 23. Axial distribution of the added mass for the rectangular cylinder (L/B=10)

vibration. This is a case in which physical intuition does not always work. It should be recognized that the above discussion is valid only for an infinitely high frequency of oscillation and for the special geometry of the spheroid. A later chapter will study how the constant local J factor changes when the free surface exists.

For blunt 3-D bodies such as a rectangular tank or a circular cylinder with vertical ends, the discrepancy near the ends between strip theory and 3-D theory is significant. Near the midship section, strip theory is a quite good approximation; however, it becomes a very poor approximation as it approaches the ends. Figures 22 and 23 compare 2-D and 3-D theories for the sectional added mass of heaving and vibrating circular and rectangular cylinders (L/B=10), respectively.

For a vibrating spheroid, the ratio of 3-D pressure to 2-D pressure is given by

$$\frac{p^{3\text{-}D}}{p^{2\text{-}D}} = \frac{(V_1 - \frac{V_3}{5})W_1 + \frac{W_3 V_3}{5}(1-5\mu^2)}{V_1 - V_3\mu^2} \quad .$$

For the spheroid, the pressure ratio is identical to the local J factor (81). For heave, the 3-D pressure varies like $\sqrt{1-\mu^2}$, while the sectional added mass by 3-D theory varies like $(1-\mu^2)$ in an axial direction. The pressure found by 2-D strip theory varies like $\sqrt{1-\mu^2}$, and the sectional added mass computed by 2-D theory varies like $(1-\mu^2)$ in an axial direction. Thus, the pressure ratio becomes identical to the local J factor through cancellation of the same factor.

F. Total J Factor

The total J factor is defined as the ratio of the actual

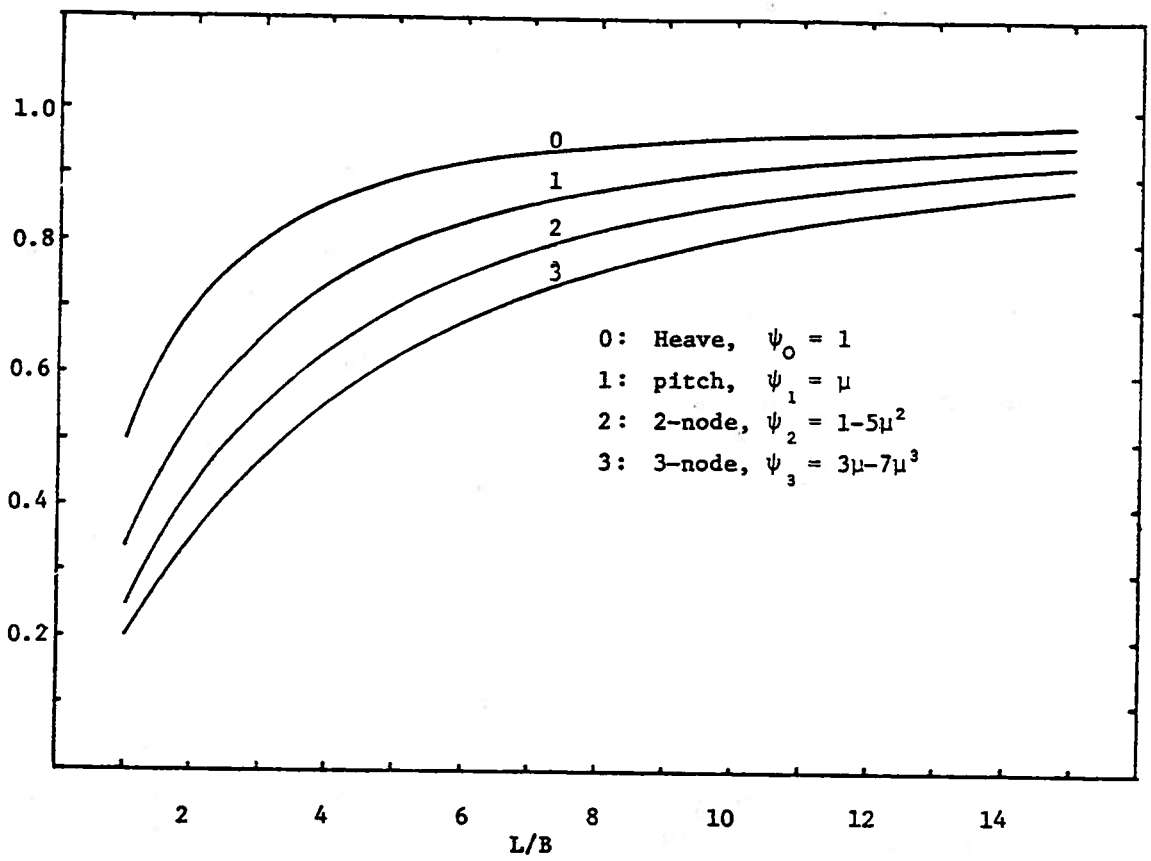

Figure 24. Total J factor of the vibrating spheroid in normal mode

added mass computed using the 3-D theory to the added mass computed using the strip theory. For a springing spheroid, the J factor becomes

$$J = \frac{(V_1 - \frac{V_3}{5})^2 W_1 + \frac{8}{175} V_3^2 R_3}{(V_1 - \frac{V_3}{5})^2 + \frac{8}{175} V_3^2} \quad .$$

Figure 24 shows the total J factor for various L/B ratios of a spheroid for various normal modes of vertical vibration. For heave, the J factor approaches 0.5 for a sphere and 1 for the infinitely long circular cylinder. For the 2-node vibration ($1-5\mu^2$), the J factor becomes 0.25 for a sphere and approaches 1 for the 2-D circular cylinder. The more slender the spheroid, the better the strip solution for estimating the added mass. The strip theory value is a better approximation for the lower modes than for the higher modes of vibration.

G. Summary

The pressure distribution and sectional added mass for a vibrating spheroid, circular cylinder, and rectangular cylinder are computed by the 3-D source distribution method. The numerical solution from any approximation method is very stable since there is no resonance phenomena inside the bodies. The three dimensional solutions are compared with the strip solutions.

The 3-D effect on the added mass distribution for the vibrating spheroid is evenly spread along the entire length because of its particular geometry and its normal mode. However, the 3-D effect on the added mass distribution for the blunt 3-D body is significant near ends. For the same geometry, end effect is more significant for the higher mode than for the lower mode of vibration.

V. 3-D FREE SURFACE PROBLEM

No analytic solution exists for the 3-D arbitrary body. Thus, analysis must depend on either the generalized multipole expansion method or the integral equation method. In general, the integral equation method is preferred for the 3-D arbitrary body. Various forms of the integral equations for the 3-D unsteady oscillation problem are derived in chapter II.

This paper employs the integral equation method by using 3-D wave source distribution. Irregular frequency phenomenon is removed by using a modified Green's function. The pressure distribution and sectional added mass and damping coefficients for the heaving spheroid are computed. The 3-D effect on the added mass is also investigated.

A. Integral Equation by 3-D Wave Source

The Fredholm integral equation of the second kind using 3-D wave source distribution is given by

$$-\frac{\sigma(P)}{2}-\frac{1}{4\pi}\iint_S \sigma(Q)\frac{\partial G}{\partial n_p}(P,Q)\, dS(Q) = n_i(P), \qquad (23)$$

where

$$\frac{\partial G}{\partial n_p} = n_x\frac{\partial G}{\partial x} + n_y\frac{\partial G}{\partial y} + n_z\frac{\partial G}{\partial z} \quad .$$

The various forms of the Green's functions and their derivatives are derived in Appendix A. The integral equation using source distribution is solved by several numerical methods.

B. Irregular Frequency of the Interior Dirichlet Problem

The integral equation method is powerful because it can be applied to an arbitrary three-dimensional body. It has,

however, the inherent disadvantage of a resonance problem with the complementary interior flow at an infinite set of eigenfrequencies similar to that of the 2-D problem (section III-C). The eigenfrequencies of simple 3-D bodies can be predicted.

The eigenfrequency of the interior Dirichlet problem ($\phi=0$ on the boundary) for a rectangular tank can be computed by using the method of the separation of variables. For the symmetrical mode, the eigensolution is given by

$$\phi^{m,n} = \cos \frac{(2m-1)\pi x}{L} \cos \frac{(2n-1)\pi y}{B} \sinh \gamma^{m,n} (z+T), \qquad (83)$$

for $m,n = 1,2,3\ldots$,

where L is the length, B is the beam, T is the draft of the tank, and

$$\gamma^{m,n} = \sqrt{\left[\frac{(2m-1)\pi}{L}\right]^2 + \left[\frac{(2n-1)\pi}{B}\right]^2} .$$

Note that the 3-D coordinate system from Figure 1 is used. The eigenfrequency of oscillation is determined from the free surface condition:

$$\frac{(\omega_{m,n})^2}{g} = \gamma^{m,n} \coth \gamma^{m,n} T .$$

The lowest eigenfrequency becomes

$$\frac{\omega^2 B}{2g} = \sqrt{\left(\frac{\pi B}{2L}\right)^2 + \left(\frac{\pi}{2}\right)^2} \coth \sqrt{\left(\frac{\pi T}{L}\right)^2 + \left(\frac{\pi T}{B}\right)^2} . \qquad (84)$$

The anti-symmetrical modes can be obtained similarly. The lowest eigenfrequency of the rectangular tank is plotted versus length/beam ratio and beam/draft ratio in Figure 25. For an infinitely long narrow tank, the eigenfrequency for the symmetrical mode becomes that of a 2-D rectangle.

For the circular tank, the method of separation of variables in cylindrical coordinates is used. The eigen solution is given by

$$\phi^{m,n}(R,\theta,z) = \sinh \gamma(z+T) J_m(\gamma^{m,n} R) \cos m\theta, \text{ for } m,n=0,1,2,$$

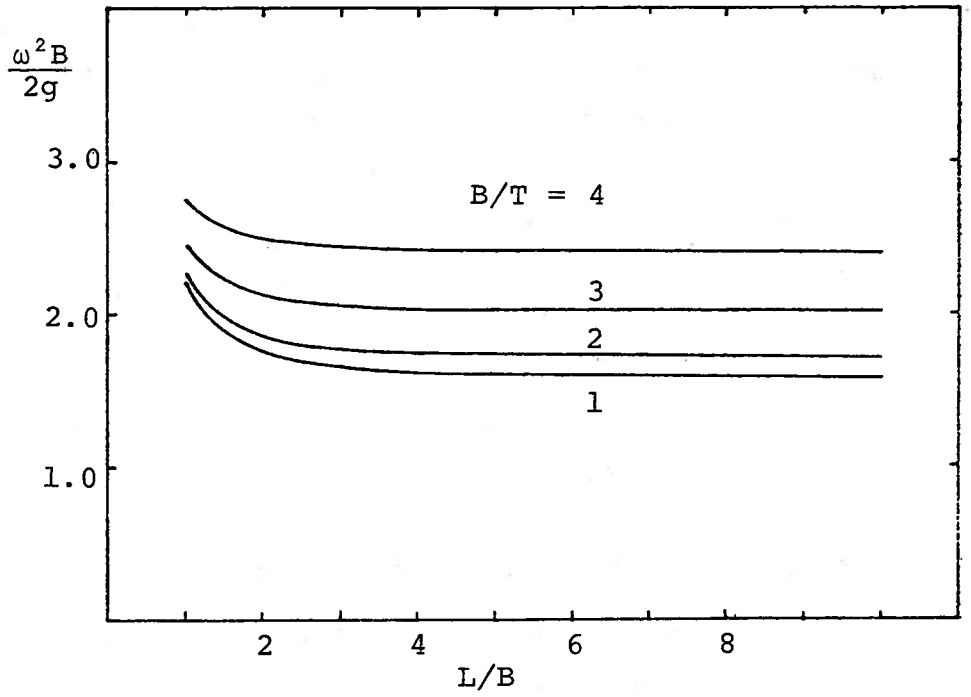

Figure 25. Lowest eigenfrequency for the rectangular cylinder

where $\gamma^{m,n}$ is determined from

$$J_m(\gamma^{m,n}R) = 0, \text{ on } R=a ,$$

and a is the radius of the circular tank.
The eigenfrequency of oscillation is given by

$$\frac{(\omega_{m,n})^2}{g} = \gamma^{m,n} \coth \gamma^{m,n}T .$$

The lowest eigenfrequency of oscillation becomes

$$\frac{\omega^2 a}{g} = 2.445 , \text{ for } \frac{a}{T} = 1 .$$

The irregular frequency phenomena of the integral equation method can be removed by modifying the fundamental form of the Green's function. A modified Green's function is constructed by adding a line of sources at the free surface on the center line. It is presented by

$$\tilde{G}(P,Q) = G(P,Q) - \frac{C}{2\pi i} G(P,Q_0)G(Q,Q_0) \cos \frac{\pi\xi}{L} ,$$

where G is the original form of the Green's function, Q_0 is the point at $(\xi,0,0)$, and $G(P,Q_0)$ is a source located at ξ of the center line. Refer to Chapter III-B for the 2-D case.

C. Linear Algebraic Equation Method

The macroscopic numerical procedure used to solve the integral equation based on source distribution is described as follows:

i) approximate the body surface by a number of plane quadrilateral elements;
ii) compute the influence coefficient matrix for induced normal velocity and induced velocity potential;
iii) compute the generalized normals of the elements;
iv) solve the simultaneous linear algebraic equation compute the source density;
v) compute the velocity potential on the hull by integrating the computed source density over the hull surface;

vi) integrate the hydrodynamic pressure on the hull in the direction of the desired motion to compute the hydrodynamic coefficients.

(Details of the numerical procedures are given in Appendix B.)

D. Iterative Methods

Similar to the 2-D free surface problem, various iterative methods are used to solve the integral equation: successive approximation by Neumann series, the frequency iteration method, and the improved iteration method using the Bucker-Chertock series.

1. Successive approximation by Neumann series

Successive approximation by Neumann series is described in III-C-2 for the 2-D free surface problem. The numerical scheme similar to the 2-D case is applied for the 3-D problem. Successive approximation does not converge for all frequencies of oscillation. The successive approximation does not converge for the low frequency. It is found, however, that the successive approximation method converges well for the high frequency.

2. Frequency iteration by using an infinite fluid solution

The frequency iteration method for the three-dimensional case is similar to the 2-D problem (III-C-3). The first iteration gives the infinite fluid source density, and the free surface effect is corrected gradually by successive iterations. The frequency iteration method converges for the high frequency of oscillation. However, it does not converge for the low frequency. Figure 26 shows that the frequency iteration method converges well for $\nu b=4$, but

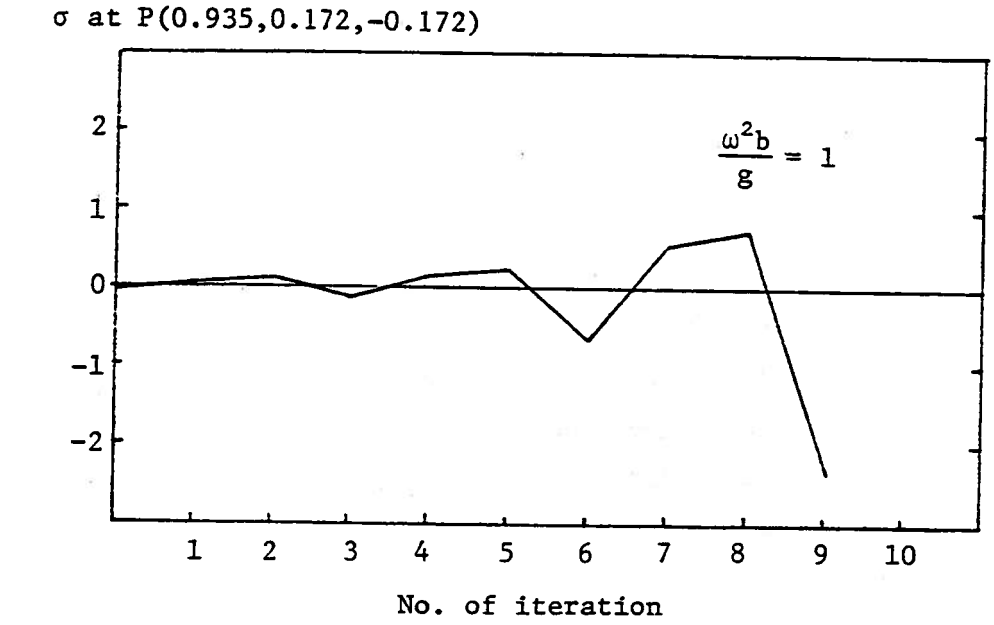

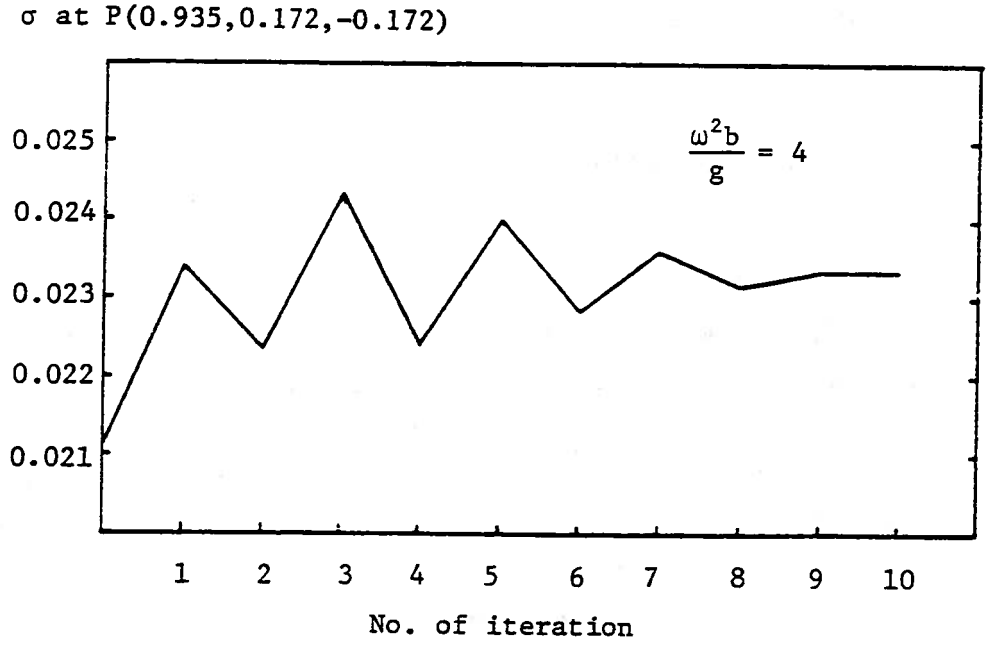

Figure 26. Convergence of the source density for the heaving sphere by the frequency iteration

diverges very fast for $\nu b = 1$. The convergence rates of both iteration methods are almost same. If one method converges, then the other method also converges.

The two fundamental questions for the iteration methods are: Do the iterative solutions converge? If so, do they converge to right solution? It is found that the iteration solutions converge to the right solution, if they converge. The rate of the convergence of iteration depends on the first approximation. For the high frequency, the infinite fluid solution as a first approximation may be sufficient enough for the convergence. This paper studies the convergence condition of the iteration method to find out why it does not converge for all frequencies. (For the low frequency, successive approximation by Neumann series and frequency iteration do not converge.) An improved iteration method by Buckner and Chertock is applied for the low frequency ranges to improve the convergence. (See Figure 27)

3. Improved iteration method

Let us assume that there is a convergent series in σ:

$$\sigma = \Delta\sigma^{(1)} + \Delta\sigma^{(2)} + \cdots\cdots .$$

Substituting σ into the integral equation (36), we can rewrite the integral equation as

$$(\Delta\sigma^{(1)}+\Delta\sigma^{(2)}+\cdots.) - \tau K(\Delta\sigma^{(1)}+\Delta\sigma^{(2)}+\cdots.) = -2f$$

Let $\tau = 1$,

$$\Delta\sigma^{(1)} = -2f(1-H)$$

and

$$\Delta\sigma^{(n)} = [H+(1-H)K]\Delta\sigma^{(n-1)} \quad \text{for } n\geq 2 ,$$

where H is any real number or complex number.
We then get a new sequence as follows:

$$\sigma^{(1)} = -2f(1-H)$$

$$\sigma^{(2)} = \Delta\sigma^{(1)}+[H+(1-H)K]\Delta\sigma^{(1)} ,$$
$$= (1+\tilde{K})\tilde{f} , \qquad (88)$$

where

$$\tilde{K} = H+(1-H)K,$$

and

$$\tilde{f} = -2f(1-H).$$

By induction, we get

$$\sigma^{(n)} = (1 + \tilde{K} + \tilde{K}^2 + ... \tilde{K}^{n-1})\tilde{f} , \qquad (89)$$

where $\tilde{K}^n$ is n-th iterate of new operator $\tilde{K}$.
Let us rewrite the equation (88) as

$$\sigma^{(2)} = -2f(1-H)+[H+(1-H)K]\Delta\sigma^{(1)},$$
$$= H\sigma^{(1)}+(1-H)[-2f+K\sigma^{(1)}].$$

By induction, we get the n-th sequence,

$$\sigma^{(n)} = H\sigma^{(n-1)}+(1-H)[-2f+ K\sigma^{(n-1)}], \qquad (90)$$

which is the Buckner's sequence. Buckner has demonstrated that the new sequence (90) converges to the unique solution if H satisfies the necessary and sufficient condition,

$$0 \leq H < 1 ,$$

except for the eigenfrequencies. Chertock (1968) gives a more useful condition of convergence in the iterative solution. He finds that if the maximum reciprocal eigenvalue of the kernel matrix is larger than the unit circle, the original Neumann series does not converge. The domain of convergence for the new sequence is inside the circle with its center at $H/(H-1)$ and its radius $\frac{1}{H}$. The circle passes through the point (1,0). If the kernel matrix has a real eigenvalue (1,0), the improved iteration method would not converge.

For the unsteady oscillation problem, the kernel matrix of the integral equation is a function of wave frequency. For each wave frequency, there is a set of characteristic values of the kernel matrix. If any one of the characteristic values is not 1, the solution exists uniquely. This

condition is sufficient for the linear algebraic equation method to work, since the determinant of the kernel matrix is not singular. This condition is not sufficient, however, for the iterative method to converge. The more restrictive condition is required for the iteration method to converge. This condition is given in theorem 4 of the section II-E. The maximum reciprocal eigenvalue of the kernel matrix is beyond the unit circle for the low frequency of oscillation. Thus, the iterative solution diverges. At the eigenfrequencies of the interior Dirichlet problem, at least one of the reciprocal eigenvalues of the kernel matrix is 1. Consequently, the iteration solution would not converge at these frequencies. For the high frequency of oscillation, the iterative method converges well since all the reciprocal eigenvalues of the kernel matrix are within the radius of convergence.

E. Hydrodynamic Pressure, Added Mass, and Damping Coefficients

The non-dimensional hydrodynamic pressure (61) was derived in section III-D from the linearized Bernoulli equation:

$$\frac{p}{\rho g a} = \nu\phi \quad . \tag{61}$$

The longitudinal distribution of the hydrodynamic pressure for the heaving spheroid is shown in Figure 28. The girthwise distributions of the pressure at various sections are shown in the Figure 29. The 3-D pressure distribution is compared with the 2-D pressure near midship and near the ends in Figure 30 and 31, respectively.

The hydrodynamic forces are obtained by integrating the hydrodynamic pressure caused by the forced-motion in the direction of that mode over the mean submerged surface of the ship:

$$F_i = \iint_S p\, n_i\, ds = \rho g a \nu \tilde{F}_i \tag{91}$$

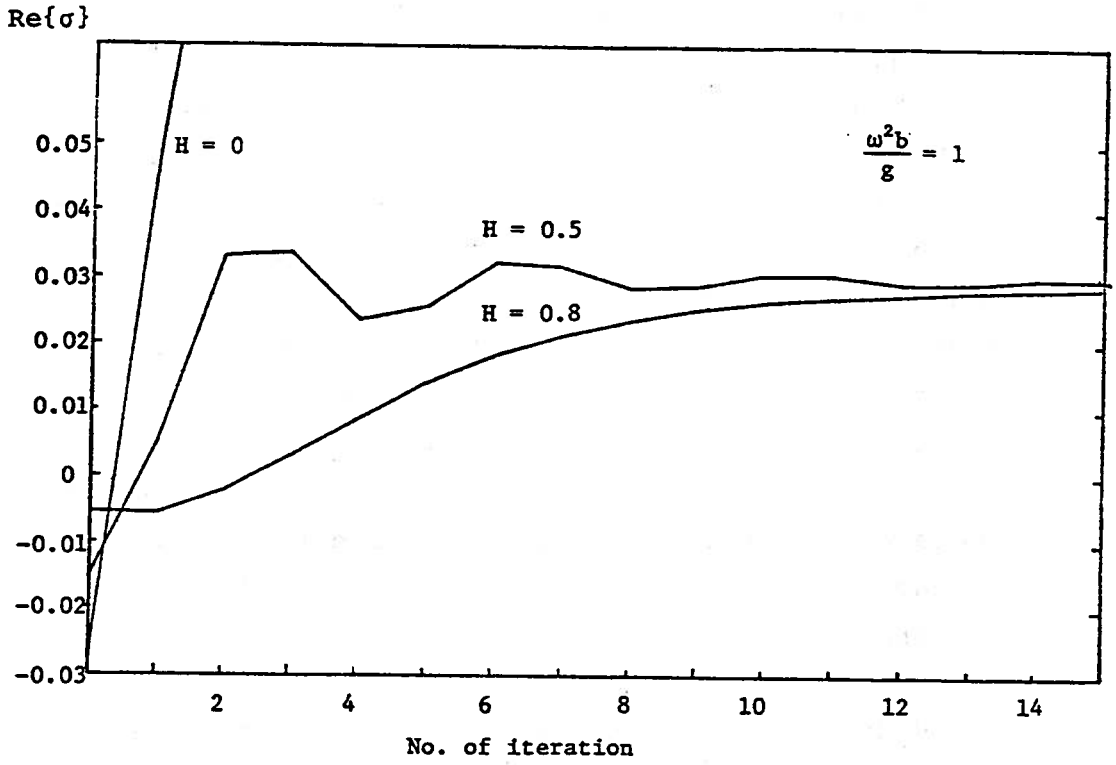

Figure 27. Convergence of the source density for the heaving sphere by the improved iteration method

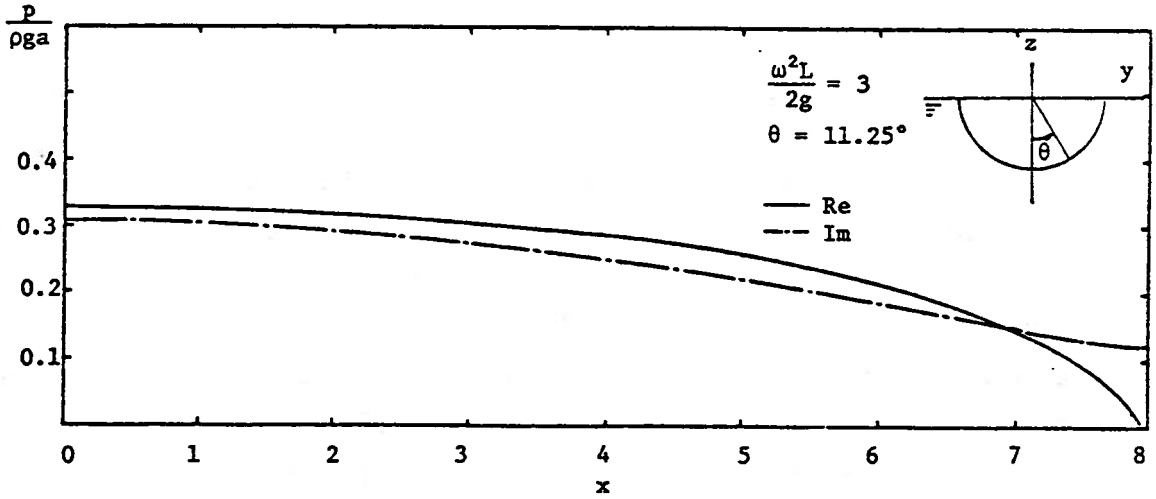

Figure 28. Longitudinal distribution of the pressure for the heaving spheroid (L/B=8)

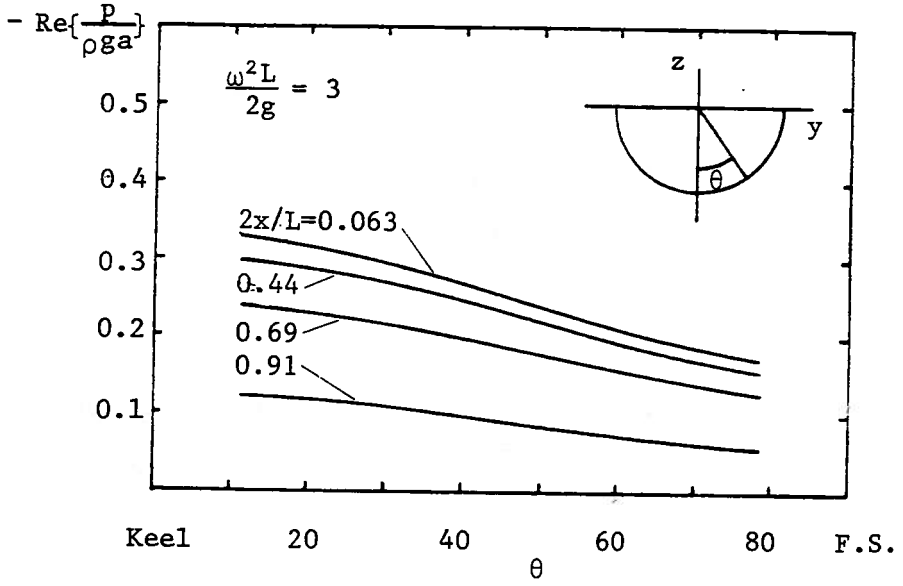

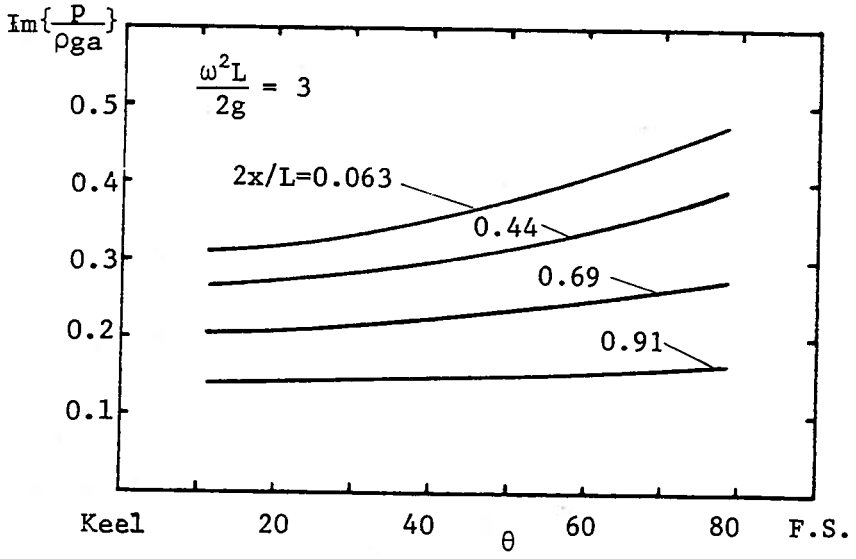

Figure 29. Pressure variation across the sections of the heaving spheroid (L/B=8)

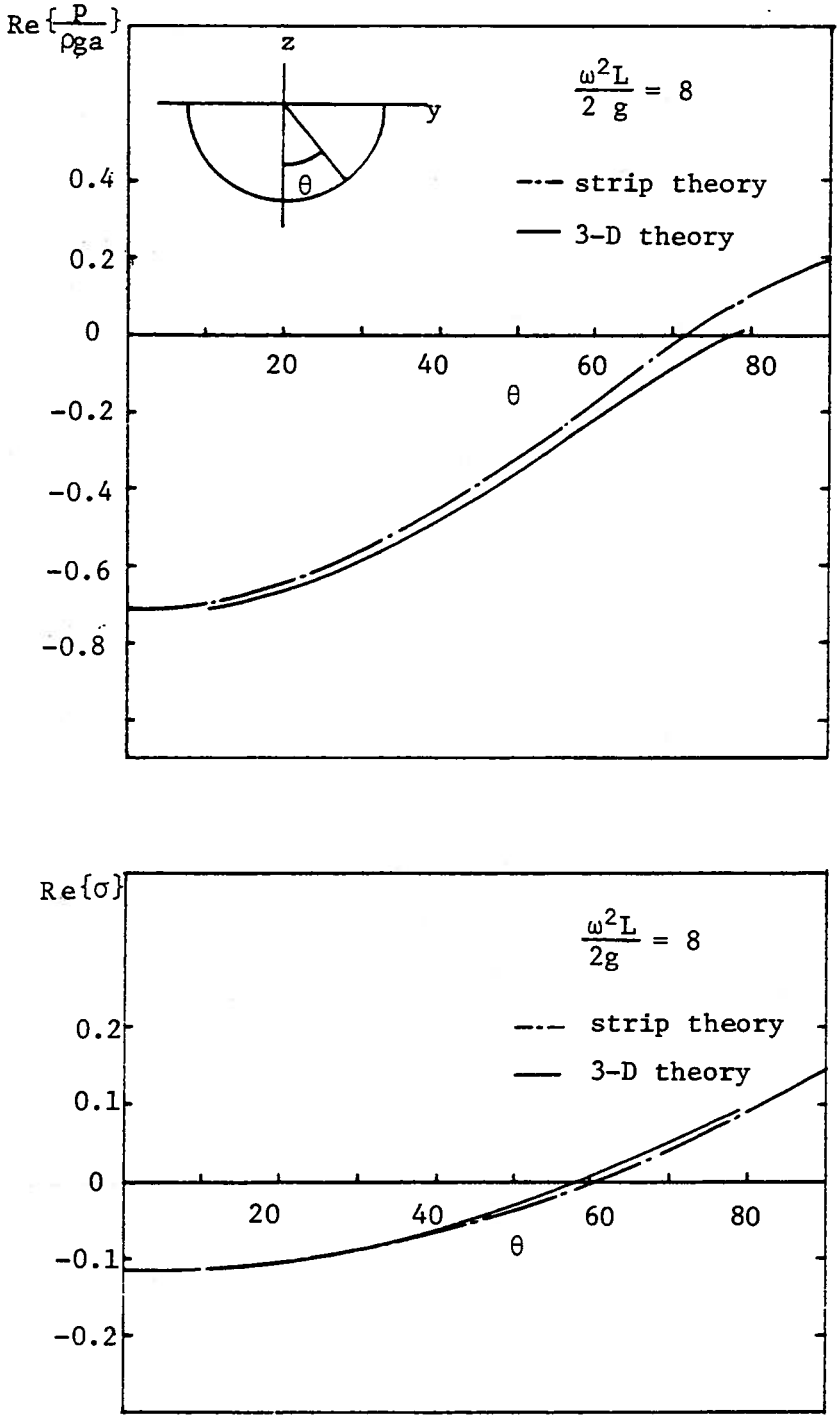

Figure 30. Girthwise distribution of the pressure and the source density near the midship (μ=0.063) of the heaving spheroid (L/B=8)

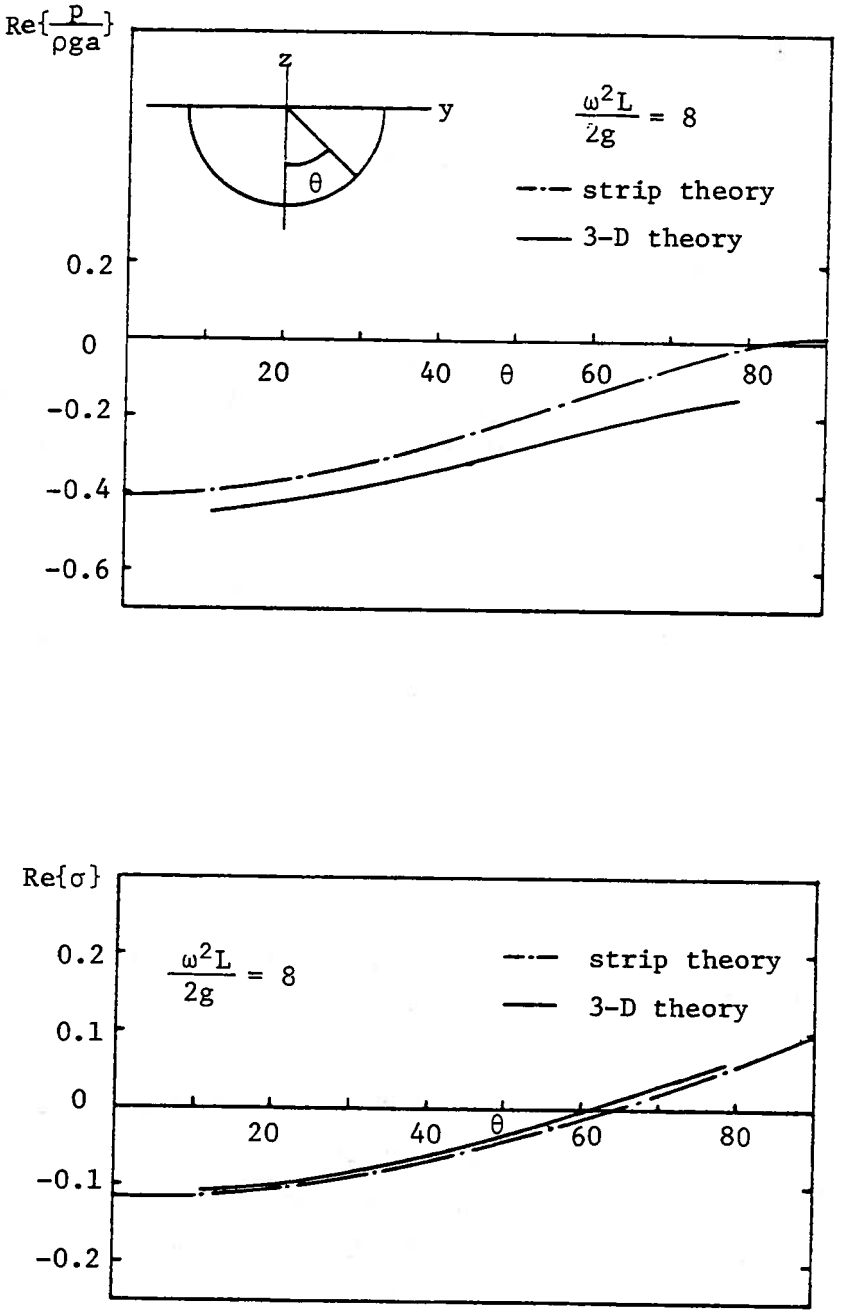

Figure 31. Girthwise distribution of the pressure and the source density near the end (μ=0.8) of the heaving spheroid (L/B=8)

where the non-dimensional hydrodynamic force, $\tilde{F}_i$, is given by

$$\tilde{F}_i = \iint_S \phi n_i \, dS \ .$$

The complex amplitude of the hydrodynamic forces due to forced motion is expressed in terms of added mass and damping coefficients as

$$F_i = - \left(-MC_a\omega^2 a + iMC_d\omega^2 a\right) \ , \qquad (92)$$

where M is the mass of the displaced fluid, C_a is the added mass coefficient, and C_d is the damping coefficient. The first term in the parenthesis is the force in phase with the acceleration of the body motion. The second term is the force in phase with the velocity of the body motion. By equating (91) and (92), the added mass coefficient and damping coefficient are defined, respectively, as follows:

$$C_a = \frac{\mathrm{Re}[\tilde{F}_i]}{V}$$

and

$$C_d = \frac{-\mathrm{Im}[\tilde{F}_i]}{V} \ ,$$

where V is the displaced volume of the body.

The added mass and damping coefficients for a heaving spheroid (L/B=8) are shown in Figures 32 and 33, respectively. The symmetry of the spheroid has been utilized to reduce the size of the linear algebraic equation. Forty elements have been used to approximate the quadrant of the semi-spheroid. The accuracy of the result depends on the number of elements used to represent the body surface. It also depends on how the elements are distributed over the surface. In general, more elements should be distributed over a region where body shape changes rapidly. For the high frequency of oscillation, more elements are needed for accuracy.

The three dimensional added mass is compared with the

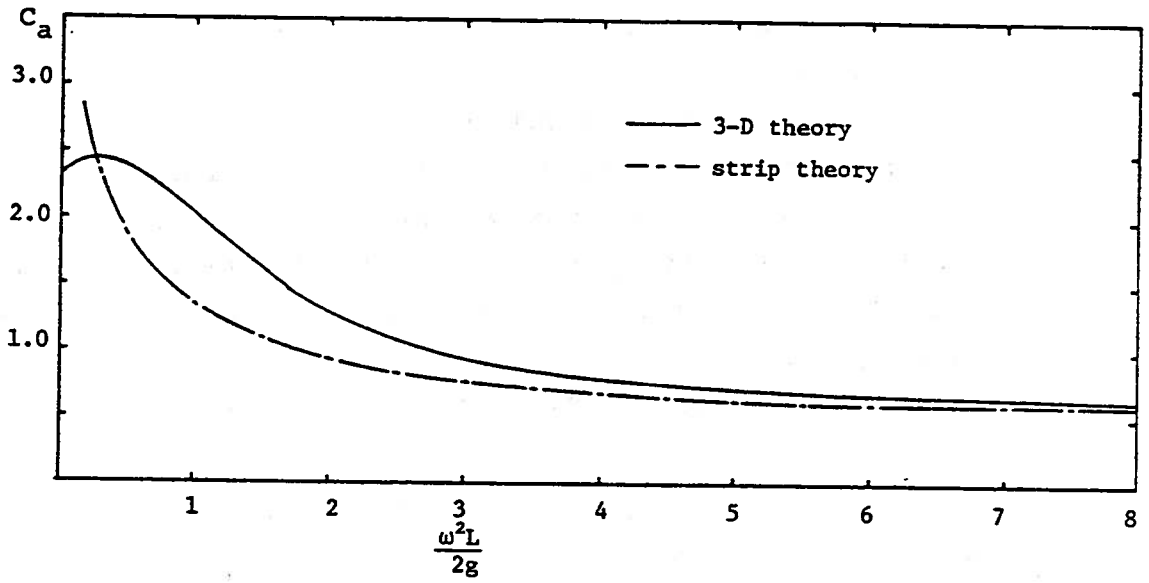

Figure 32. Added mass coefficient for the heaving spheroid (L/B=8)

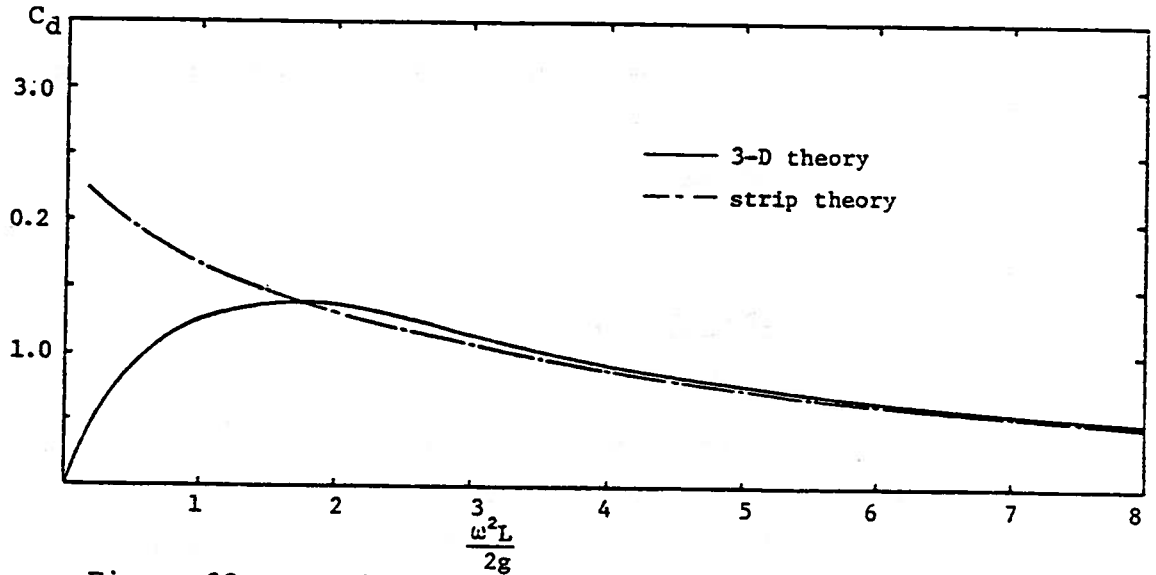

Figure 33. Damping coefficient for the heaving spheroid (L/B=8)

strip theory added mass for the heaving spheroid in Figure 32. The two theories have a completely different asymptotic behavior for the low frequency limit. Added mass becomes infinite using the strip theory, while it is finite using 3-D theory. Thus, the error by strip theory becomes infinite for the low frequency limit. For the high frequency limit, the error by strip theory is finite. The error by strip theory for the infinitely high frequency limit is 5.5% for the heaving spheroid of L/B ratio 8 (Figure 24).

For finite frequencies , the total J factor lies between the two limits. For a fairly high frequency of oscillation, the strip theory approximates the 3-D result well. Eventually the error would approach the finite value of the high frequency limit.

F. Sectional Added Mass, Damping Coefficients, and the 3-D Effect

The sectional hydrodynamic force is computed from the pressure integration over the contour at station x:

$$\tilde{F}_j(x) = \int_{C(x)} \phi n_i \frac{d\ell}{\sqrt{1-n_1^2}} \quad .$$

The sectional added mass and damping coefficients are defined as

$$C_a(x) = \frac{\mathrm{Re}[\tilde{F}_j(x)]}{A_0} ,$$

and

$$C_d(x) = \frac{-\mathrm{Im}[\tilde{F}_j(x)]}{A_0} ,$$

where A_0 is the sectional area at midship.

The spheroid is chosen to see the 3-D effect on the sectional added mass distribution along the x axis under the presence of the free surface, since the spheroid has a unique geometry for which the strip theory solution is a constant ratio of the 3-D exact solution in the infinite fluid. In

other words, the strip solution produces a constant error ratio not only near the ends, but also near midship. This error ratio decreases as the spheroid becomes more slender.

Figures 34 through 36 show the sectional added mass distribution for the various frequencies ($\omega^2 L/2g = 3,8,12$) using both 3-D and 2-D theories. For the low frequency ($\omega^2 L/2g=3$), the sectional added mass distribution from the 2-D strip solution is quite different from the three-dimensional result (see Figure 34). Moreover the ratio of the 3-D added mass to the 2-D added mass is not constant at each section. The local J factor varies relatively slowly along the middle section. As it approaches the end of spheroid, the J factor moves toward zero. The strip theory overestimates the sectional added mass near the end. But the strip theory underestimates the total added mass, since the strip solution underestimates near midship which is the source of the main contribution. (It is not offset by the strip thoery overestimations near the ends.) For the high frequency ($\omega^2 B/2g = 12$), the sectional added mass computed by the strip theory still deviates from the 3-D solution, but the deviation is smaller than in the lower frequency case. Near the end of the spheroid, the strip theory still overestimates the sectional added mass. However, this region of discrepancy is narrowly restricted to the very end. The total J factor is 0.987. The strip solution overestimates the 3-D solution. The total J factor would eventually approach a high frequency limit of 0.945 (see Figure 24). As the frequency increases, the sectional added mass distribution of the strip thory approaches the 3-D result with a constant error ratio. The 3-D effect near the end disappears in the high frequency limit.

Figure 37 through 39 show the sectional added mass distribution for the vibrating spheroid using both 3-D and 2-D theories. The differences between the 3-D and 2-D added mass distribution are greater for the low frequency than for the high frequency.

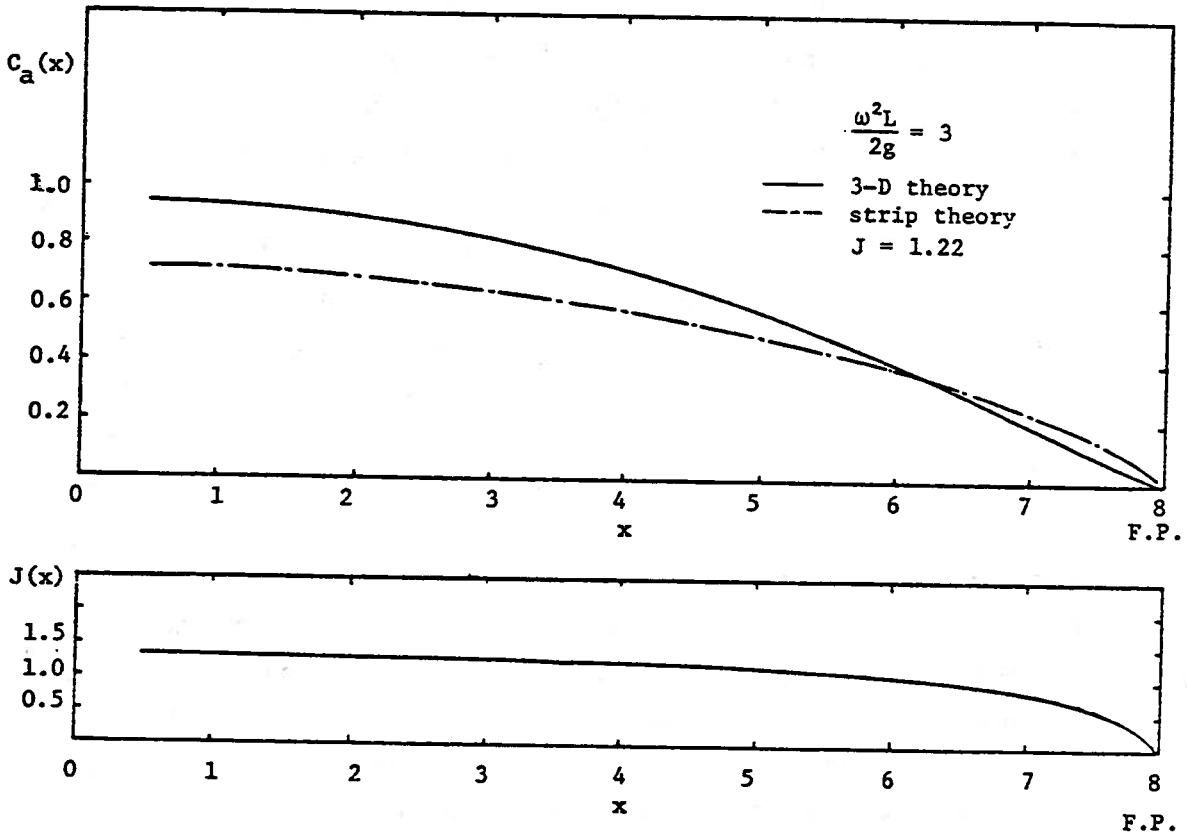

Figure 34 . Axial distribution of the added mass coefficient for the heaving spheroid (L/B=8)

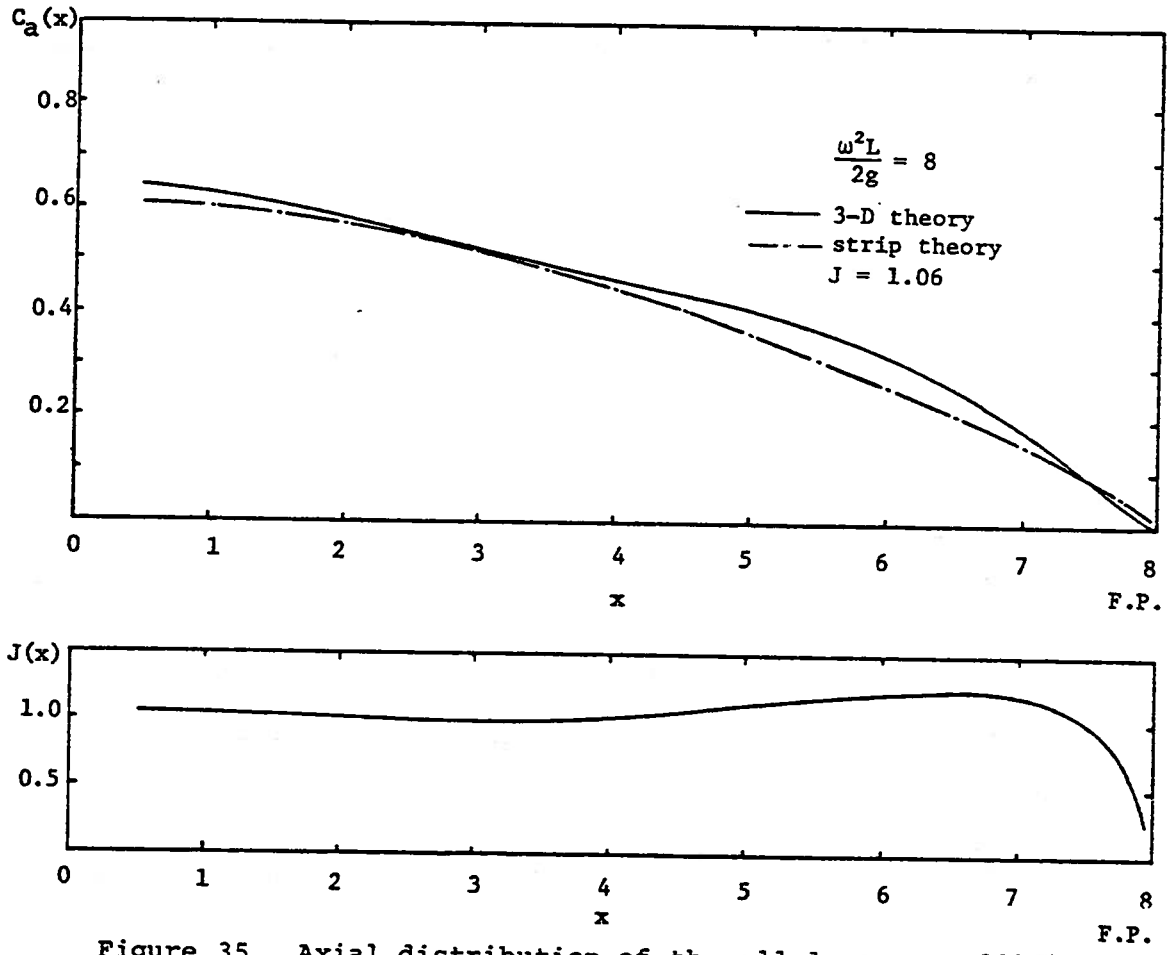

Figure 35. Axial distribution of the added mass coefficient for the heaving spheroid (L/B=8)

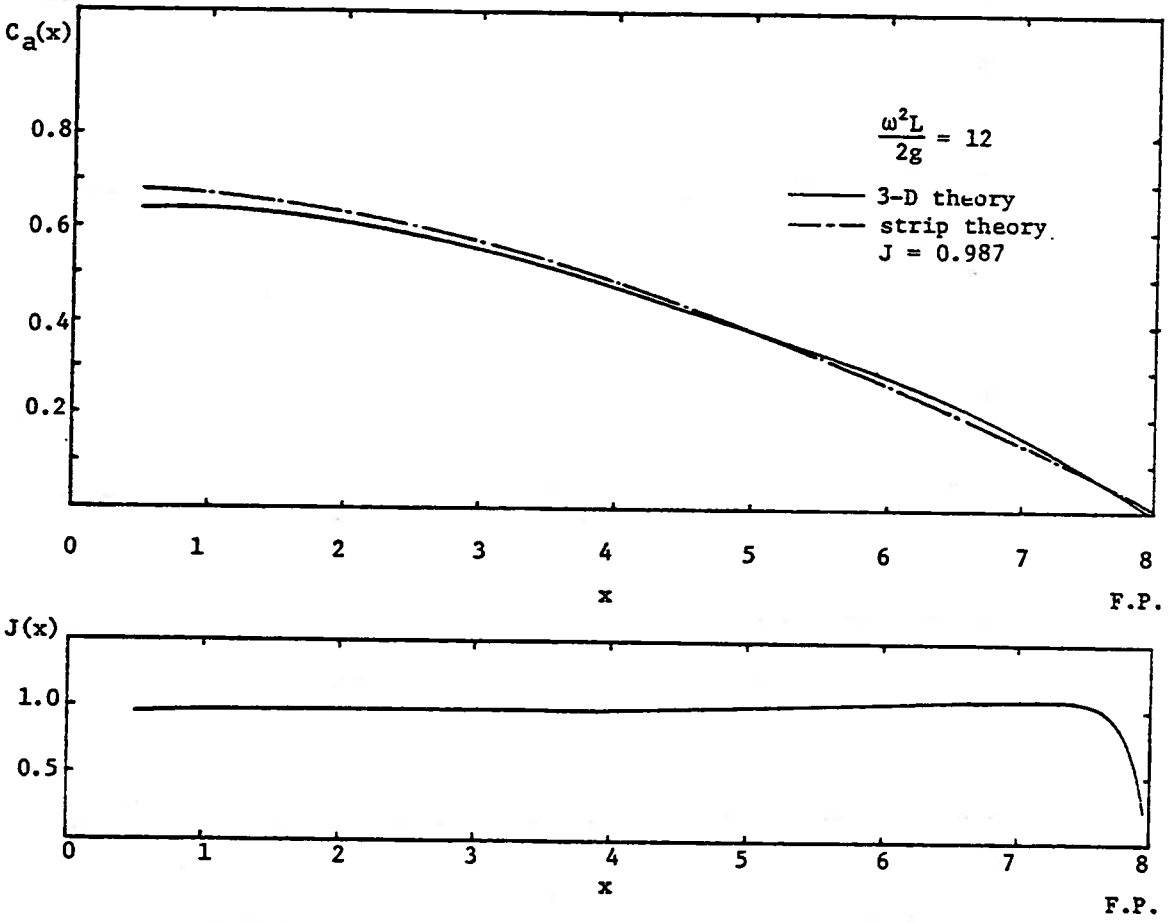

Figure 36. Axial distribution of the added mass coefficient for the heaving spheroid (L/B=8)

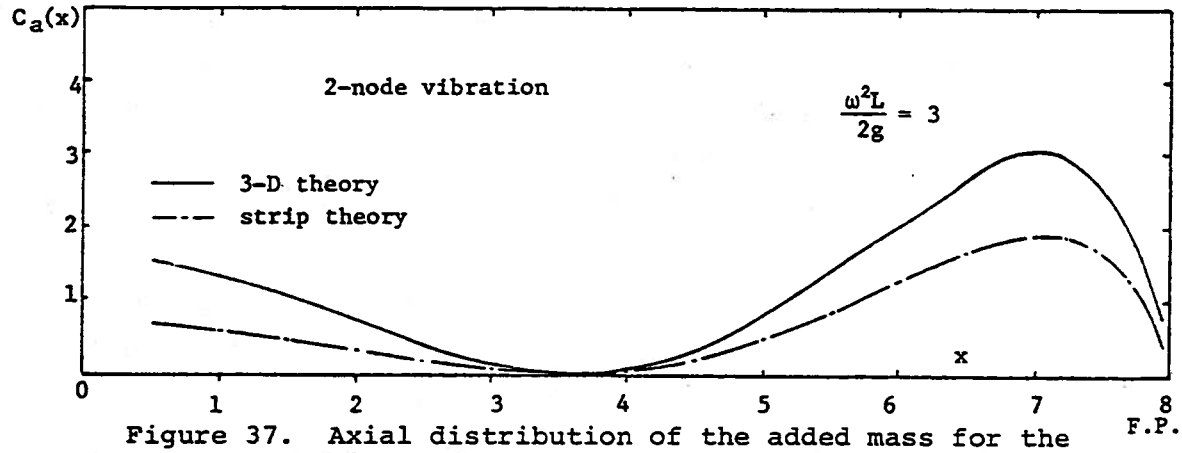

Figure 37. Axial distribution of the added mass for the vibrating spheroid

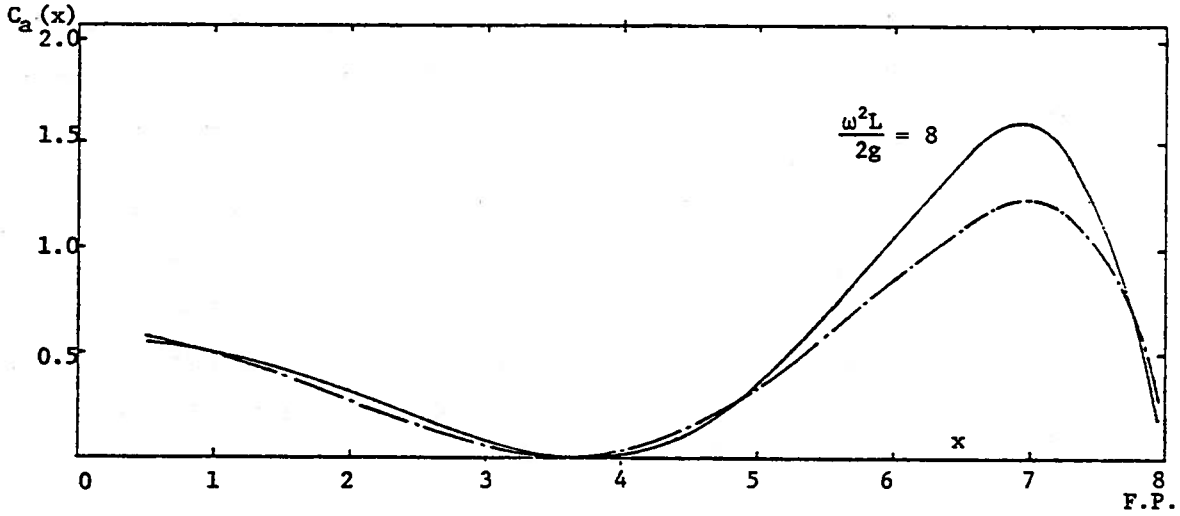

Figure 38. Axial distribution of the added mass for the vibrating spheroid

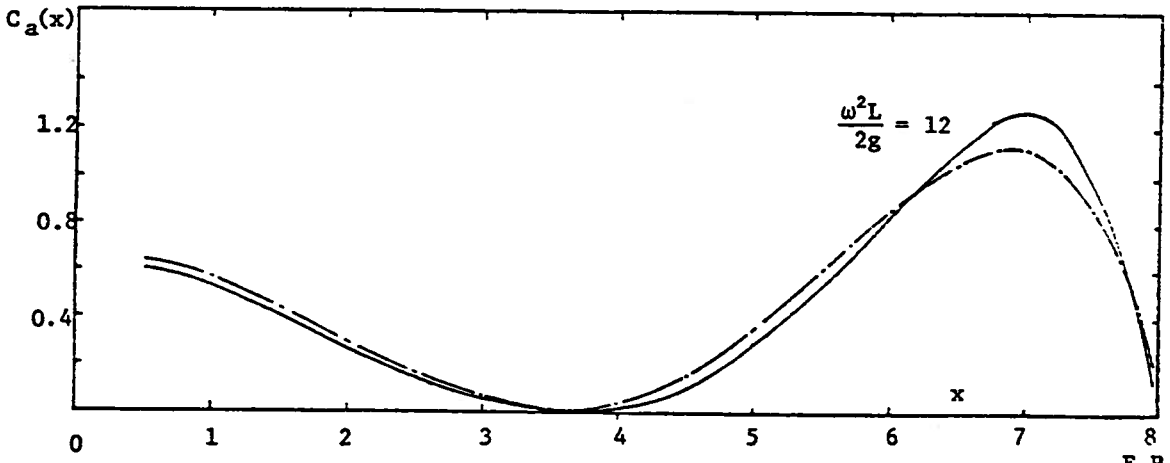

Figure 39. Axial distribution of the added mass for the vibrating spheroid

H. Summary

The Fredholm integral equation of the second kind derived by using sources is applied to solve the exact 3-D radiation problem. The integral equation is solved by several different methods: equivalent linear algebraic equations, successive approximation by Neumann series, improved iteration using Buckner-Chertock series, and frequency iteration using the infinite fluid solution. This 3-D source distribution method can be applied for a general arbitrary body, for which the 2-D strip theory cannot be applied. The body surface need not be slender or analytically defined. It must, however, be smooth enough to have a continuous normal vector. The method may give less accurate results for a body with sharp edges where the normal vector has discontinuity. However, for a practical computation, the edge can be rounded to give a finite curvature.

The pressure distribution, added mass coefficient, and damping coefficient for the heaving spheroid at the free surface are computed. The 3-D effect on the added mass is also studied. The 3-D effect on the added mass distribution is more significant for the low frequency than for the high frequency of oscillation. The total added mass found by strip theory gives a poorer approximation for the low frequency than for the high frequency limit. For a fairly high frequency, the strip theory is a good approximation.

VI. WAVE EXCITING FORCES

Exciting forces caused by waves can be computed by several different methods. One method solves the diffraction problem directly. The exact diffraction problems are difficult to solve. No analytic solutions exist for an arbitrary three-dimensional body. Thus, one has to depend on numerical methods. Various forms of integral equations (23), (28), and (32) are available to solve the diffraction problem. One is the integral equation (23) which uses a source distribution. The integral equation method requires large storage space and computing time, since the symmetry condition of the body geometry cannot be utilized for oblique wave. A new diffraction problem must be solved for each wave heading angle.

Alternatively, the direct diffraction problem can be avoided by use of the Haskind reciprocity relationship, which can determine the total force by the diffracted waves without solving the diffraction problem. The total force is converted into an integral involving the forced motion potential by the application of Green's theorem. Thus, we need to know only the forced motion velocity potential, which we must solve for the hydrodynamic coefficients of the equation of motion. Furthermore, it is not necessary to solve the problem for each wave heading angle. However, Haskind's method does not give the actual pressure distribution. The identity of the actual pressure distribution has already been lost by applying Green's theorem in the whole fluid domain. The integrand of the Haskind formula cannot be identified as the actual force distribution; however, the actual force distribution is not necessary to set up the equation of motion. Only the total integrated exciting forces are needed to set up the equation of motion. If one wanted

to compute the load distribution or the bending moment at midship, refer to an alternative method derived by Ogilvie (1971).

This study uses the Haskind formula to compute the exciting forces resulting from the diffracted wave, because it is an efficient and economical method, especially for the symmetric body. The author solves the direct diffraction problem by source distribution method and computes the pressure distribution and sectional forces for the head sea. These results are compared with Faltinsen's (1971) results and Lee's experimental results(unpublished, described by Faltinsen).

A. Wave Exciting Forces by Haskind Formula and Strip Theory

The complex amplitude of the wave exciting forces is obtained by integrating the pressure caused by incident and diffracted waves over the hull surface:

$$F_i^{w*} = -i\omega\rho \iint_S (\Phi_0 + \Phi_7)\, n_i\, dS \,, \tag{93}$$

where Φ_0 is the complex amplitude of the incident wave potential, which is given by

$$\Phi_0 = \frac{igh}{\omega} e^{\nu z} e^{-i(\nu x \cos\chi + \nu y \sin\chi)} \,,$$

h is the wave amplitude, ν is the wave number, χ is the heading angle of the wave, and Φ_7 is the complex amplitude of the diffracted wave potential.

Applying the Haskind reciprocity relationship and hull boundary condition to (93), we get

$$F_i^{w} = -i\omega\rho \iint_S (\Phi_0\, n_i - \phi_i \frac{\partial \Phi_0}{\partial n})\, dS \,. \tag{94}$$

The first term in the integral of (94) is the well-known Froude-Kryloff force, while the second term is the diffracted wave force. Since we know ϕ_i from the forced motion prob-

---

*Superscript w denotes wave action. The wave exciting force F^w, should be distinguished from the hydrodynamic force resulting from forced motion.

lem, the diffracted wave force is obtained by simple integration. Non-dimensionalizing the wave force (94) by the hydrostatic force, we get

$$\frac{F_i^w}{\rho g h A_w} = \frac{1}{A_w}\iint_S (\phi_0 \, n_i - \phi_i \frac{\partial \phi_0}{\partial n}) dS, \qquad (95)$$

where A_w is water plane area and non-dimensional potential of incident wave is given by $\phi_0 = \omega\Phi_0/igh$. The real and imaginary parts of the exciting forces are the forces in phase with the water elevation and vertical velocity component, respectively. The amplitudes and phase angles of wave forces causing heave on the spheroid are shown in Figures 41 and 42. The phase angle is defined as the leading angle of wave force over the wave crest at midship.

For the strip theory* , ϕ_i is replaced by 2-D potential in Haskind formula (94) assuming that forced motion potential satisfies approximately the 2-D Laplace equation near the body of the hull. Furthermore, the 3-D normal also is replaced by the 2-D normal, assuming that the body geometry changes slowly in x direction. Thus we get the 2-D version of the Haskind formula from (94):

$$F_i^w = \rho h \int_{-L/2}^{L/2} dx \left[g e^{-i\nu x \cos\chi} \int_{C(x)} N_i e^{-i\nu y \sin\chi} e^{\nu z} d\ell \right.$$
$$\left. - e^{-i\nu x \cos\chi} \int_{C(x)} \omega^2 (N_3 - iN_2 \sin\chi) e^{-i\nu y \sin\chi} e^{\nu z} \phi_i^{2\text{-}D} d\ell \right].$$

This is the same as the sum of the equations (149) and (150) of Salvesen, Tuck, and Faltinsen (1970). By replacing the integral of the 2-D potential with the 2-D sectional added mass and damping coefficients using (65), we get

$$F_3^w = \rho h \int_{-L/2}^{L/2} dx \, e^{i\nu x} e^{-\nu T(x)} \left[g b(x) - A_0 \omega^2 \{ C_a(x) - i \, C_d(x) \} \right],$$

for heave in head sea which is the sum of equation (32) and (33) of Salvesen, Tuck, and Faltinsen (1970). T(x) is the effective draft of section at x, b(x) is the half beam of the section, and A_0 is the sectional area at the midship.

---

*Strip theory refers to Salvesen, Tuck, and Faltinsen's strip theory (1970) unless otherwise specified. This should be distinguished from Faltinsen's diffraction theory (1971).

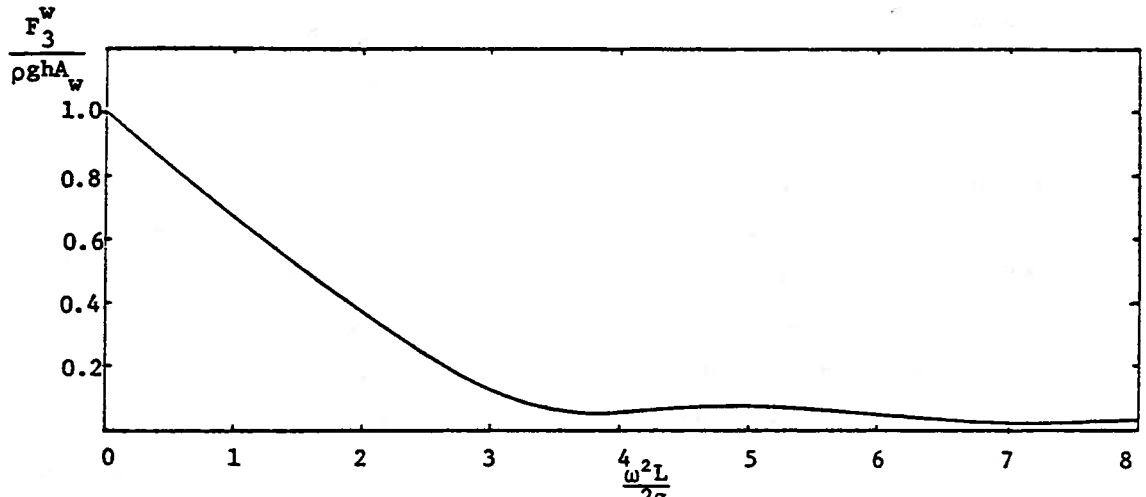

Figure 40. Amplitude of the wave force on the spheroid (L/B=8) for heave

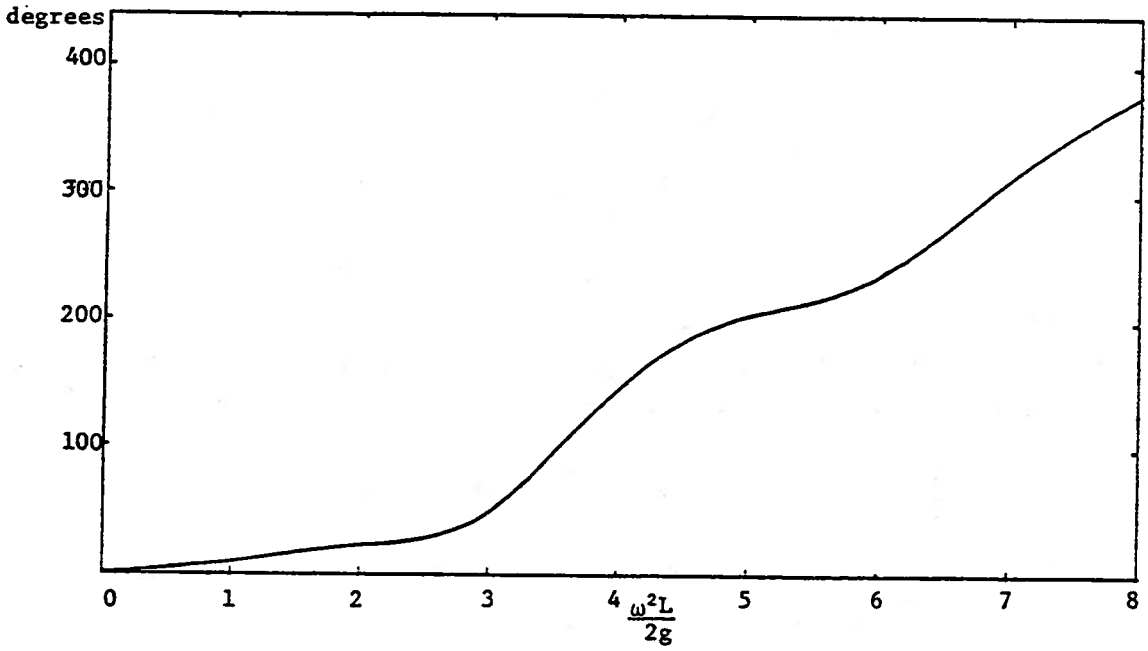

Figure 41. Phase lead of the wave force on the spheroid (L/B=8) for heave

B. Direct Diffraction Problem and Wave Pressure

The diffracted wave potential is computed by solving the integral equation (23) by using source distribution:

$$-\frac{\sigma}{2}7 - \frac{1}{4\pi}\iint_S \sigma_7(Q)\frac{\partial G}{\partial n_P}(P,Q)\,dS(Q) = -\frac{\partial \phi_0}{\partial n} \quad . \tag{23}$$

The numerical method to solve the integral equation is the same as the 3-D radiation problem, except for the body boundary condition. The numerical method is described in Appendix B. Once the unknown source density is determined from the body boundary condition, the non-dimensional diffracted wave potential is computed by

$$\phi_7(P) = -\frac{1}{4\pi}\iint_S \sigma_7(Q)G(P,Q)\,dS(Q) \quad .$$

The dimensional form of the diffracted wave potential is given by

$$\Phi_7 = \frac{igh}{\omega}\phi_7 \quad .$$

The complex amplitude of the wave pressure caused by diffracted and incident waves is represented in terms of velocity potential:

$$p^w = -i\omega\rho(\Phi_0 + \Phi_7).$$

The wave pressure is non-dimensionalized by hydrostatic pressure:

$$\frac{p^w}{\rho g h} = \phi_0 + \phi_7 \quad .$$

Note that the wave pressure has both the real and imaginary parts. The amplitude and phase angle of the wave pressure are computed. The distribution of wave pressure is compared with Faltinsen's results and C. M. Lee's experimental results with the spheroid for short waves ($\lambda/L=0.5$) in a head sea. These results are shown in Figures 42 through 44. Note that Faltinsen's results and C. M. Lee's results are for the low speed case ($F_n=0.082$), while the 3-D result is for zero

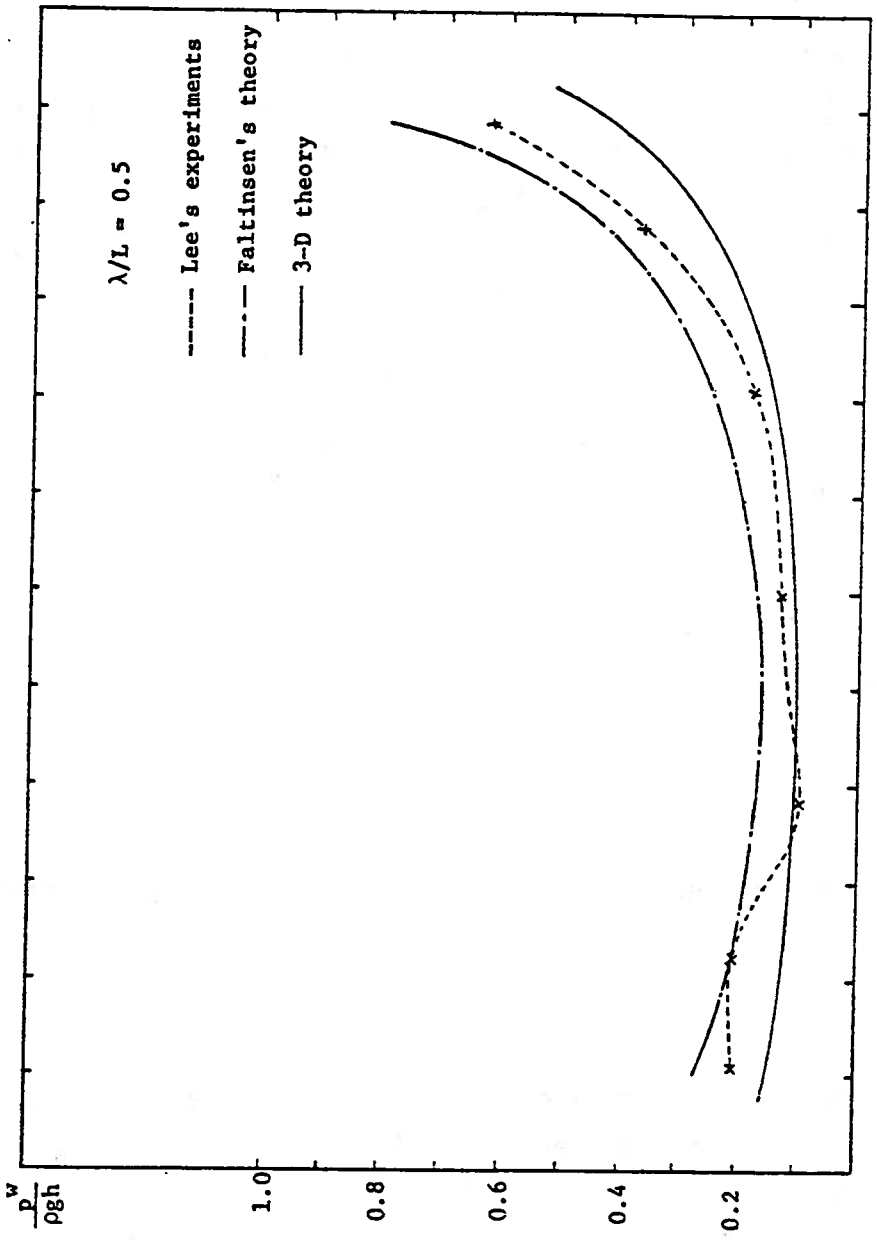

Figure 42. Longitudinal distribution of the wave pressure along the keel of the spheroid (L/B=6)

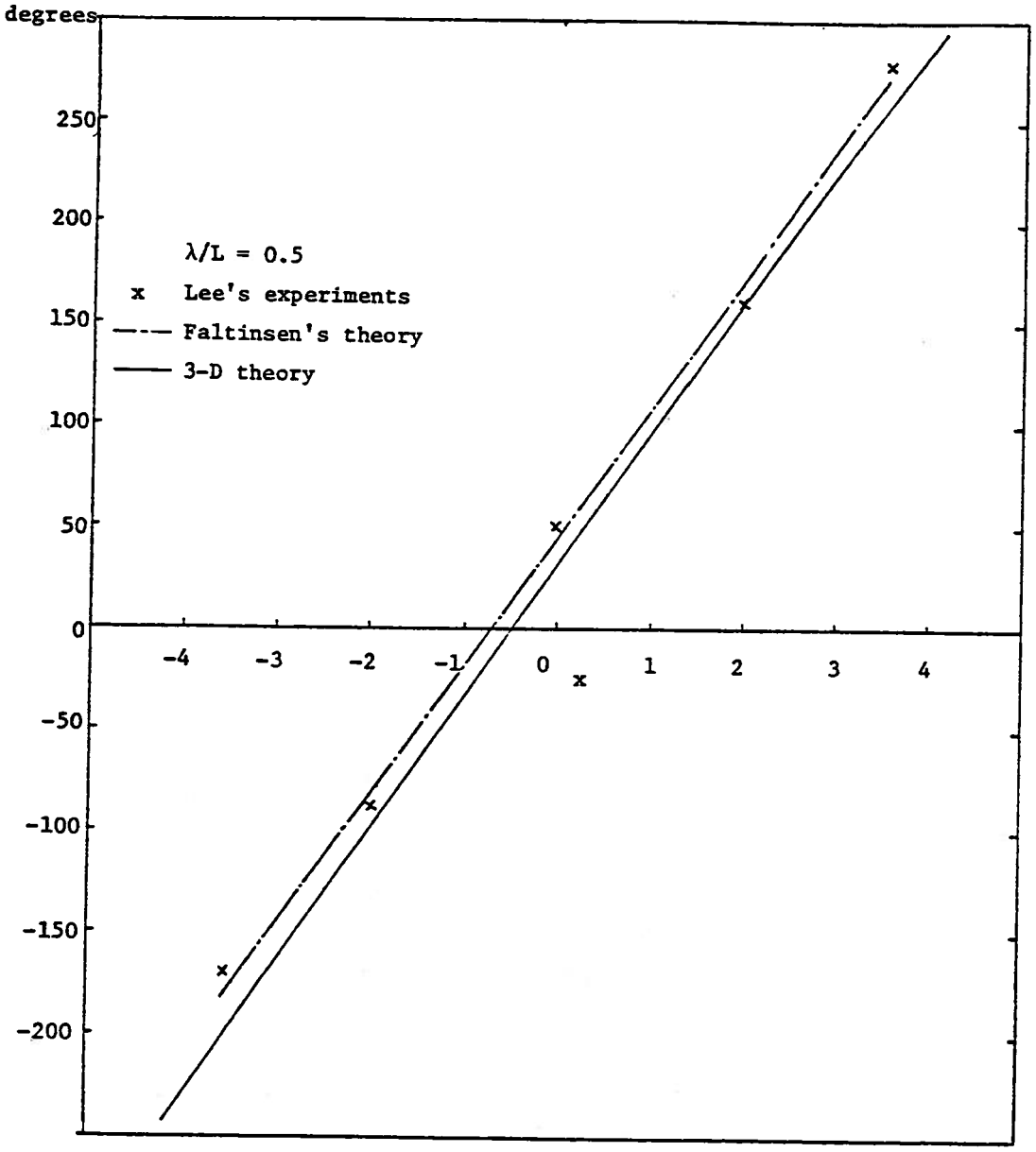

Figure 43. Longitudinal distribution of the phase angle of the wave pressure on the spheroid (L/B=6)

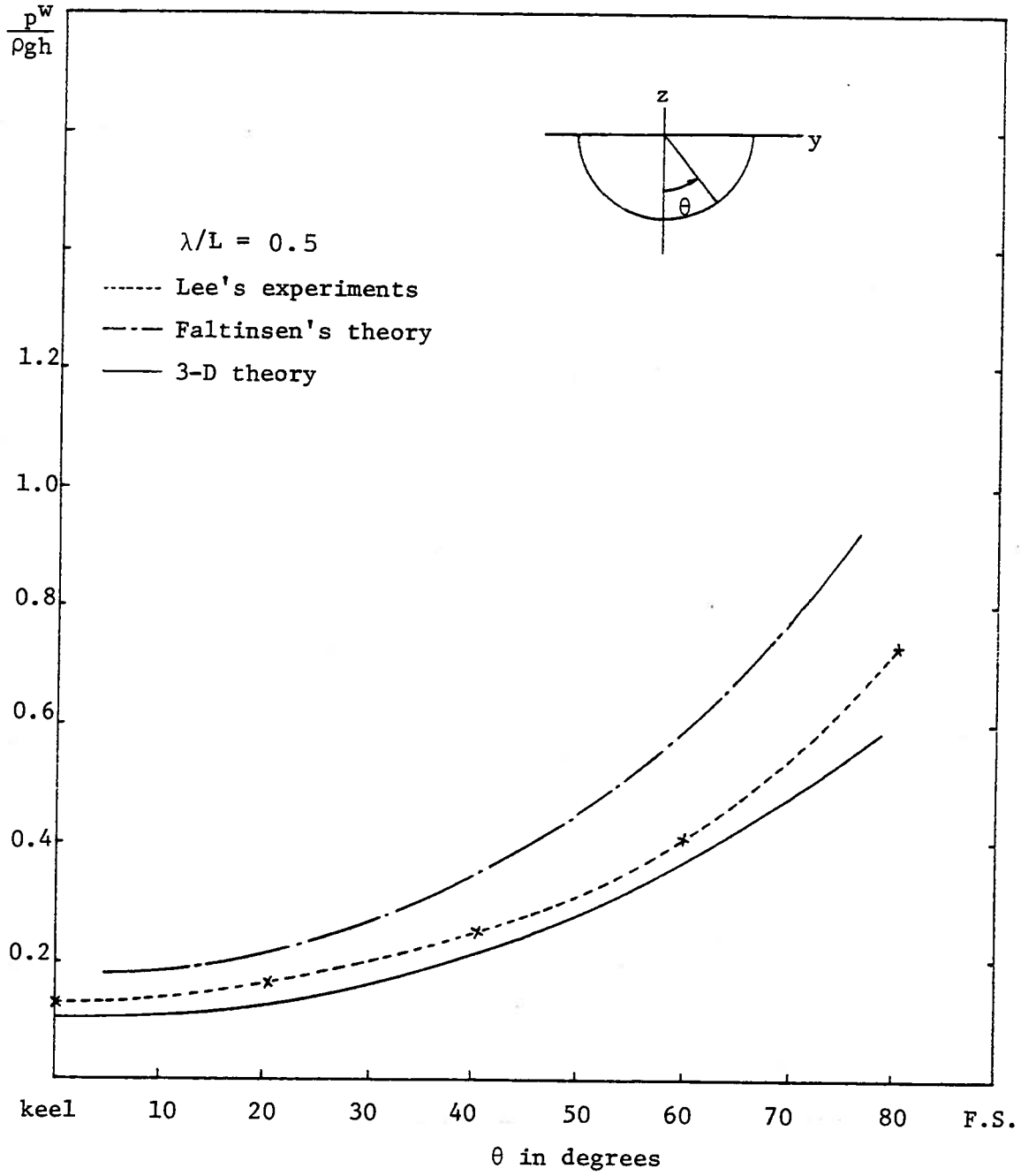

Figure 44. Pressure variation along the midship section of the spheroid (L/B=6)

speed. Figure 42 shows the longitudinal distribution of pressure along the keel of the spheroid (L/B=6). 3-D theory gives the lowest value, even though all the results show similar qualitative behavior. Figure 43 shows the longitudinal distribution of the phase angle of the pressure. Faltinsen's theory predicts the phase angle to be 45 degrees before the phase angle of the Froude-Kriloff pressure, while 3-D diffraction theory shows a lower value of 30.4 degrees. Figure 44 shows the girthwise pressure variation along the midship section. Faltinsen's results overestimate those found using 3-D theory.

C. Distribution of the Sectional Wave Forces

Newman (1970) proposed a method to compute the distribution of the wave forces by applying Green's theorem directly in the 2-D domain. However, one has to solve the 2-D boundary value problem, the governing equation for which is the 2-D Helmholz equation instead of the 2-D Laplace equation.

Ogilvie (1974) derives a similar relationship to compute the wave force per unit length without solving the diffraction problem. He applies Green's theorem in the 3-D strip with width Δx and evaluates the integrals over all the boundary surfaces.

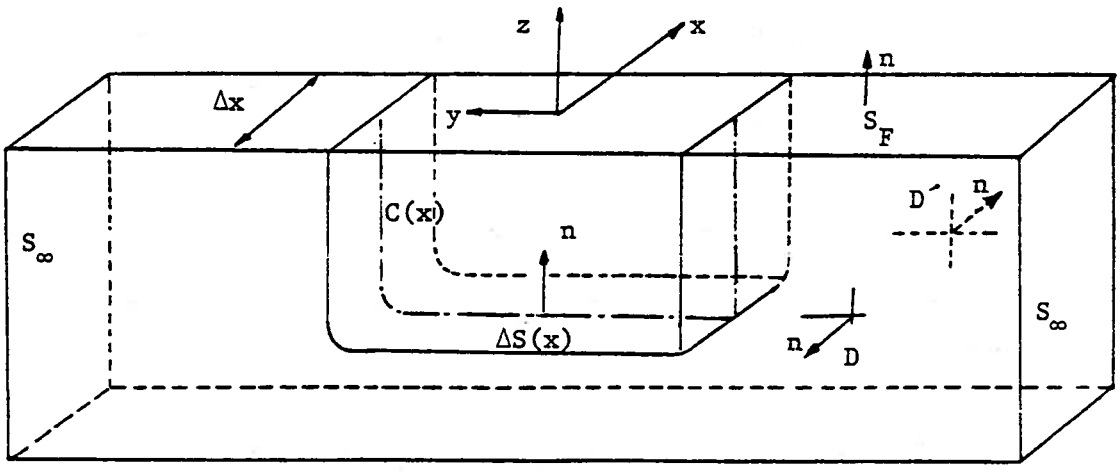

Figure 45. Strip along which sectional force is computed.

Applying Green's theorem to the strip shown in Figure 45, we get

$$\iint_{\Sigma S} \left(\frac{\partial \phi_i}{\partial n} \Phi_7 - \phi_i \frac{\partial \Phi_7}{\partial n}\right) dS = 0,$$

where ΣS includes all the boundary surfaces. Since ϕ_i and Φ_7 satisfy the same free surface and radiation conditions, the integral over those surfaces vanishes. The integral over D and D´ remains, however. Then we get the sectional wave exciting force on the strip S(x) at x as

$$\Delta F^W(x) = -i\omega\rho \left[\iint_{S(x)} \left(\Phi_0 n_i - \phi_i \frac{\partial \Phi_0}{\partial n}\right) dS - \iint_{D+D'} \left(\Phi_7 \frac{\partial \phi_i}{\partial n} - \phi_i \frac{\partial \Phi_7}{\partial n}\right) dS \right]. \tag{96}$$

The integral over D and D´ can be combined as

$$\iint_{D+D'} \left(\frac{\partial \phi_i}{\partial n} \Phi_7 - \phi_i \frac{\partial \Phi_7}{\partial n}\right) dS \simeq \Delta x \iint_D \frac{\partial}{\partial x}\left(\frac{\partial \phi_i}{\partial x}\Phi_7 - \phi_i \frac{\partial \Phi_7}{\partial x}\right) dS,$$

$$= \Delta x \iint_D \left(\Phi_7 \frac{\partial^2 \phi_i}{\partial x^2} - \phi_i \frac{\partial^2 \Phi_7}{\partial x^2}\right) dS.$$

If we further assume that (97)

$$\frac{\partial^2 \phi_i}{\partial x^2} \simeq -k^2 \phi_i \text{ , and } \frac{\partial^2 \Phi_7}{\partial x^2} \simeq -k^2 \Phi_7, \text{ where } k = \nu \cos \chi,$$

the integral over D also vanishes. However, this ϕ_i must satisfy the 2-D Helmholz equation rather than the 3-D Laplace equation. The integral over D will not vanish, however, since we have only

$$\frac{\partial^2 \phi_i}{\partial x^2} = -\frac{\partial^2 \phi_i}{\partial y^2} - \frac{\partial^2 \phi_i}{\partial z^2} \text{ , and } \frac{\partial^2 \Phi_7}{\partial x^2} = -\frac{\partial^2 \Phi_7}{\partial y^2} - \frac{\partial^2 \Phi_7}{\partial z^2}.$$

By using the equation (97) and some manipulation, we get the wave force per unit length as

$$\frac{\Delta F^W(x)}{\Delta x} = -i\omega\rho \left[\int_{C(x)} \left(\Phi_0 n_i - \phi_i \frac{\partial \Phi_0}{\partial n}\right) \frac{d\ell}{\sqrt{1-n_1^2}} - \iint_D \left(\frac{\partial^2 \phi_i}{\partial x^2}\Phi_7 - \frac{\partial^2 \Phi_7}{\partial x^2}\phi_i\right) dS \right], \tag{98}$$

where ϕ_i is 3-D exact potential and n_i is still the 3-D normal. This formula is exact since no strip assumption is made, but it is not useful for practical computation since the second integral includes the diffracted wave potential, which we want to avoid. The first integral is the integrand of the Haskind formula (94). Thus, the integral over D is the difference between the 3-D sectional force and the integrand of the Haskind formula. The difference is greater for short waves than for long waves.

The sectional forces caused by waves are computed from direct pressure integration along the girth of the section. Non-dimensionalizing the sectional wave forces results in

$$\frac{F^W(x)\ \nu}{\rho g h} = \int_{C(x)} (\phi_0 + \phi_7)\ n_i\ \frac{d\ell}{\sqrt{1-n_1^2}} \quad .$$

The instantaneous profiles of the sectional wave force for the heave of a spheroid is shown in Figure 46.

D. 3-D Effect on Wave Exciting Forces

The longitudinal distribution of the wave exciting forces for heave is computed by solving the direct 3-D diffraction problem for the two different waves ($\nu L/2 = 3,8$). The sectional wave forces on the spheroid determined by 3-D diffraction theory are compared with those computed by 3-D Haskind formula, and 2-D strip theory in Figures 47 and 48. The 3-D theory shows the end effects for head seas because of the significant deformation of the waves near the ship's bow and stern. The wave force determined by 3-D theory has a higher value near the bow and lower value near the stern than that of the strip theory for head sea. The 3-D theory and Haskind formula show asymmetrical behavior about the midship, while the 2-D theory is symmetrical fore and aft.

The strip theory does not predict the attenuation of the wave forces for the head sea. It does not distinguish differences in the magnitude of wave forces near the bow and near the stern. The difference between the 3-D theory and the integrand of the Haskind formula is significant especially for the short waves. This confirms that the integrand of the Haskind formula cannot be identified as an actual force distribution. The discrepency between the theories for the wave force distribution is greater for the short waves than for the long waves. However, the phase angle shows good agreement between theories.

The integrated forces from the bow to station x are plotted in Figure 49. It shows that the integrated wave force determined by Haskind formula approaches the total force determined by the 3-D diffraction theory. This confirms that the Haskind formula should be used for computing the total force, not for the distribution of forces.

Figures 50 and 51 show the distribution of the wave forces for the springing mode. The attenuation of the wave forces along the spheroid is more significant for the springing mode than for the heave.

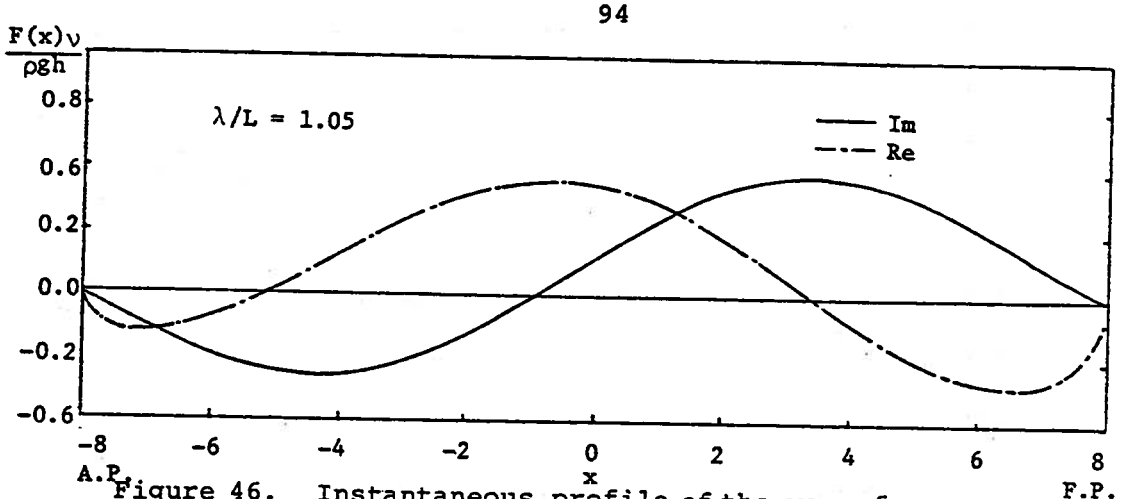

Figure 46. Instantaneous profile of the wave force on the spheroid (L/B=8) for heave (νL/2 = 3) in head sea

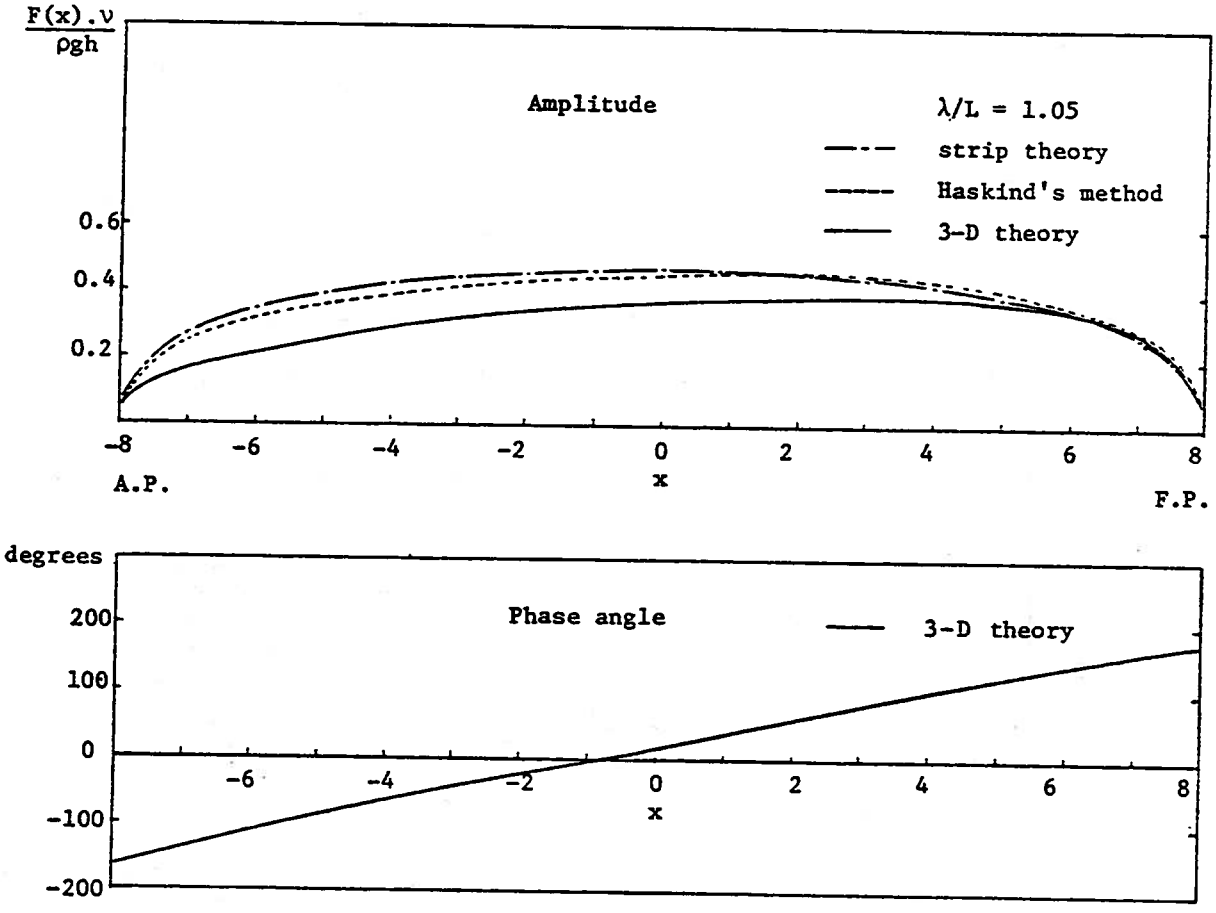

Figure 47. Longitudinal distribution of the wave force on the spheroid for heave (νL/2 = 3)

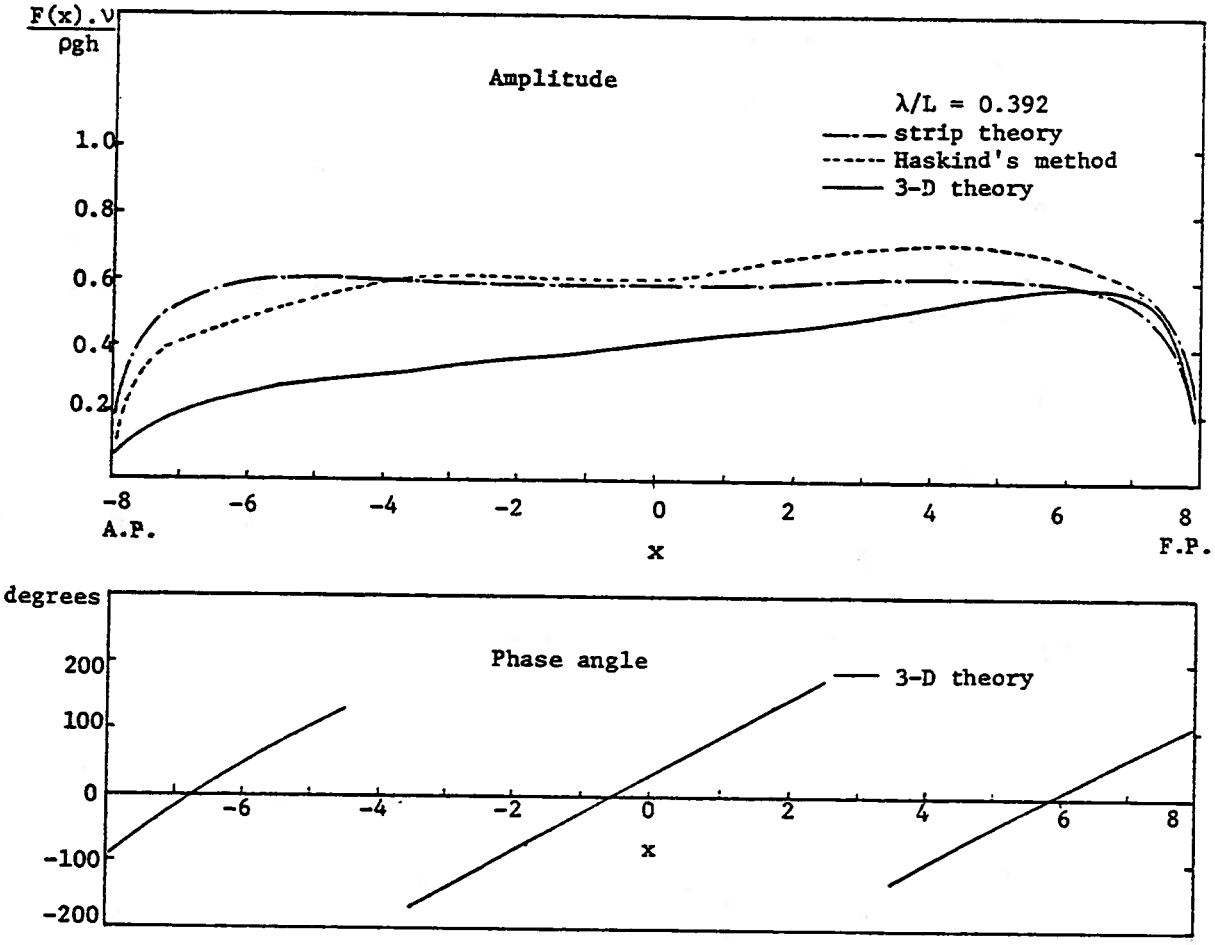

Figure 48. Longitudinal distribution of the wave force on the spheroid for heave ($\nu L/2 = 8$)

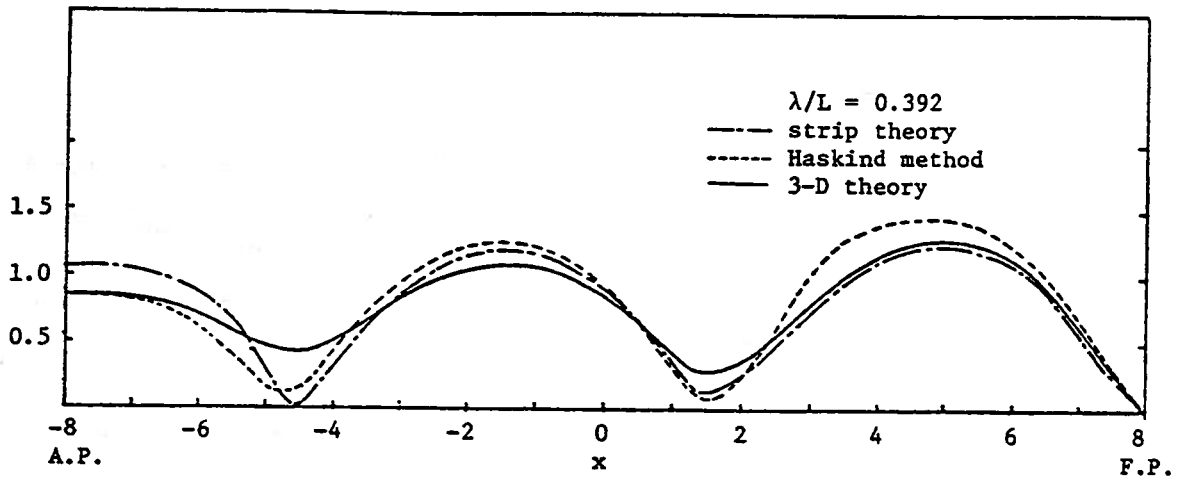

Figure 49. Wave force summed up to section x from the bow of the spheroid ($\nu L/2 = 8$)

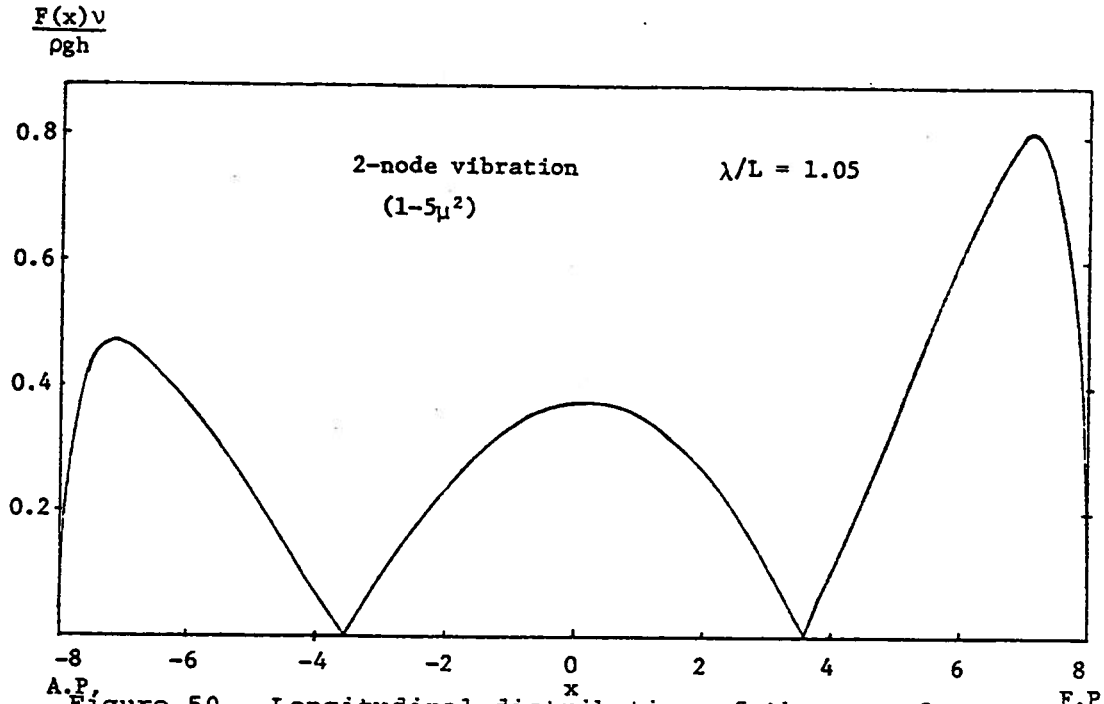

Figure 50. Longitudinal distribution of the wave force on the spheroid for springing (νL/2=3)

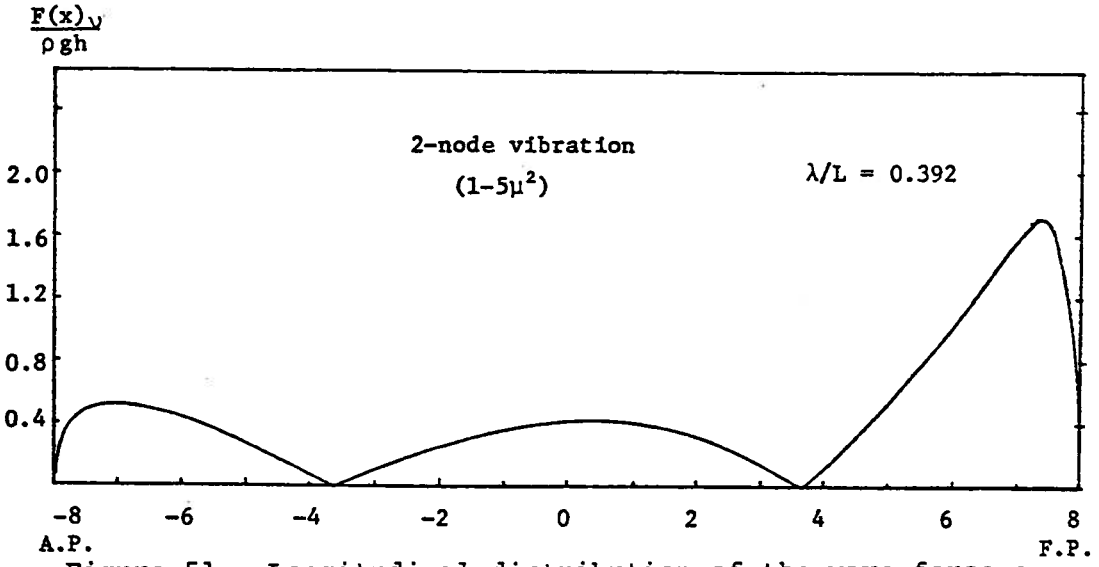

Figure 51. Longitudinal distribution of the wave force on the spheroid for springing (νL/2=8)

VII. SUMMARY

The three-dimensional boundary value problem for the unsteady motion of a ship oscillating at the free surface in a head sea has been formulated for the zero-forward speed. Various forms of the integral equation methods are formulated. The integral equation method by using three-dimensional source distribution is developed to compute the added mass, damping coefficients, and wave exciting forces on a ship.

The integral equation is solved numerically by three different methods: successive approximation by Neumann series, frequency iteration using the infinite fluid solution, and linear algebraic equations. Iterative methods converge for the high frequencies of oscillation, but not for the low frequencies. The iteration methods require more stringent condition on the kernel matrix than does the linear algebraic equation method. The iteration methods are studied to determine why they do not converge for all frequency ranges. An improved iteration method using the Buckner-Chertock series is applied to improve the convergence in the lower frequency range.

The integral equation using source distribution fails at a discrete infinite number of the eigenfrequencies of the interior Dirichlet problem. The difficulty near these eigenfrequencies can be removed by using a new form of the Green's function. The new Green's function is constructed by adding a point source at the origin to the fundamental Green's function given for the 2-D problem. The new Green's function produces a new integral equation which removes the numerical difficulty near these eigenfrequencies. The three-dimensional problem with free surface is approached similarly. The modified form of the Green's function is constructed by adding a line of sources along the centerline at the free surface to the fundamental Green's function. This modifica-

tion cures the irregular frequency phenomenon at these eigen-frequencies.

It is accepted in the field that short waves cause the strip theory to fail for the computation of wave exciting forces. First study, investigates the three-dimensional effects on the hydrodynamic coefficients. It finds the strip theory is completely wrong for the zero frequency limit. The added mass coefficient found by strip theory is infinite for the zero frequency limit, while the 3-D theory gives a finite limit. For the high frequency limit, the error by strip theory is finite. The more slender is the ship, the better the result of strip theory. The 3-D effect on the added mass is spread evenly along the entire length of the spheroid for the infinitely high frequency; it is not concentrated at the ends. The 3-D effect on the generalized added mass is greater for the higher mode than for the lower mode of the vibrating spheroid. But strip theory is a good approximation for fairly high frequencies. The 3-D effect on the hydrodynamic coefficients (added mass and damping) is quite small for the heaving slender spheroid.

Next, the study looks at the 3-D effects of the wave exciting forces for the head sea. The direct diffraction problem is solved by the 3-D source distribution method. The amplitude and phase angle of the pressure distribution are compared with Faltinsen's results and Lee's experimental results for the heaving spheroid. All the results show similar trends near the bow and stern. However, Faltinsen's theory overestimates the 3-D result.

The axial distribution of the wave exciting forces is computed by the three-dimensional diffraction theory, the 3-D Haskind formula, and the 2-D strip theory developed by Salvesen, Tuck and Faltinsen (1970). For wave force distribution, the strip theory underestimates the 3-D theory near the bow and overestimates it near the stern. The 3-D theory finds that, in head sea, greater forces occur near the bow than the stern, and the forces decrease as the wave passes along

the ship. The discrepency between the theories is quite small for the long waves ($\lambda/L = 1.05$), but the difference becomes much greater for the short waves ($\lambda/L = 0.392$), because more diffraction occurs for the short waves. The difference between the Haskind formula and 3-D diffraction theory for the force distribution due to short waves is significant. The study confirms that the integrand of the Haskind formula cannot be identified as an actual force distribution. It has a physical meaning only when the total integrated force is considered.

APPENDICES

APPENDIX A. GREEN'S FUNCTION

1. Derivation of the 3-D Green's Function

The various forms of 3-D Green's functions are derived in this appendix. The boundary value problem for the Green's function is similar to that for the velocity potential, with the exception of the boundary condition on the hull. The Green's function is not required to satisfy the complicated body boundary condition. It should satisfy the following equations:

$$\left(\frac{\partial}{\partial x^2} + \frac{\partial}{\partial y^2} + \frac{\partial}{\partial z^2}\right)G = -\frac{1}{4\pi}\,\delta(x-\xi)\delta(y-\eta)\delta(z-\zeta) \quad \text{in the fluid region,} \tag{A-1}$$

$$\frac{\partial G}{\partial z} - \nu G = 0 \quad \text{on} \quad z=0\ , \tag{A-2}$$

$$\lim_{z\to-\infty}\frac{\partial G}{\partial z} = 0\ , \tag{A-3}$$

and

$$\lim_{R\to\infty}\sqrt{R}\left(\frac{\partial G}{\partial R} + i\nu G\right) = 0\ , \tag{A-4}$$

where $R = \sqrt{(x-\xi)^2+(y-\eta)^2}$.

Note that G is the complex velocity potential of a source of strength, -4π . Time factor $e^{i\omega t}$ has been suppressed.

Let G and $\tilde{G}$ be the Fourier transform pair. Then, in x,y plane and k_x,k_y plane, we get

$$\tilde{G}(k_x,k_y,z) = \frac{1}{2\pi}\int_{-\infty}^{\infty}\int_{-\infty}^{\infty} G(x,y,z)\,e^{-i\{k_x(x-\xi)+k_y(y-\eta)\}}dxdy\ , \tag{A-5}$$

and

$$G(x,y,z) = \frac{1}{2\pi}\int_{-\infty}^{\infty}\int_{-\infty}^{\infty}\tilde{G}(k_x,k_y,z)\,e^{i\{k_x(x-\xi)+k_y(y-\eta)\}}dk_xdk_y\ . \tag{A-6}$$

A change of variables gives Fourier transform pairs in the R,θ plane and the k,β plane as follows:

$$\tilde{G}(k,\beta,z) = \frac{1}{2\pi}\int_0^{\infty} RdR \int_{-\pi}^{\pi} G(R,\theta,z)e^{-ikR\cos(\theta-\beta)}\,d\theta \ , \qquad (A-7)$$

and

$$G(R,\theta,z) = \frac{1}{2\pi}\int_0^{\infty} kdk \int_{-\pi}^{\pi} \tilde{G}(k,\beta,z)e^{ikR\cos(\theta-\beta)}d\beta \ , \qquad (A-8)$$

where $R = \sqrt{(x-\xi)^2+(y-\eta)^2}$,

$x-\xi = R\cos\theta$, $y-\eta = R\sin\theta$,

and $k_x = k\cos\beta$, $k_y = k\sin\beta$.

Let $G = 1/r + G_0$,

where $r = \sqrt{(x-\xi)^2+(y-\eta)^2+(z-\zeta)^2}$.

G_0 is the harmonic part of the Green's function. The singular part is $1/r$ from the well-known potential theory. Taking the Fourier transform of the Laplace equation, we get an ordinary differential equation for $\tilde{G}_0$,

$$\frac{d^2\tilde{G}_0}{dz^2} - k^2\tilde{G}_0 = 0 \qquad (A-9)$$

The solution of the differential equation (A-9) is an exponential form. Only positive k is needed to produce a finite solution, as $z\to-\infty$. It is given by

$$\tilde{G}_0 = A_0(k,\beta)e^{kz} \ . \qquad (A-10)$$

The Fourier transform of the free surface condition (A-2) is given by

$$\frac{d\tilde{G}}{dz} - \nu\tilde{G} = 0 \quad , \quad \text{on} \quad z = 0 \ . \qquad (A-11)$$

From the free surface condition, we can determine A_0 as

$$A_0(k,\beta) = \frac{(k+\nu)e^{k\zeta}}{(k-\nu)k} \ . \qquad (A-12)$$

Thus we find the Fourier transform of G is

$$\tilde{G} = \frac{e^{-k|z-\zeta|}}{k} + \frac{(k+\nu)e^{k(z+\zeta)}}{(k-\nu)k} \quad , \tag{A-13}$$

where the following integrals were used in the derivation:

$$J_0(kR) = \frac{1}{2\pi}\int_0^{2\pi} e^{-ikR\cos\beta}d\beta \quad , \tag{A-14}$$

$$\int_0^{\infty} \frac{R}{\sqrt{R^2+z^2}} J_0(kR)dR = \frac{e^{-k|z|}}{k} \quad . \tag{A-15}$$

Inverting the Fourier transform of G,(A-13), produces the Green's function as:

$$G = \frac{1}{r} + \bar{\int_0^{\infty}} \frac{k+\nu}{k-\nu} e^{k(z+\zeta)} J_0(kR)dk \quad , \tag{A-16}$$

where the bar on the integral sign denotes that this is a principal value integral. Integral (A-14) and

$$\int_0^{\infty} e^{-k|z-\zeta|}J_0(kR)dk = \frac{1}{\sqrt{R^2+(z-\zeta)^2}} \tag{A-17}$$

are used in the derivation of (A-16).

The radiation condition remains to be satisfied. For large R, (A-16) becomes, asymptotically,

$$G \sim -2\pi\nu e^{\nu(z+\zeta)}Y_0(\nu R).$$

In order to insure the outgoing wave with $e^{+i\omega t}$, we add a harmonic solution, $-2\pi i\nu e^{\nu(z+\zeta)}J_0(\nu R)$. The Green's function then behaves as follows:

$$G \sim -2\pi i\nu e^{\nu(z+\zeta)}H_0^{(2)}(\nu R) \quad , \text{ for large } \nu R,$$

where $H_0^{(2)}$ is the Hankel function of the second kind. Finally we obtain a Green's function as

$$G = \frac{1}{r} + \bar{\int_0^{\infty}} \frac{k+\nu}{k-\nu} e^{k(z+\zeta)}J_0(kR)dk - 2\pi i\nu e^{\nu(z+\zeta)}J_0(\nu R) \quad . \tag{A-18}$$

Using the integral (A-17), Green's function (A-18) becomes,

$$G = \frac{1}{r} - \frac{1}{r^*} + 2\int_0^\infty \frac{ke^{k(z+\zeta)}}{k-\nu} J_0(kR)dk - 2\pi i\nu e^{\nu(z+\zeta)} J_0(\nu R) \quad , \tag{A-19}$$

where

$$r^* = \sqrt{(x-\xi)^2+(y-\eta)^2+(z+\zeta)^2} \quad .$$

Using the integral (A-18) again, Green's function (A-19) becomes

$$G = \frac{1}{r} + \frac{1}{r^*} + 2\nu\int_0^\infty \frac{e^{k(z+\zeta)}}{k-\nu} J_0(kR)dk - 2\pi i\nu e^{\nu(z+\zeta)} J_0(\nu R) \quad . \tag{A-20}$$

Next Havelock's form of Green's function is derived from (A-20). Combining the principal value integral with the imaginary part, Green's function (A-20) then can be represented as

$$G = \frac{1}{r} + \frac{1}{r^*} + 2\nu\int_{0\frown}^\infty \frac{e^{k(z+\zeta)}}{k-\nu} J_0(kR)dk \quad , \tag{A-21}$$

where $\frown$ denotes the path along the indented semi-circle over the singularity at $k=\nu$.

Next we evaluate the contour integral with the indented semi-circle above the simple pole. Substituting $\frac{1}{2}[H_0^{(1)}(kR) - H_0^{(2)}(kR)]$ for $J_0(kR)$, the contour integral is written as

$$\int_{0\frown}^\infty \frac{e^{k(z+\zeta)}}{k-\nu} J_0(kR)dk = \frac{1}{2}[I_1+I_2] \quad , \tag{A-22}$$

where

$$I_1 = \int_{0\frown}^\infty \frac{e^{k(z+\zeta)}}{k-\nu} H_0^{(1)}(kR)\ dk \ ,$$

and

$$I_2 = \int_{0}^{\infty} \frac{e^{k(z+\zeta)}}{k-\nu} H_0^{(2)}(kR)\, dk \quad .$$

Then we evaluate the integrals I_1 and I_2 by use of residue theorem. The residue theorem states that

$$\int_{\Sigma C} = \pm 2\pi i \, \Sigma \text{ residues} \quad , \tag{A-23}$$

where ΣC denotes all the contours, and $\pm$ signs are assigned to represent the counterclockwise and the clockwise direction of integration, respectively. The paths of integration are shown in Figure A.1. Jordan's Lemma causes the integral over C_R to vanish. There is no residue in path 1. Thus the integral I_1 becomes

$$I_1 = -\int_{\infty}^{0} \frac{e^{im(z+\zeta)}}{im-\nu} H_0^{(1)}(imR)\, idm \quad . \tag{A-24}$$

From Abramowitz and Stegun (1964), we get

$$H_0^{(1)}(imR) = \frac{2K_0(mR)}{\pi i} \quad ,$$

where K_0 is the modified Bessel function.

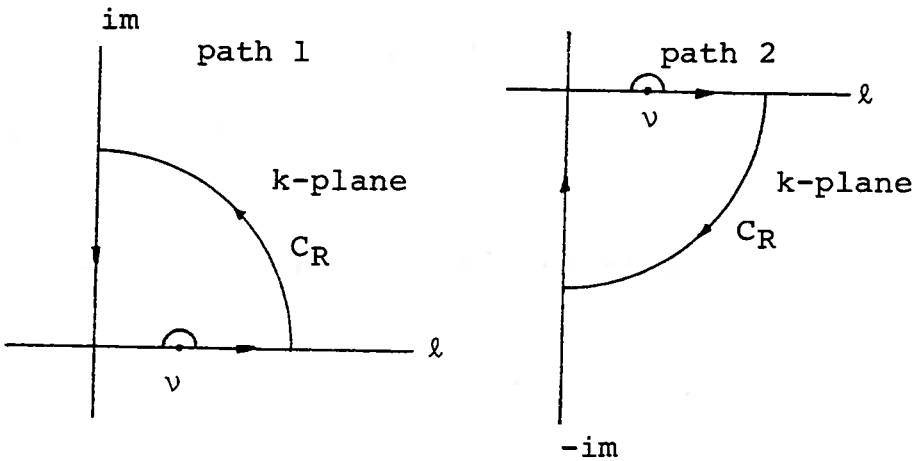

Figure A.1. Paths of integration in the complex plane

Replacing $H_0^{(1)}(imR)$ by $\frac{2K_0(mR)}{\pi i}$ produces

$$I_1 = -\frac{2}{\pi}\int_0^{\infty} \frac{(\nu+im)e^{im(z+\zeta)}}{\nu^2+m^2} K_0(mR)\,dm \ .$$

By using the residue theorem (A-23), I_2 is represented by

$$I_2 = i\int_{\infty}^{0} \frac{e^{-im(z+\zeta)}}{-im-\nu} H_0^{(2)}(-imR)\,dm - \text{Residue} \ .$$

In explanation, the integral over C_R vanishes in the fourth quadrant by Jordan's Lemma. We have a residue inside path 2, and the negative sign occurs because of the clockwise direction of integration. Replacing $H_0^{(2)}(-imR)$ by $-\frac{2}{\pi i}K_0(mR)$ and evaluating the residue, we get

$$I_2 = -\frac{2}{\pi}\int_0^{\infty} \frac{(\nu-im)e^{-im(z+\zeta)}}{\nu^2+m^2} K_0(mR)\ dm - 2\pi i\nu e^{\nu(z+\zeta)} H_0^{(2)}(\nu R).$$

Adding I_1 and I_2, and after some algebraic manipulation, Havelock's form of Green's function is obtained as follows:

$$G = \frac{1}{r} + \frac{1}{r^*} - \frac{4\nu}{\pi}\int_0^{\infty} \left[\frac{\nu\cos m(z+\zeta) - m\sin m(z+\zeta)}{\nu^2+m^2}\right] K_0(mR)\,dm$$

$$-2\pi i\nu e^{\nu(z+\zeta)} H_0^{(2)}(\nu R) \ . \qquad \text{(A-25)}$$

Next we derive Haskind's form of Green's function. Let

$$I = \int_0^{\infty} \left[\frac{\nu\cos m(z+\zeta) - m\sin m(z+\zeta)}{\nu^2+m^2}\right] K_0(mR)\ dm \ .$$

A change of variables produces

$$I = \int_0^{\infty} \left[\frac{\cos u\nu(z+\zeta) - u\sin u\nu(z+\zeta)}{1+u^2}\right] K_0(u\nu R)\ du \ . \qquad \text{(A-26)}$$

The z-derivative of I is

$$\frac{\partial I}{\partial z} = \int_0^\infty \left[\frac{-u\nu \sin u\nu(z+\zeta) - u^2 \nu \cos u\nu(z+\zeta)}{1+u^2}\right] K_0(u\nu R)\,du \quad . \tag{A-27}$$

Adding (A-26) and (A-27) results in a first order ordinary differential equation after some algebraic manipulation:

$$\nu I - \frac{\partial I}{\partial z} = \nu \int_0^\infty \cos u\nu(z+\zeta) K_0(u\nu R)\,du \quad . \tag{A-28}$$

The integral in the right-hand side of (A-28) is obtained by using the formula 6.671-14 from Gradshteyn and Ryzhik (1965):

$$\int_0^\infty \cos u\nu(z+\zeta) K_0(u\nu R)\,du = \frac{\pi}{2\sqrt{R^2+(z+\zeta)^2}} \quad . \tag{A-29}$$

The solution of the differential equation (A-28) is given as

$$I = -\frac{\pi}{2} e^{\nu(z+\zeta)} \int_0^{z+\zeta} \frac{e^{-\nu u}\,du}{\sqrt{R^2+u^2}} + Ce^{\nu(z+\zeta)} \quad . \tag{A-30}$$

By evaluating I at the point $(z+\zeta)=0$ in both (A-26) and (A-30) and equating them together, we can determine the constant C as:

$$C = \int_0^\infty \frac{K_0(u\nu R)\,du}{1+u^2} = \frac{\pi^2}{4}\left[H_0(\nu R) - Y_0(\nu R)\right] \quad , \tag{A-31}$$

where H_0 is the Struve function of zero order. Putting (A-31) and (A-30) into (A-25), the Green's function becomes

$$G = \frac{1}{r} + \frac{1}{r^*} + 2\nu e^{\nu(z+\zeta)} \int_0^{z+\zeta} \frac{e^{-u\nu}}{\sqrt{R^2+u^2}}\,du - \pi\nu e^{\nu(z+\zeta)}\left[H_0(\nu R) - Y_0(\nu R)\right]$$

$$-2\pi i\nu e^{\nu(z+\zeta)} H_0^{(2)}(\nu R) \quad . \tag{A-32}$$

The Green's function (A-32) is an efficient form for the practical computation since it separates the oscillatory

outgoing waves from the monotonically decaying local disturbance. From Gradshteyn and Ryzhik (6.566), we get

$$H_0(\nu R) - Y_0(\nu R) = \frac{2}{\pi}\int_0^\infty \frac{e^{-\nu u}\,du}{\sqrt{R^2+u^2}} \quad . \tag{A-33}$$

Substituting (A-33) into (A-32) and combining the integrals, yields

$$G = \frac{1}{r} + \frac{1}{r^*} - 2\nu e^{\nu(z+\zeta)}\int_{z+\zeta}^\infty \frac{e^{-\nu u}du}{\sqrt{R^2+u^2}} - 2\pi i\nu e^{\nu(z+\zeta)}H_0^{(2)}(\nu R) \quad . \tag{A-34}$$

By change of variable, $u-\xi=w$, we get

$$G = \frac{1}{r} + \frac{1}{r^*} + 2\nu e^{\nu z}\int_\infty^z \frac{e^{-\nu w}\,dw}{\sqrt{(x-\xi)^2+(y-\eta)^2+(w+\zeta)^2}} - 2\pi i\nu e^{\nu(z+\zeta)}H_0^{(2)}(\nu R), \tag{A-35}$$

which is the Green's function derived by Haskind.

2. Evaluation of 3-D Green's Function and Its Derivatives

In order to solve the integral equation by source distribution, the Green's function must be computed numerous times. Computing the Green's function and its derivatives in order to construct the kernel matrix of the integral equation is the most time consuming part of the total computation. An efficient form of the Green's function is definitely needed. Many different forms of Green's function (A-18), (A-19), (A-20), (A-21), (A-25), (A-32) and (A-35) are available. One can be derived from the other by deforming the path of integration and evaluating the integrals.

The most common forms (A-18), (A-19) and (A-20), which include the principal value integral, are inefficient to compute because the integrand, which includes the Bessel function of the first kind, is rapidly oscillating for large kR, and also because of numerical difficulty near the singularity at $k=\nu$. Havelock's form (A-25) of Green's function separates the outgoing wave from the local distur-

bance. However, it includes the integral of the oscillating function. Green's function (A-33) and the original Haskind form (A-35) explicitly separate the oscillatory outgoing waves from the local disturbance. Local disturbance is represented by an exponentially decaying integral. For numerical computation, a modified form (A-32) from Haskind's form is efficient for computation, especially for large kR. By change of variable, (A-32) is rewritten as

$$G = \frac{1}{r} + \frac{1}{r^*} + 2\nu e^{\nu(z+\zeta)} \int_0^{\nu(z+\zeta)} \frac{-e^{-u}du}{\sqrt{(\nu R)^2+u^2}} - \pi\nu e^{\nu(z+\zeta)} [H_0(\nu R)+Y_0(\nu R)]$$

$$- 2\pi i\nu e^{\nu(z+\zeta)} J_0(\nu R) \ .$$

Differentiating G with respect to x produces

$$G_x^{\dagger} = -(x-\xi)\left(\frac{1}{r^3} + \frac{1}{r^{*3}}\right) - 2\nu^3(x-\xi)e^{\nu(z+\zeta)} \int_0^{\nu(z+\zeta)} \frac{e^{-u}\,du}{[(\nu R)^2+u^2]^{3/2}}$$

$$-\pi\nu^2 e^{\nu(z+\zeta)} \frac{(x-\xi)}{R} \left\{\frac{2}{\pi} - H_1(\nu R) - Y_1(\nu R)\right\} + 2\pi i\nu^2 e^{\nu(z+\zeta)} \frac{(x-\xi)}{R} J_1(\nu R) . \qquad \text{(A-36)}$$

Similarly, the y-derivative of the Green's function is obtained as

$$G_y = -(y-\eta)\left(\frac{1}{r^3} + \frac{1}{r^{*3}}\right) - 2\nu^3(y-\eta)e^{\nu(z+\zeta)} \int_0^{\nu(z+\zeta)} \frac{e^{-u}\,du}{[(\nu R)^2+u^2]^{3/2}}$$

$$-\pi\nu^2 e^{\nu(z+\zeta)} \frac{(y-\eta)}{R} \left\{\frac{2}{\pi} - H_1(\nu R) - Y_1(\nu R)\right\} + 2\pi i\nu^2 e^{\nu(z+\zeta)} \frac{(y-\eta)}{R} J_1(\nu R) . \qquad \text{(A-37)}$$

---

†Subscripts x, y, and z denote the partial derivatives with respect to x,y,z, respectively.

Finally, the z derivative of G is obtained as

$$G_z = \frac{-(z-\zeta)}{r^3} - \frac{(z+\zeta)}{r^{*3}} + 2\nu^2 e^{\nu(z+\zeta)} \int_0^{\nu(z+\zeta)} \frac{e^{-u}\, du}{\sqrt{(\nu R)^2+u^2}}$$

$$-\pi\nu^2 e^{\nu(z+\zeta)} \{ H_0(\nu R)+Y_0(\nu R) \} + \frac{2\nu}{r^*} - 2\pi i\nu^2 e^{\nu(z+\zeta)} J_0(\nu R) \quad . \tag{A-38}$$

3. Derivation of the 2-D Green's function from the 3-D Green's function

The two-dimensional Green's function can be derived in a manner similar to that of the three-dimensional one. Various forms of two-dimensional Green's functions have been derived by John (1950), Haskind (1953), Thorne (1953), and Ogilvie (1978).

In Chapter IV, two-dimensional source densities have been used as a first approximation of the 3-D source density along the parallel middle body. In this appendix, 2-D source density is derived from the 3-D source density for an infinitely long uniform cylinder. The 2-D Green's function is derived from the 3-D Green's function for the infinite fluid case and also for the free surface case.

a. Infinite fluid case

The 3-D velocity potential is represented by the distribution of the 3-D sources over the hull:

$$\phi = -\frac{1}{4\pi} \int_{-L/2}^{L/2} d\xi \int_{C(\xi)} \frac{d\ell\ \sigma(Q)}{\sqrt{1-n_1^2}} \left[\frac{1}{\sqrt{(x-\xi)^2+R_o^2}} - \frac{1}{\sqrt{(x-\xi)^2+R_o^{*2}}} \right] , \tag{A-39}$$

where $R_o=\sqrt{(y-\eta)^2+(z-\zeta)^2}$, and $R_o^*=\sqrt{(y-\eta)^2+(z+\zeta)^2}$.

For an infinitely long uniform cylinder, $n_1=0$, and $\sigma(\xi,\eta,\zeta)=\sigma(\eta,\zeta)$. Interchanging the order of integration of (A-39) results in

$$\phi = -\frac{1}{4\pi}\int_{C(\xi)} d\ell\ \sigma(\eta,\zeta)\int_{-L/2}^{L/2}\left[\frac{1}{\sqrt{(x-\xi)^2+R_o^2}} - \frac{1}{\sqrt{(x-\xi)^2+R_o^{*2}}}\right] d\xi \ . \tag{A-40}$$

Now

$$I_1 = \int_{-L/2}^{L/2} \frac{1}{\sqrt{(x-\xi)^2+R_o^2}}\, d\xi \ , \quad I_2 = \int_{-L/2}^{L/2} \frac{-1}{\sqrt{(x-\xi)^2+R_o^{*2}}}\, d\xi \ .$$

Separating the limits of this integration into two parts, results in

$$I_1 = \lim\left[\int_{-L/2}^{x} \frac{d\xi}{\sqrt{(x-\xi)^2+R_o^2}} + \int_{x}^{L/2} \frac{d\xi}{\sqrt{(x-\xi)^2+R_o^2}}\right] \ .$$

Evaluating the integrals, we get

$$I_1 = -\log\left|(x-\xi)+\sqrt{(x-\xi)^2+R_o^2}\right|_{-L/2}^{x} + \log\left|(\xi-x)+\sqrt{(x-\xi)^2+R_o^2}\right|_{x}^{L/2}$$

$$= -2\log(R_o) + \log\ (x+\tfrac{L}{2} + \sqrt{(x+\tfrac{L}{2})^2+R_o^2})$$

$$+\log(\tfrac{L}{2}-x+\sqrt{(x-\tfrac{L}{2})^2+R_o^2}) \tag{A-41}$$

Similarly,

$$I_2 = 2\ \log R_o^* - \log[(x+\tfrac{L}{2})+\sqrt{(x+\tfrac{L}{2})^2+R_o^{*2}}] - \log[(\tfrac{L}{2}-x)+\sqrt{(x-\tfrac{L}{2})^2+R_o^{*2}}] \ .$$

Combining I_1 and I_2 and taking $L\to\infty$ as the limit, we get

$$\lim_{L\to\infty}(I_1+I_2) = -2(\log R_o - \log R_o^*) \tag{A-42}$$

This is the 2-D Green's function for the infinite fluid. The velocity potential therefore becomes the 2-D velocity potential by substituting (A-42) into (A-40):

$$\phi = + \frac{1}{2\pi} \int_C \sigma[\log R_o - \log R_o^*] \, d\ell \ . \tag{A-43}$$

b. Free Surface Case

$$\phi = - \frac{1}{4\pi} \int_{-L/2}^{L/2} d\xi \int_{C(\xi)} \frac{d\ell\sigma(Q)}{\sqrt{1-n_1^2}} \left[\frac{1}{r} - \frac{1}{r^*} + 2 \underbrace{\int_0^\infty \frac{ke^{k(z+\zeta)}}{k-\nu} J_0(k\sqrt{(x-\xi)^2+(y-\eta)^2})\, dk}_{\curvearrowright} \right] . \tag{A-44}$$

For the infinitely long uniform cylinder,

$$n_1 = 0 \quad \text{and} \quad \sigma(\xi,\eta,\zeta) = \sigma(\eta,\zeta) \ .$$

Interchanging the order of integration in (A-44), we get

$$\phi = - \frac{1}{4\pi} \int_C d\ell\sigma(\eta,\zeta) \int_{-L/2}^{L/2} \left[\frac{1}{r} - \frac{1}{r^*} + 2 \underbrace{\int_0^\infty \frac{ke^{k(z+\zeta)}}{k-\nu} J_0(k\sqrt{(x-\xi)^2+(y-\eta)^2})\, dk}_{\curvearrowright} \right] d\xi . \tag{A-45}$$

Now, let

$$I_3 = \int_{-L/2}^{L/2} d\xi \underbrace{\int_0^\infty \frac{ke^{k(z+\zeta)}}{k-\nu} J_0(k\sqrt{(x-\xi)^2+(y-\eta)^2})\, dk}_{\curvearrowright} \ . \tag{A-46}$$

Interchanging the order of integration, we get

$$I_3 = \underbrace{\int_0^\infty dk \, \frac{ke^{k(z+\zeta)}}{k-\nu}}_{\curvearrowright} \int_{-\infty}^{\infty} J_0(k\sqrt{(x-\xi)^2+(y-\eta)^2})\, d\xi \ . \tag{A-47}$$

Let

$$I_4 = \int_{-\infty}^{\infty} J_0(k\sqrt{(x-\xi)^2+(y-\eta)^2})\, d\xi \ . \tag{A-48}$$

By change of variables, I_4 becomes

$$\int_{-\infty+x}^{\infty+x} J_0(k\sqrt{\xi'^2+(y-\eta)^2}) \, d\xi' \ .$$

Deleting the prime sign and considering the section at x=0 for simplicity since it should be the same for any section, we get

$$I_4 = \int_{-\infty}^{\infty} J_0(k\sqrt{\xi^2+Y^2})\,d\xi \ ,$$

where $(y-\eta)$ is replaced by Y. Using the addition theorem (9.1.75) from Abramowitz and Stegun, I_4 becomes

$$2\int_0^{\infty} d\xi \sum_{n=-\infty}^{\infty} J_n(k\xi)\ J_n(kY)\ \cos\frac{n\pi}{2} \ . \qquad \text{(A-49)}$$

Changing the integral and summation of (A-49), we get

$$I_4 = 2 \sum_{n=-\infty}^{\infty} J_n(kY)\ \cos\frac{n\pi}{2}\int_0^{\infty} d\xi\ J_n(k\xi) \qquad \text{(A-50)}$$

From Gradshteyn and Ryzhik (6.511),

$$\int_0^{\infty} d\xi\ J_n(k\xi) = \frac{1}{k} \qquad \text{(A-51)}$$

Substituting (A-51) into (A-50) gives

$$I_4 = \frac{2}{k} \sum_{n=-\infty}^{\infty} J_n(kY)\ \cos\frac{n\pi}{2} \ . \qquad \text{(A-52)}$$

Using the relationship $J_{-n}=(-1)^n J_n$, (A-52) becomes

$$I_4 = \frac{2}{k}\ [J_0-2J_2+2J_4+\ldots] \ . \qquad \text{(A-53)}$$

Using the formula (9.1.47) from Abramowitz and Stegun (1964), (A-53) becomes

$$I_4 = \frac{2}{k}\cos\ (kY) \ . \qquad \text{(A-54)}$$

Substituting (A-54) into (A-47), I_3 becomes

$$I_3 = \int_0^{\infty} \frac{dke^{k(z+\zeta)}\cos k(y-\eta)}{k-\nu} \ . \qquad \text{(A-55)}$$

Using (A-42) and (A-55) into (A-45) yields

$$\phi = \frac{1}{2\pi}\int_C d\ell\sigma\left[\log R_o - \log R_o^* - 2\int_0^\infty \frac{dk e^{k(z+\zeta)}}{k-\nu}\cos\{\nu(y-\eta)\}\right] . \qquad \text{(A-56)}$$

The 2-D Green's function has been obtained from the 3-D Green's function. The 2-D source density is the limiting value of the 3-D source density for the infinitely long uniform cylinder.

APPENDIX B

NUMERICAL METHOD FOR INTEGRAL EQUATION

1. General procedure

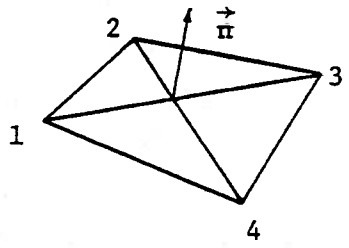

Figure B.1 Plane quadrilateral element and unit normal

The integral equation is approximated by a set of linear algebraic equations. The approximation involves the approximate evaluation of the integral of the Green's function and approximate representation of the body surface. The body surface is approximated by a number of plane quadrilateral elements over which the source density is assumed constant. Then the integral equation (23) is approximated as

$$-\frac{\sigma}{2}(P) \sum_{Q=1}^{N} \sigma_i(Q) \iint_{S(Q)} \frac{1}{4\pi} \frac{\partial G(P,Q)}{\partial n_P} \, dS = n_i(P) \ , \qquad \text{(B-1)}$$

where $S(Q)$ is the area of the element Q.

The plane quadrilateral element is formed from the four input points. Geometric information such as the coordinates of the centroid, the element of the transformation matrix, the maximum diagonal, the area, and the second moment of the area, are computed. The unit normal vectors are computed by taking the cross product of the two diagonal vectors.

In matrix form, we get

$$[I(P,Q)]\ \{\sigma(Q)\} = \{n_i(P)\} ,$$

where

$$I(P,Q) = -\frac{1}{4\pi}\iint\frac{\partial G(P,Q)}{\partial n_P}dS(Q) \quad \text{for } P \neq Q , \tag{B-2}$$

$$= -\frac{1}{2} - \frac{1}{4\pi}\iint\frac{\partial G(P,Q)}{\partial n_P}dS(Q) \quad \text{for } P = Q .$$

The induced velocity vector at the centroid of the P-th element due to Q-th element with unit source density is computed. The induced normal velocity at P is obtained by taking the dot product of the induced velocity vector with the unit normal vector of the P-th element.

The boundary value n_i (P) is computed by using the geometric information of the unit normal vector. For the linear motion of the rigid body, n_i is defined by

$$\vec{n} = (n_1, n_2, n_3) , \text{ for } i = 1,2,3 .$$

For the rotational motion of the rigid body, n_i is defined by

$$\vec{r} \times \vec{n} = (n_4, n_5, n_6) , \text{ for } i = 4,5,6 .$$

For the vertical mode of the vibration, we get n_i as

$$n_i = n_3\psi_i(x) ,$$

where $\psi_i(x)$ is i-th mode of the vertical vibration.

Once we compute the kinematic boundary condition on the hull, we can solve the linear algebraic equation by matrix inversion or decomposition methods. The influence coefficient matrix is computed only once for all modes of motion. The left-hand side of the integral equation does not change unless we make use of the symmetry characteristics. Computation of the influence coefficients is the most time consuming part of the total computation.

When the solution for the source density is obtained, the velocity potential is computed at the centroid of each element (P) by integrating the product of source density and Green's function over all the elements (Q):

$$\phi(P) = -\frac{1}{4\pi}\sum_{Q=1}^{N}\sigma(Q)\iint_{S(Q)} G(P,Q)\, dS(Q) \quad . \tag{B-3}$$

In discrete form, we get

$$[J(P,Q)]\ \{\sigma(Q)\} = \{\phi(P)\} \ ,$$

where J(P,Q) is the influence coefficient for the induced velocity potential which is given by

$$J(P,Q) = -\frac{1}{4\pi}\iint_{S(Q)} G(P,Q)\, dS(Q) \quad . \tag{B-4}$$

For symmetrical bodies, only the nonredundant part of the body surface is necessary to construct plane quadrilateral elements. The reflected part of the body is taken into account by using a symmetrical or antisymmetrical relation of its source density with the source density of its original element.

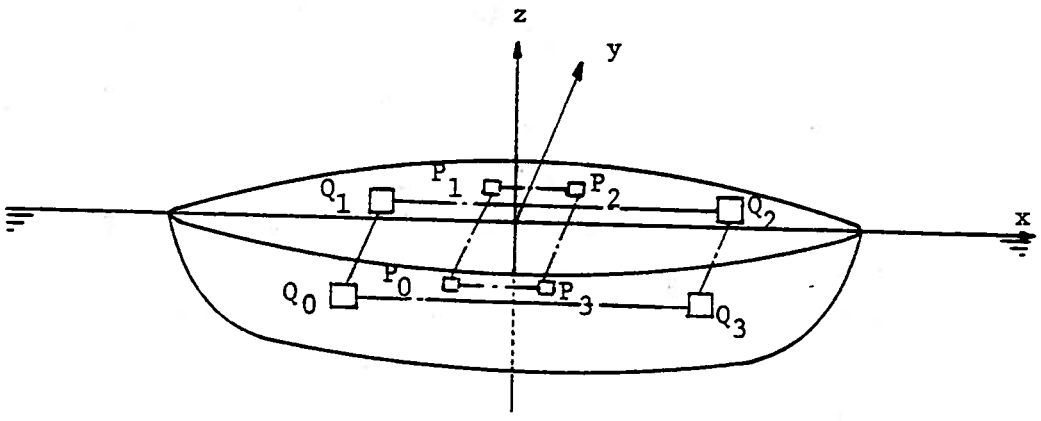

Figure B.2 Symmetry of the ship

a. Symmetrical ship with one plane of symmetry

For a body with one plane of symmetry (x-z plane), only a half of the body surface is needed to solve the equation. The source density on the reflected element of the ship is symmetrical or anti-symmetrical with that of the original element. For the heave or any other symmetrical mode of vertical vibration,

$$\sigma(Q_0) = \sigma(Q_1) ,$$

where the subscript o denotes the basic element, and the subscript 1 denotes the 1st reflected element with respect to x-z plane (See Figure B-2). By using symmetry of the source density, we get

$$\begin{aligned} n_i(P_0) &= \sum_{Q_i=1}^{N} [\sigma(Q_0) I(P_0,Q_0) + \sigma(Q_1) I(P_0,Q_1)] , \\ &= \sum_{Q_i=1}^{N} \sigma(Q_0) [I(P_0,Q_0) + I(P_0,Q_1)] . \end{aligned} \tag{B-5}$$

In order to compute $I(P_0,Q_1)$, certain symmetrical or anti-symmetrical relations in the derivative of G are used. For example, x component of the induced velocity at P_0 due to Q_1 is identical to that of induced velocity at P_1 due to Q_0. Thus we get

$$\begin{aligned} I(P_0,Q_1) &= -\frac{1}{4\pi} \iint_{S(Q_1)} [n_x \frac{\partial G}{\partial x}(P_0,Q_1) + n_y \frac{\partial G}{\partial y}(P_0,Q_1) + n_z \frac{\partial G}{\partial z}(P_0,Q_1)] dS , \\ &= -\frac{1}{4\pi} \iint_{S(Q_0)} [n_x \frac{\partial G}{\partial x}(P_1,Q_0) - n_y \frac{\partial G}{\partial y}(P_1,Q_0) + n_z \frac{\partial G}{\partial z}(P_1,Q_0)] dS . \end{aligned} \tag{B-6}$$

All the geometric quantities for the reflected element are obtained from its basic element. Once the induced normal velocity at P due to all reflected elements is computed, induced normal velocity at the next P-th element due to the same Q-th element is computed to make use of the already computed geometric data of Q-th element. The influence coefficient I(P,Q) is computed column by column.

Similarly to the induced normal velocity, the velocity potential is given by

$$\phi(P_o) = \Sigma[\sigma(Q_o)J(P_o,Q_o) + \sigma(Q_1)J(P_o,Q_1)],$$

$$= \Sigma\sigma(Q_o)[J(P_o,Q_o) + J(P_o,Q_1)]. \qquad \text{(B-7)}$$

A symmetry condition,

$$J(P_o,Q_1) = J(P_1,Q_o) ,$$

is used to computed the induced potential at P_o due to the reflected element Q_1.

b. Symmetrical ship with two planes of symmetry

For the body with two planes of symmetry (x-z and y-z planes), only a quadrant of the body surface is needed to sovle the problem. For the heave or symmetrical mode of vertical vibration, the source density on the reflected elements are identical:

$$\sigma(Q_o) = \sigma(Q_1) = \sigma(Q_2) = \sigma(Q_3),$$

where subscripts 2 and 3 denote the 2nd reflected and 3rd reflected elements of the basic element. (See Figure B.2) By using the relationship between the source densities of the reflected elements, we get

$$n_i(P_o) = \sum_{Q_i=1}^{N} \sigma(Q_o)[I(P_o,Q_o)+I(P_o,Q_1)+I(P_o,Q_2)+I(P_o,Q_3)] \qquad \text{(B-8)}$$

By applying the symmetry or antisymmetry in the derivatives of Green's function, we get alternative form of $I(P_o,Q_2)$:

$$I(P_o,Q_2) = -\frac{1}{4\pi}\iint_{S(Q_2)}[n_x\frac{\partial G}{\partial n}(P_o,Q_2)+n_y\frac{\partial G}{\partial y}(P_o,Q_2)+n_z\frac{\partial G}{\partial z}(P_o,Q_2)]dS,$$

$$= -\frac{1}{4\pi}\iint_{S(Q_o)}[-n_x\frac{\partial G}{\partial x}(P_2,Q_o)-n_y\frac{\partial G}{\partial y}(P_2,Q_o)+n_z\frac{\partial G}{\partial z}(P_2,Q_o)]dS. \qquad \text{(B-9)}$$

Similarly, we get

$$I(P_o,Q_3) = -\frac{1}{4\pi}\iint_{S(Q_o)}[-n_x\frac{\partial G}{\partial x}(P_3,Q_o)+n_y\frac{\partial G}{\partial y}(P_3,Q_o)+n_z\frac{\partial G}{\partial z}(P_3,Q_o)]dS. \qquad \text{(B-10)}$$

The velocity potential is given by

$$\phi(P_o) = \sum_{Q_i=1}^{N} \sigma(Q_o)[J(P_o,Q_o)+J(P_o,Q_1)+J(P_o,Q_2)+J(P_o,Q_3)]. \quad \text{(B-11)}$$

By applying the symmetry relations, $J(P_o,Q_2)=J(P_2,Q_o)$ and $J(P_o,Q_3)=J(P_3,Q_o)$, we get

$$\phi(P_o) = \sum_{P_i=1}^{N} \sigma(Q_o)[J(P_o,Q_o)+J(P_1,Q_o)+J(P_2,Q_o)+J(P_3,Q_o)]. \quad \text{(B-12)}$$

The other modes of motion can be treated in a similar manner using the symmetry or anti-symmetry of source density.

2. Influence coefficient matrix

The induced velocity potential at the centroid of the P-th element due to the Q-th element with constant source density is computed by

$$J(P,Q) = -\frac{1}{4\pi}\iint_{S(Q)} \frac{1}{r(P,Q)} dS - \frac{1}{4\pi} S(Q)\{G-\frac{1}{r}\}. \quad \text{(B-13)}$$

Three different formulas are used to compute the integral of (B-13).

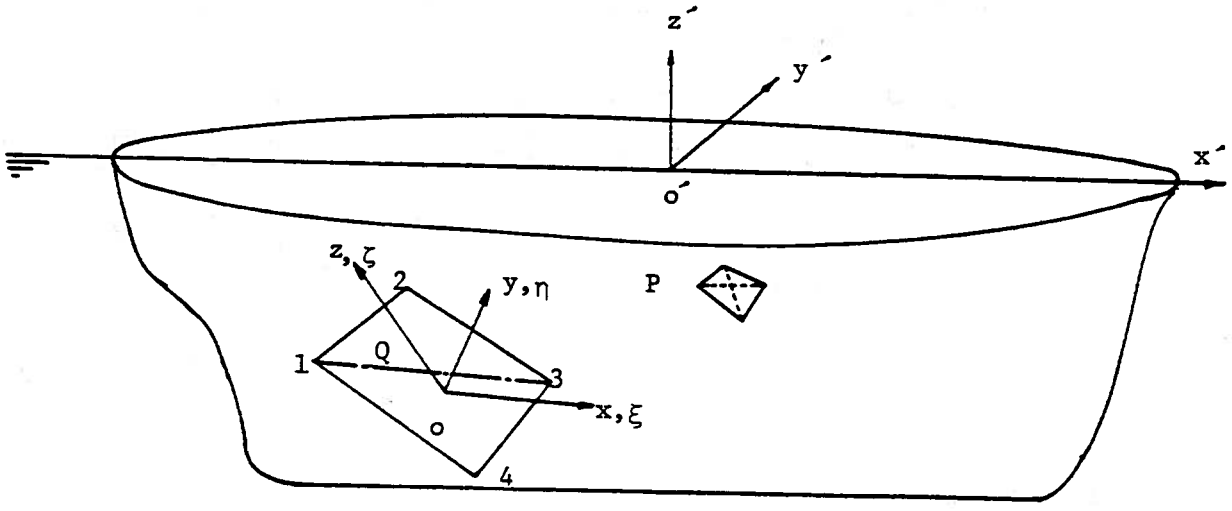

Figure B.3 Local coordinate system

a. Exact formula

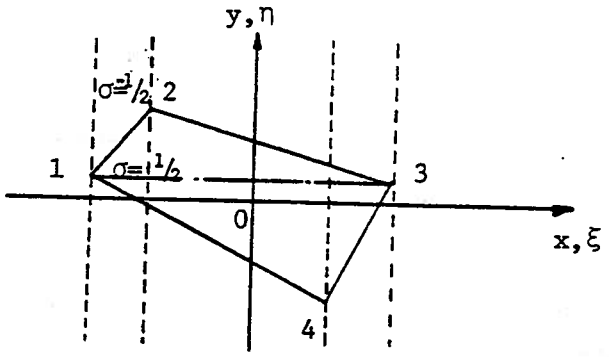

Figure B.4 Semi-infinite strips with uniform source density

Following procedures similar to those used by Hess and Smith (1962) and Faltinsen and Michelsen (1974), the integral is decomposed as the sum of the induced potential due to the two semi-infinite source strips whose boundaries consist of the side of the quadrilateral and semi-infinite lines parallel to one of the coordinate systems. The source density value of the strip on the right is +1/2, while the source density of the strip on the left is -1/2. When summed over the four sides, the surface integral over the quadrilateral is recovered, while the integrals outside of the element cancel each other:

$$\iint_{S(Q)} \frac{1}{r(P,Q)}\, dS = \sum_{i=1}^{4} K_i \ , \qquad \text{(B-14)}$$

where

$$K_i = \frac{1}{2}\int_{\xi_i}^{\xi_{i+1}} d\xi \left(\int_{-\infty}^{\eta'} - \int_{\eta'}^{+\infty} \right) \frac{d\eta}{\sqrt{(x-\xi)^2+(y-\eta)^2+z^2}} \ , \qquad \text{(B-15)}$$

and $\eta' = \eta_i + \frac{\eta_{i+1}-\eta_i}{\xi_{i+1}-\xi_i}(\xi-\xi_i)$, and (ξ_i,η_i) is the coordinates of the i-th corner point. (See Figure B.4)
The inside integrals of (B-15) are given by

$$\left(\int_{-\infty}^{\eta'} - \int_{\eta'}^{+\infty} \right) \frac{d\eta}{\sqrt{(x-\xi)^2+(y-\eta)^2+z^2}}$$

$$= -2 \log[(y-\eta')+\sqrt{(x-\xi)^2+z^2+(y-\eta')^2}\ ] \ . \qquad \text{(B-16)}$$

Substitution of (B-16) into (B-15) yields

$$K_i = \int_{\xi_i}^{\xi_{i+1}} d\xi[\ -\log\{(y-\eta')+\sqrt{(x-\xi)^2+(y-\eta')^2+z^2}\}].$$

When the argument of log becomes close to zero, we encounter numerical difficulty. In this case an alternative form is used:

$$K_i = \int_{\xi_i}^{\xi_{i+1}} d\xi[-\log\{(x-\xi)^2+z^2\}+\log\{-(y-\eta')+\sqrt{(x-\xi)^2+(y-\eta')^2+z^2}\}].$$

The first integral is given by

$$\int_{\xi_i}^{\xi_{i+1}} d\xi\ \log\{(x-\xi)^2+z^2\} = 2(\xi_{i+1}-\xi_i)-(x-\xi_i)\log\{(x-\xi_i)^2+z^2\}$$

$$-2|z|\tan^{-1}\frac{(x-\xi_i)}{|z|} + (x-\xi_{i+1})\log\{(x-\xi_{i+1})^2+z^2\}+2z\tan^{-1}\frac{(x-\xi_{i+1})}{|z|}. \qquad \text{(B-17)}$$

The second integral is computed numerically.

b. Approximation formula by quadrupole and simple pole

When the field point P(x,y,z) is far from the Q-th element, approximate formulas are used to compute the induced velocity potential.

The integrand is expanded in a power series in ξ and η about the origin,

$$\frac{1}{\sqrt{(x-\xi)^2+(y-\eta)^2+z^2}} \simeq W-W_x\xi-W_y\eta+\frac{1}{2}W_{xx}\xi^2+W_{xy}\xi\eta+\frac{1}{2}W_{yy}\eta^2 \qquad \text{(B-18)}$$

where $W = \frac{1}{\sqrt{x^2+y^2+z^2}}$, and subscripts denote the partial

derivatives. Substituting (B-18) into the integral, (B-14), and taking constant terms out of integral, we get

$$\iint_{S(Q)} \frac{ds}{\sqrt{(x-\xi)^2+(y-\eta)^2+z^2}} \simeq AW-(W_x M_x+W_y M_y) + \frac{1}{2}(W_{xx} I_{xx}+2W_{xy} I_{xy}+I_{yy} W_{yy}), \tag{B-19}$$

where A is the area of the element Q, M_x is the first moment of the area in x, M_y is the first moment of the area in y, I_{xx} is the second moment of the area in x, I_{xy} is the second cross moment of the area in x-y, and I_{yy} is the second moment of area in y. The first term is a source at the origin of the Q-th element coordinate system. The second terms are the dipoles, the axes of which are along the x axis and y axis, respectively. The third terms are quadrupoles.

Since the origin of the coordinate system is taken as the centroid of the element, all first moments M_x, M_y vanish. Thus the dipole moments are zero. Only a source and quadrupole exist.

Two approximation formulas are used: one uses a source-quadrupole for the intermediate distance; the other uses source only for a far distant point. As a criterion, the ratio of the distance of field point P to the maximum diagonal of the quadrilateral element is used to decide which approximation formula is chosen. The source-quadrupole formula is used for the ratio of 2.45, and the point source formula is used for the ratio beyond 4. Figure B.5 shows the velocity potential induced from the unit source distribution over the plane quadrilateral element by three methods: exact formula, source-quadrupole formula, and source formula.

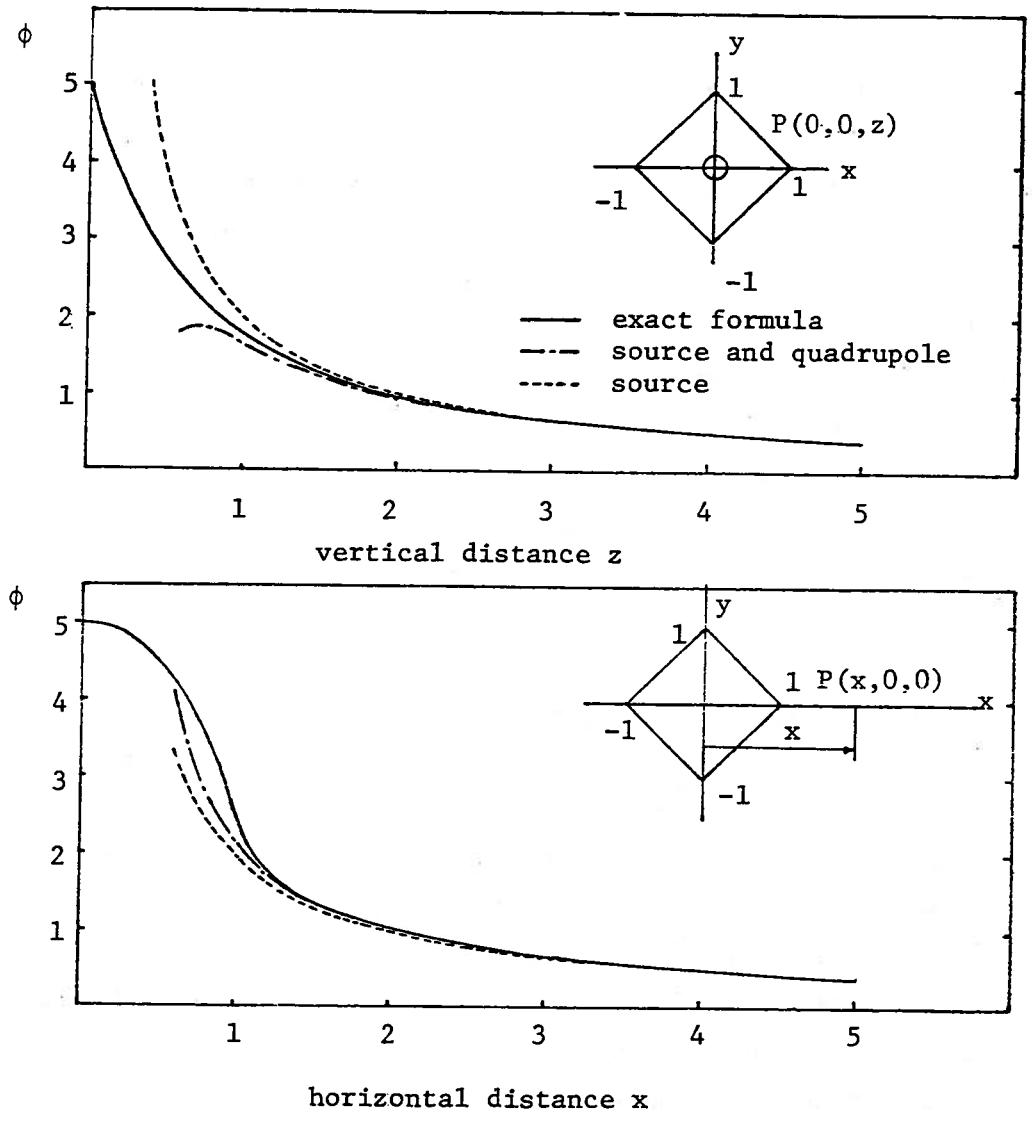

Figure B.5 Induced potential due to the plane quadrilateral element with a uniform source density

REFERENCES

REFERENCES

Abramowitz, M., and Stegun, I.A. (1964). Handbook of Mathematical Functions, Mathematics Series, 55, National Bureau of Standards, Washington.

Barakat, R. (1962). "Vertical Motion of a Floating Sphere in a Sine-Wave Sea," J. of Fluid Mech. 13, 540-556.

Brundrit, G. (1965). "A Solution to the Problem of Scalar Scattering From a Smooth, Bounded Obstacle Using Integral equations," Quart. J. Mech. Appl. Math., 18, 473-489.

Buckner, H. (1948). "A Special Method of Successive Approximations for Fredholm Integral Equations," Duke Math. J., 15, 197-206.

Burton, A.J. and Miller, G.F. (1971). "The Application of Integral Equation Methods to the Numerical Solution of Some Exterior Boundary Value Problem," Proc. Roy. Soc., Ser. A, 323, 201-210.

Chertock, G. (1964). "Sound Radiation from Vibrating Surfaces," J. Acoust. Soc. Amer., 36, 1305-1313.

Chertock, G. (1968). "Convergence of Interative Solutions to Integral Equation for Sound Radiation," Quart. J. Appl. Math., 26, 268-272.

Chertock, G. (1970). "Solutions for Sound Radiation problems by Integral Equations at the Critical Wavenumbers," J. Acoust. Soc. Amer., 47, 387-388.

Copley, L.G. (1968). "Fundamental Results Concerning Integral Representations in Acoustic Radiation," J. Acoust. Soc. Amer., 44, 28-32.

Faltinsen, O.M. (1971). "A Rational Strip Theory of Ship Motions: Part 2," Rept. No. 113, Dept. Nav. Arch. & Marine Eng., Univ. of Michigan, Ann Arbor.

Faltinsen, O.M., and Michelsen, F.C. (1974). "Motions of Large Structures in Waves at Zero Froude Number," International Symposium on the Dynamics of Marine Vehicles and Structures in Waves, London, 99-114.

Frank, W. (1967). "Oscillation of Cylinders In or Below the Free Surface of Deep Fluids," Report No. 2375, Naval Ship Res. & Dev. Center, Bethesda, MD.

Gradshteyn, I.S., Ryzhik, I.M. (1965). Tables of Integrals, Series, and Products, Academic Press, New York and London.

Haskind, M.D. (1957). "The Exciting Forces and Wetting of Ships in Waves," English Translation:DTMB Trans. No. 307.

Havelock, T. (1955). "Waves Due to a Floating Sphere Making Periodic Heaving Oscillation," Proc. Roy. Soc., Ser. A 230, 1-7.

Hess, J.L., and Smith, A.M.O. (1962). "Calculation of Non-lifting Potential Flow about Arbitrary three-dimensional Bodies," Rep. No. E.S. 40622, Douglas Aircraft Division, Long Branch, Cal.

John, F. (1950). "On the Motion of Floating Bodies. II. Simple Harmonic Motions," Comm. Pure Appl. Math., **3**, 45-101.

Jones, D.S. (1974). "Integral Equations for the Exterior Acoustic Problem," Quart. J. Mech. Appl. Math., **27**, 129-142.

Kellogg, O.D. (1929). Foundations of Potential Theory, Dover Incorporated, New York.

Kim, W.D. (1966). "On a Free Floating Ship in Waves," J. Ship Research, 10, 182-191.

Kleinman, R.E., and Roach, G.F. (1974). "Boundary Integral Equations for the Three-dimensional Helmholz Equations," SIAM Review, 16, 214-236.

Korvin-Kroukovsky, B.V., and Jacobs, W.R. (1957). "Pitching and Heaving Motions of a Ship in Regular Waves," Trans. SNAME, 65, 590-632.

Kumai, T. (1966). "A Method for Evaluating the Three-dimensional Reduction Factor of the Virtual Mass in the Vertical Vibration of Ships," Japan Shipbuilding and Marine Engineering, July, 15-21.

Lamb, H. (1932). Hydrodynamics, Sixth Edition, Dover Incorporated, New York.

Landweber, L., and Macagno, M. (1958). "Irrotational Motion of the Liquid Surrounding a Vibrating Ellipsoid of Revolution," J. of Ship Research, **2** , 37-49.

Lewis, F.M. (1929). "The Inertia of Water Surrounding a Vibrating Ship," Trans. SNAME, 37, 1-20.

Maruo, H., and Sasaki, N. (1974). "On the Wave Pressure Acting on the Surface of an Elongated Body Fixed in Head Seas," Selected Papers J. Soc. Nav. Arch. of Japan, **13**, 34-42.

Mikhlin, S.G. (1960). Integral Equations, Second Edition, The McMillan Company, New York.

Milgram, J.H. and Halkyard, J.E. (1971). "Wave Forces on Large Objects in the Sea," J. Ship Research, **15**, 115-124.

Newman, J.N. (1962). "The Exciting Forces on Fixed Bodies in Waves," J. Ship Research, 6 , 10-17.

Newman, J.N. (1970). "Applications of Slender-Body Theory in Ship Hydrodynamics," Annual Reviews of Fluid Mechanics, 2, 67-94.

Ogilvie, T.F. (1971). "On the Computation of Wave-Induced Bending and Torsion Moment," J. Ship Research, 15, 217-220.

Ogilvie, T.F. (1974). "The Fundamental Assumptions in Ship Motion Theory," Proc. International Symposium on the Dynamics of Marine Vehicles and Structures in Waves, London, 307-315.

Ogilvie, T.F., and Shin, Y.S. (1978). "Integral-Equation Solutions for Time Dependent Free Surface Problem," J. Soc. Nav. Arch. Japan, 43-53.

Ogilvie, T.F., and Tuck, E.O. (1969). "A Rational Strip Theory for Ship Motions:Part I," Report No. 013, Dept. of Naval Architecture and Marine Engineering, University of Michigan.

Ohmatsu, S. (1975). "On the Irregular Frequencies in the Theory of Oscillating Bodies in a Free Surface," Papers, Ship Res. Inst., No. 48.

Paulling, J.R. and Wood, P. (1972). "State of Art Report Seakeeping," 16th American Towing Tank Conference.

Petryshyn, W.V. (1963). "On a General Iterative Method for the Approximate Solution of Linear Operator Equation," Math. Comp. 17, 1-10.

Porter, W.R. (1960). "Pressure Distributions, Added-mass and Damping Coefficients for Cylinders Oscillating in a Free Surface," Rep. No. 82-16, Inst. Eng. Res., Univ. of Calif., Berkeley, CA.

Rall, L.B. (1955). "Error Bounds for Iterative Solutions to Integral Equations," Pacific J. Math. 5, 977-986.

Salvesen, N., and Tuck, E.O., and Faltinsen, O.M. (1970). "Ship Motions and Sea Loads," Trans. SNAME, 78, 250-287.

Samuelson, P.F. (1953). "Rapidly Converging Solutions to Integral Equations," J. Math. Phys., 31, 276-286.

Sayer, P., and Ursell, F. (1977). "Integral Equation Methods for Calculating the Virtual Mass in Water of Finite Depth," Proc. of 2nd International Conference on Numerical Ship Hydrodynamics, September, University of California, Berkeley, 176-184.

Schenck, H.A. (1968). "Improved Integral Formulation for Acoustic Radiation Problems," J. Acoust. Soc. Amer., 44, 41-58.

Tasai, F. (1959). "On the Damping Force and Added Mass of Ships Heaving and Pitching," J. Soc. Nav. Arch. of Japan, 105, 47-56.

Tein, Y.S. (1976). "Three-Dimensional Added Mass of a Vibrating Ship," Ph.D. Thesis, Dept. Nav. Arch. & Mar. Eng., Univ. of Michigan, Ann Arbor.

Troesch, A.W. (1976). "The Diffraction Potential for a Slender Ship Moving Through Oblique Waves," Rep. No. 176, Dept. Nav. Arch. & Mar. Eng., Univ. of Michigan, Ann Arbor.

Ursell, F. (1949a). "On the Heaving Motion of a Circular Cylinder on the Surface of a Fluid," Quart. J. Mech. Appl. Math. **2**, 218-231.

Ursell, F. (1953). "Short Surface Waves Due to an Oscillating Immersed Body," Proc. Roy. Soc., Ser. A, **220**, 90-103.

Ursell, F. (1973). "On the Exterior Problems of Acoustics," Proc. Camb. Phil. Soc., **74**, 117-125.

Vorus, W.S. (1971). "An Integrated Approach to the Determination of Propeller-Generated Vibratory Forces Acting on a Ship Hull," Rep. No. 072, Dept. Nav. Arch. & Mar. Eng., Univ. of Michigan, Ann Arbor.

Wagner, G. (1951). "On the Solution of Fredholm Integral Equation of the Second Kind by Iteration," J. Math. Phys., **30**, 23-30.

Wang, S. (1966). "The Hydrodynamic Forces and Pressure Distributions for an Oscillating Sphere in a Fluid of Finite Depth," Dept. Nav. Arch. & Mar. Eng., Massachusetts Institute of Technology, Cambridge.

Wehausen, J.V., and Laitone, E.V. (1960). "Surface Waves," Encyclopedia of Physics, S. Flugge/Marburg, Ed., Vol. IX, 446-778, Springer Verlag Berlin.

Yeung, R.W. (1973). "A Singularity-Distribution Method for Free Surface Flow Problems with an Oscillating Body," Rep. No. NA73-6, College of Eng., Univ. of Calif., Berkeley, CA.